REVIEW

Check for updates

Advances in surface modification of biomass and its nanostructuring for enhanced environmental remediation applications

Sandeep Kumar, ID *[a] Parminder Kaur,[ae] Chou-Yi Hsu,[b] Mohammed Ahmed Mustafa,[c] Jyoti Rani,[a] Jasmeen Kaur[a] and Sandeep Kaushal ID *[d]

The growing concerns over environmental pollution and resource sustainability have generated considerable interest in valorizing biomass waste materials as functional materials for environmental remediation. Owing to its abundance, renewability, and diverse surface functionalities, lignocellulosic biomass holds immense potential as a cost-effective adsorbent and a catalyst. However, its practical application is hindered by limitations such as low surface area, limited porosity, and insufficient reactive sites. This review systematically compiles and critically analyzes the recent advances in surface modification and nanostructuring strategies aimed at enhancing the physicochemical properties of biomass-derived materials for water and wastewater treatment. This article covers a broad spectrum of modification approaches, including physical (pyrolysis, hydrothermal carbonization, and microwave heating), chemical (acid/alkali activation and oxidative treatments), and physicochemical techniques, alongside emerging nanocomposite fabrication methods involving metal and metal oxide nanoparticle immobilization. Key focus is placed on how these modifications improve surface area, porosity, functional group distribution, and catalytic activity, thereby augmenting the adsorption and degradation capacities of biomass materials. Mechanistic insights into contaminant removal processes – adsorptive, degradative, and synergistic pathways – are elaborated, thus correlating materials' properties with their pollutant removal efficiencies. Additionally, this review outlines the characterization techniques essential for evaluating structural, morphological, and surface chemistry alterations in modified biomass materials. By bridging the fragmented literature and integrating mechanistic perspectives with material design principles, this review highlights the potential of engineered biomass-based materials as sustainable alternatives for environmental remediation. It also identifies research gaps, proposing future directions focused on scalable, eco-friendly modification techniques, performance optimization, and comprehensive environmental impact assessments. This work aspires to guide the development of next-generation biomass-derived materials for advanced, sustainable, and economically viable pollutant remediation technologies.

1. Introduction

Biomass refers to organic matter derived from living organisms, such as plants, animals, and microorganisms.[1] Examples of biomass include wood, agricultural residues, animal manure, and organic waste (Fig. 1). It serves as a renewable energy source that can be utilized through various processes like combustion, fermentation, and conversion into biofuels (*e.g.*, ethanol and biodiesel) and other bioproducts. The renewable aspect of biomass lies in its ability to be replenished relatively quickly compared to fossil fuels, which take millions of years to form.[2] The substantial quantities of agro-waste pose significant challenges to effective waste management practices.[3] Burning of the crop residues is a common practice that results in the non-recovery of potential resources and release of greenhouse gases and air pollutants. The crop residues are estimated to contain 80% nitrogen (N), 25% phosphorus (P), 50% sulphur (S), and 20% potassium (K), all of which are lost during burning.[4] Treating biomass as waste

[a] *Department of Chemistry, Akal University, Talwandi Sabo, Bathinda 151302, Punjab, India. E-mail: sandeepchem83@gmail.com*

[b] *Thunderbird School of Global Management, Arizona State University Tempe Campus, Phoenix, Arizona 85004, USA*

[c] *Department of Biology, College of Education, University of Samarra, 34010, Iraq*

[d] *Regional Institute of Education, National Council of Educational Research and Training, Ajmer, Rajasthan, India. E-mail: kaushalsandeep33@gmail.com*

[e] *Department of Chemistry, Guru Kashi University, Talwandi Sabo, Bathinda 151302, Punjab, India*

Fig. 1 Renewable sources of biomass.

can have significant environmental, economic, social, and sustainability implications. The utilization of biomass offers numerous environmental advantages, including reducing greenhouse gas emissions, promoting waste reduction and recycling, and providing an alternative to fossil fuels.[5] The implementation of effective waste management strategies that prioritize resource recovery, recycling, and utilization of biomass can help mitigate these impacts and promote a more sustainable approach to biomass management.[6]

The waste biomass may act as a clean, sustainable, and renewable energy source that can be used as a potential resource for converting into valuable products for use in removing pollutants from soil and water. The majority of adsorbents are derived from agricultural sources, such as leaves, bark, seeds, fruit peels, and flowers, fish scales, algae, bacteria, and fungi. Lignocellulosic agro-waste is the most abundant renewable energy resource, with additional agronomic and environmental applications.[7] Agricultural biomass residues have a similar composition to other lignocellulosic materials, with cellulose 40–50%, hemicellulose 20–30%, lignin 20–25%, and ash 1–5%.[8] Lignin is an aromatic polymer containing various functionalities such as carbonyl (–CO–), hydroxyl (–OH), and methyl (–CH$_3$) groups. Hemicellulose and cellulose are aliphatic compounds with carbonyl, hydroxyl, and ether functionalities as a part of their polymeric structure. These functional groups contain oxygen atoms, which have a

strong tendency to bind positively charged heavy metal ions and small organic contaminants by different physical interactions such as hydrogen bonding, electrostatic, or van der Waals interactions.[9] Thus, using agricultural waste for environmental remediation is a beneficial and cost-effective process.

Agricultural biomass, derived from various agricultural sources, possesses distinct characteristics that differentiate it from conventional adsorbents commonly used in environmental remediation processes. These characteristics include a relatively lower surface area, pore size, and pore volume compared to traditional adsorbents like activated carbon or zeolites. The lower surface area, pore size, and pore volume of agricultural biomass limit its adsorption capacity and efficiency in removing pollutants from contaminated water or soil.[10] Adsorption, a process where contaminants are physically or chemically bound to the surface of the adsorbent material, relies on the availability of active sites and pore structures for effective pollutant removal.[11] Since agricultural biomass has an inherently smaller surface area and fewer pores, its adsorption capacity may be insufficient for efficient pollutant removal, especially for contaminants present in high concentrations or requiring specific adsorption conditions.[12] To overcome these limitations and harness the potential of agricultural biomass materials as adsorbents for environmental remediation, innovative strategies need to be developed. These strategies may include:

1.1. Surface modification

The chemical or physical treatments can be applied to agricultural biomass to enhance its surface properties, increase surface area, and create more active sites for adsorption. The adsorption performance of biomass can be improved by employing techniques such as impregnation, chemical activation, or thermal treatment that can modify the surface chemistry and morphology of biomass.[13]

1.2. Nanostructuring

Incorporating nanomaterials, such as nanoparticles or nanocomposites, onto the surface of agricultural biomass can enhance its adsorption capacity and selectivity. Nanostructuring increases the surface area by introducing additional adsorption sites, thus facilitating the removal of a wide range of pollutants with higher efficiency.[14,15] Moreover, the biomass-derived nanomaterials also exhibits enhanced photocatalytic application for the removal of recalcitrant organic contaminants through Fenton-like heterogeneous processes.[16]

1.3. Composite materials

Combining agricultural biomass with other adsorbent materials, such as activated carbon, clay minerals, or polymers, can create composite materials with synergistic adsorption properties. These composite materials combine the strengths and advantages of both components, resulting in enhanced adsorption performance and versatility for environmental remediation applications.[14]

1.4. Functionalization

Introducing functional groups or chemical moieties onto the surface of agricultural biomass can modify its surface chemistry and improve its affinity towards specific pollutants.[17] The functionalization allows for targeted adsorption of contaminants and enhances the selectivity and efficiency of agricultural biomass-based adsorbents.[18]

1.5. Optimization of operating conditions

Optimizing process parameters such as pH, temperature, contact time, and adsorbent dosage can maximize the adsorption efficiency of agricultural biomass-based adsorbents. By understanding the adsorption mechanisms and kinetics involved one can help tailor the operating conditions to achieve optimal pollutant removal performance.[19]

By employing these strategies, agricultural biomass materials can be effectively utilized as adsorbents for environmental remediation processes, offering a sustainable and cost-effective solution for pollutant removal from water and soil environments. These advancements not only address the challenges associated with the inherent properties of agricultural biomass, but also contribute to the development of innovative and eco-friendly adsorption technologies for environmental protection and sustainability. Over the past few decades, there has been a significant increase in interest within the research community towards the development of sustainable technologies for removing contaminants (Fig. 2). However, existing literature reviews have predominantly focused either on the adsorptive
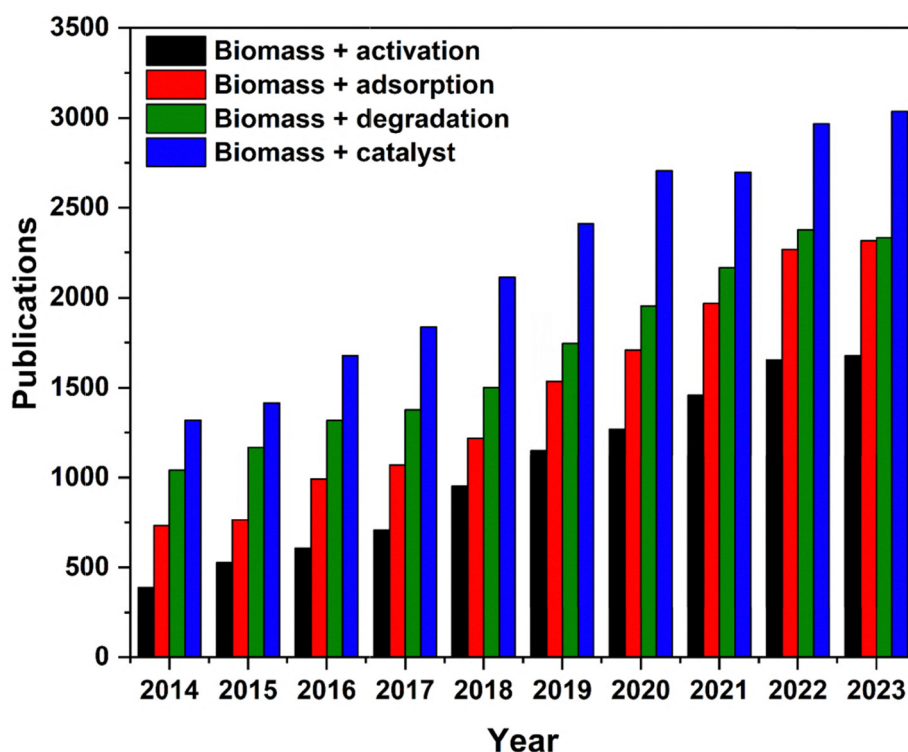

Fig. 2 Research trend of contaminant remediation utilizing biomass-derived materials over the last decade (searching keywords: ''biomass + activation; adsorption; degradation; and catalyst; source: Web of Science).

removal of contaminants using biomass and its derivatives or on mere compiling the sustainable surface modification techniques, often neglecting the intricate structural changes within the biomass and its derived nanocomposites and the underlying mechanisms of contaminant removal. In this comprehensive review, we provide an extensive discussion on surface modification techniques, elucidating the structural changes induced in biomass *via* various activation processes, while discussing the characterization techniques employed to analyze surface modifications and the mechanisms underlying the contaminant removal. Moreover, we also provide a comprehensive summary of the diverse environmental remediation applications of biomass and its carbon-rich derivatives, offering a holistic perspective on the subject.

The sharp increase in publications after 2017 reflects several converging research trends. First, the global emphasis on sustainable and low-cost materials for water and wastewater treatment significantly raised the profile of biomass-derived carbons as eco-friendly alternatives to activated carbon. Second, advancements in nanostructuring techniques enabled the integration of biomass with metal and metal oxide nanoparticles, leading to multifunctional composites that combined adsorption with catalytic degradation. Third, the introduction of persulfate- and peroxymonosulfate-based advanced oxidation processes, often mediated by biochar or activated carbon, opened new avenues for tackling recalcitrant organic contaminants. In parallel, the expansion of photocatalytic and electrochemical approaches using biomass-derived supports further drove research interest. Collectively, these innovations account for the steep rise in scientific output observed after 2017.

2. Surface modification techniques for lignocellulosic biomass

Surface modification techniques for biomass involve altering the surface properties of biomass materials to enhance their performance or functionality for specific applications. To improve its efficiency in wastewater treatments lignocellulose biomass can be modified using various physical and chemical treatments (Fig. 3).

2.1. Physical modification of biomass

Physical methods of surface modification of biomass involve altering the surface properties of biomass materials without introducing chemical changes. Biomass can undergo modification through a variety of physical processes, including cutting, grinding, ball milling, boiling, steaming, autoclaving, thermal drying, and pyrolysis.[20] These methods effectively alter the surface area and particle size of the biomass, enhancing its adsorption capabilities.

2.1.1. Pretreatment of biomass. For the synthesis of activated carbon, pretreatment of biomass is the first step, which involves: (a) acid washing that removes soluble and insoluble metals, ash, and lignin from the raw precursor, whereas hot water washing primarily removes soluble ions. Alkaline pretreatment of lignocellulosic biomass removes silicone and expands the internal structure by dissolving some of the lignin; (b) crushing, to obtain a powder sample; (c) drying at 100 °C, to remove moisture and obtain constant weight; and (d) sieving, to obtain homogeneous particles in a specific range.[21]

2.1.2. Pyrolysis of biomass. Pyrolysis presents an alternative technique for transforming biomass into valuable products like biochar, bio-oil, and syngas under oxygen-deprived conditions at temperatures spanning from 300 to 900 °C.[22] The process of pyrolysis can be categorized into slow pyrolysis and fast pyrolysis based on factors such as temperature, heating rate, pressure, and duration. The fast pyrolysis offers significant advantages by boosting bio-oil yield, reaching up to 75% from biomass, with a rapid heating rate, exceeding 200 °C min^{-1}, and a residence time of less than 10 s. However, the slow pyrolysis occurs within the temperature range of 400 to 600 °C, operates at atmospheric pressure, featuring a relatively lengthy residence time exceeding 1 h and low heating rates of 5–7 °C min^{-1}.[23] This method mainly yields biochar while producing limited amounts of condensed bio-oil, syngas, and hydrocarbons.

2.1.3. Hydrothermal carbonization. Recently, hydrothermal carbonization has become more popular for making activated carbon compared to the traditional thermal carbonization method in an inert atmosphere. This is because the hydrothermal carbonization method doesn't necessitate the initial step of drying the biomass.[24] In contrast to pyrolysis, it is observed as a cost-effective way to produce hydrochar because the hydrothermal carbonization is generally performed at low temperatures (180 to 250 °C) under pressure in water. When water is present, several chemical reactions occur, including hydrolysis, dehydration, decarboxylation, aromatization, and re-condensation. The resulting hydrochar contains a large number of oxygenated functional groups like hydroxylic, carboxylic, and phenolic, which make it more hydrophilic and also improve its ability to adsorb substances.[24]

2.1.4. Microwave heating. Microwave irradiation for heating has gained significant attention from researchers owing to its capacity to transfer heat effectively at the molecular level. This enables a more uniform and rapid thermal conductivity from the heat source. The microwave heating technique can be integrated with physical and/or chemical activation processes to produce activated carbons (ACs) with enhanced performance, employing either a single-stage or two-stage activation procedure. One-step microwave (MW) activation offers distinct advantages such as a more condensed structure, smaller footprint, and simpler operation compared to traditional two-step activation methods.[25] Two-step MW activation processes typically involve carbonization and subsequent activation of the char, with either activation or carbonization conducted under MW irradiation. MW heating offers numerous advantages over conventional heating methods, including uniform and internal heating, rapid and selective heating, ease of control, straightforward setup, insensitivity to particle size and shape, and reduced pretreatment requirements for biomass.[26]
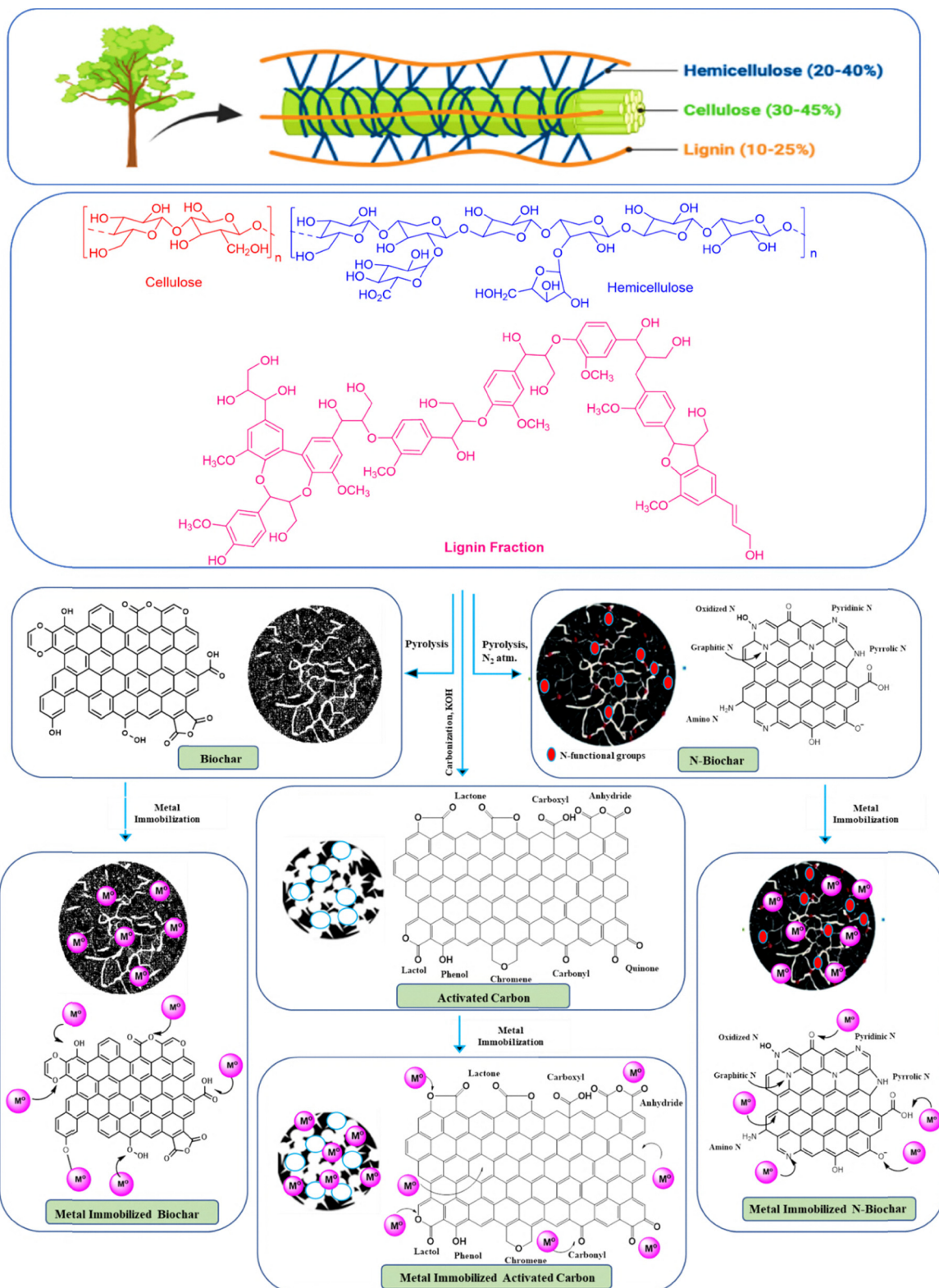
Fig. 3 Schematic representation of biomass-derived carbon materials (biochar, hydrochar, and activated carbon) and their surface modification/metal immobilization pathways for environmental remediation applications.

2.2. Chemical modification

Chemical modification of biomass involves altering its chemical composition through various chemical treatments commonly employed for surface modification of agricultural biomass to enhance its properties for various applications.

2.2.1. Acid modification of biomass. Acid modification represents a typical wet oxidation process commonly employed for surface alteration. Mineral acids and oxidants such as HNO_3, H_2O_2, $HClO$, H_2SO_4, H_3PO_4, and HCl are utilized in acid modification processes, while organic acids like acetic, carboxylic acid, formic acid, and oxalic are rarely used due to their weaker effect stemming from their low strength. The acidification of the adsorbent surface enhances its acidic behavior and hydrophilic nature by reducing mineral content. Adsorbents with an acidic surface feature oxygen-containing functional groups such as carboxyl, carbonyl, quinone, hydroxyl, lactone, and carboxylic anhydride.[19] These functional groups are typically situated on the outer surfaces or edges of the basal plane on activated carbon, significantly influencing the material's chemical properties.[27] Researchers have extensively explored the utilization of acid-modified adsorbents for water decontamination purposes, reflecting ongoing efforts in this area.

2.2.2. Alkaline modification of biomass. Modifying adsorbents with reducing agents can markedly alter their surface functional groups, leading to significant enhancements in their adsorption capacities. This process tends to improve the relative abundance of alkali groups and render the surface more non-polar, thereby improving the adsorption capacity for non-polar substances. When subjected to alkali treatment, an adsorbent acquires a positive charge on its surface, which in turn boosts the adsorption of negatively charged species. Surface reduction can be achieved through treatments involving $NaOH$, KOH, $LiOH$, Na_2SiO_3, Na_2CO_3, and various oxides.[19]

2.3. Physico-chemical activation of biomass

Activated carbon finds wide-ranging applications, including the removal of various contaminants from water and wastewater, as well as in capacitors, battery electrodes, catalytic supports, and gas storage materials. These applications arise from its desirable characteristics, including its large surface area and porosity, along with its surface chemistry capable of interacting with molecules possessing specific functional groups.[28] Over the past few decades, there has been growing recognition of the potential of biowaste to yield low-cost adsorbents, leading to numerous studies assessing the characteristics and efficacy of activated carbon derived from various biowaste sources for wastewater pollutant removal (Table 1).

Activated carbon is conventionally produced through two primary activation methods: (a) physical activation; and (b) chemical activation. The physical activation involves two distinct thermal stages. Initially, the carbonaceous precursor undergoes pyrolysis or carbonization at high temperatures, typically between 700–900 °C, in an inert atmosphere to prevent combustion. This step eliminates heteroatoms and releases volatiles, resulting in chars with high carbon content (where

increased carbonization temperature enhances carbon content), but limited porosity development. The subsequent stage of physical activation is gasification, entailing the selective removal of the most reactive carbon atoms through controlled gasification reactions to induce the characteristic porosity of activated carbons.[73] The gasification temperature varies depending on the gasification agent utilized, typically water vapor, CO_2, or O_2/air. Water vapor or CO_2 gasification commonly occurs at temperatures ranging around 700–900 °C, whereas gasification using pure O_2 or air requires much lower temperatures (around 300–450 °C) due to the higher reactivity of O_2 compared to CO_2 and water vapor. The use of O_2 complicates gasification control and porosity development due to its high reactivity and exothermic nature.[74] Generally, CO_2 serves as the preferred activation gas due to its cleanliness and ease of handling and facilitation of activation process control owing to its slow reaction rate at elevated temperatures. Jiang et al. used pyrolysis in the presence of CO_2 and N_2 as a physical activator to obtain activated hybrid willow biomass.[75] Pallares et al. activated barley straw biomass by regulating the gas flow rate of compressed gas cylinders containing N_2 and CO_2, along with steam produced using a steam generator at 150 °C.[29]

On the other hand, the process of chemical activation involves impregnating a biomass material with a chemical reagent and then activating it, whether the material is raw or carbonized. The activation can be achieved in one-step or two-steps. In the one-step process, the raw precursor is mixed with the activating agent and then is subjected to carbonization. In the two-step process, the pre-carbonized biomass is treated with the activating agent, and then it is again subjected to carbonization. Strong bases ($NaOH$ and KOH), acids (H_2SO_4, H_3PO_4, HCl, HF, etc.), or salts ($ZnCl_2$ and $CaCl_2$) are employed as activating agents. In single-step activation, a strong base such as KOH is typically used.[28] After activation, the last step involves the washing to remove the remaining activating agents or reaction byproducts that occlude the newly formed porosity and drying. Ogungbenro et al. synthesized activated carbon form data seed biomass using a two-step activation process involving pyrolysis of biomass under a CO_2 atmosphere followed by treatment with chemical activators such as KOH and H_2SO_4.[76] Suarez and Centeno obtained activated carbon from apple bagasse using pyrolysis under CO_2 and then activation with KOH under a N_2 atmosphere.[31] Mesoporous activated carbon from Kenaf,[32] cashew,[33] corn straw,[34] sawdust biomass,[35] and Corncob[36] was obtained using single step pyrolysis under the N_2 atmosphere in the presence of H_3PO_4 as a chemical activator. The activated carbon from Jujun grass,[37] Lecithin,[38] and Wheat straw[39] biomass was obtained by two-step hydrothermal carbonization with KOH and H_3PO_4 as a chemical activator. Sangeetha et al. synthesized activation carbon in the presence of $ZnCl_2$ from the coconut shell.[41]

2.4. Nanostructuring of biomass and its derivatives

The fabrication of these biomaterials with inorganic nanoparticles such as metal/metal oxides will not only increase their

Table 1 Synthetic approaches involving surface modification of biomass

Biomass	Process type	Pre-treatment	Activator	Activating conditions	Ref.
Barley straw	Two-step	Carbonization, N_2 atm.	CO_2 and steam	800 °C in CO_2 and 700 °C in steam	29
Date seeds	Single step	None	KOH/H_2SO_4	600–900 °C, N_2 atm.	30
Apple bagasse	Two-step	Pyrolysis with CO_2, 800 °C	KOH	800 °C, N_2 atm.	31
Kenaf	Single step	None	H_3PO_4	600 °C, N_2 atm.	32
Cashew nut	Single step	None	H_3PO_4	400–700 °C, N_2 atm.	33
Corn straw	Single step	None	H_3PO_4	300 °C, N_2 atm.	34
Pine wood sawdust	Single step	None	H_3PO_4	800 °C, N_2 atm.	35
Corncob	Single step	None	H_3PO_4	450–850 °C, N_2 atm.	36
Jujun grass	Two-step	Hydrothermal carbonization	KOH	900 °C, N_2 atm.	37
Lecithin	Two-step	Hydrothermal carbonization	KOH	900 °C, N_2 atm.	38
Wheat straw	Two-step	$ZnCl_2$ catalytic hydrothermal carbonization (200 °C)	H_3PO_4	500 °C, N_2 atm.	39
Cotton shell	Single step	None	KOH	600 °C, N_2 atm.	40
Coconut shell	Single step	None	$ZnCl_2$	500 °C, N_2 atm.	41
Tobacco stalks	Two-step	Carbonized at 700 °C	None	1000 °C, 5 h	42
Shiitake mushroom	Single step	None	None	300 °C, 500 °C, 700 °C	43
Rape straw	Two-step	Carbonized at 700 °C	KOH	750 °C	44
Sunflower	Two-step	650 °C	Ag/vitamin C/and H_2O_2	None	45
Rice straw	Two-step	700 °C	Tannic acid	None	46
Food and plant waste	Single step	None	None	300 °C	47
Cow manure	Single step	None	None	Carbonized at 300 °C, 500 °C, and 700 °C, N_2 atm.	48
Pomelo peels	Two-step	Carbonized at 400 °C	KOH	600, 700, 800, and 900 °C, N_2 atm.	49
Wheat Straw	Single step	None	None	600 °C, N_2 atm.	50
Rice husk	Single step	None	NaOH	None	51
Seaweed	Two-step	500 °C	NaOH	800 °C, N_2 atm.	52
Rice Husk	Single step	None	NaOH	None	53
Hazelnut Shell	Two-step	None	KOH	950 °C	54
Rice husk	Two-step	None	KOH	950 °C	54
Corn Stalks	Two-step	None	KOH	950 °C	54
Erythrina speciosa	Single-step	None	$ZnCl_2$	None	55
Animal dung	Two-step	None	KOH and $ZnCl_2$	Hydrothermal activation	56
Bamboo	Two-step	None	KOH	700 °C	57
Sesame straw	Two-step	None	KOH, $Ca(OH)_2$	Calcination	58
Thevetia neriifolia	Two-step	None	H_3PO_4, 400 °C	800 °C N_2 atm.	59
Acacia wood	Two-step	500 °C, N_2 atm.	KOH	110 °C, Microwave oven	60
Haematoxylum campechianum	Two-step	None	H_3PO_4	500 °C	61
Sugar cane bagasse	Two-step	None	$ZnCl_2$	500 °C N_2 atm.	62
Rice husk	Two-step	None	$NaOH/CH_3COOH/H_3PO_4$	700 °C	63
Kesambi wood	Two-step	400 °C	H_2SO_4	110 °C, oven	64
Sawdust	Two-step	None	KOH	800 °C N_2 atm.	65
Biomass peels	Two-step	None	H_3PO_4	600 °C	66
Pistachio wood	Single step	None	NH_4NO_3	800 °C N_2 atm.	67
Date press cake	Two-step	500 °C	NaOH	750 °C N_2 atm	68
Rice husk	Single step	None	NaOH	None	69
Corn cob	Single step	None	HCl	None	69
Baobab fruit shells	Single step	None	H_3PO_4	200–900 °C N_2 atm	70
Poplar flour and walnut shell	Single step	None	None	1000 °C	71
Soybean biomass	Single step	None	None	900 °C	72

surface area for contaminant absorption, but also make them efficient catalysts for studying various organic contaminant degradation processes.[77] The adsorption tendencies of biomass materials complemented with the catalytic efficiencies of inorganic nanoparticles generate a synergistic effect, which is effective in the removal of various contaminants from their aqueous solution.[78] Fe is a pure metal and magnetic in nature; thus, a magnetic biochar can be obtained when Fe is immobilized on biochar. Nano-sized Fe, also known as nanoscale zero-valent iron (nZVI), is highly unstable in the environment; however, many studies have confirmed that coating nZVI on biochar could be an efficient approach to getting a stable nZVI@biochar composite with simultaneous high reactivity due to dispersive nZVI on biochar.[15] The removal mechanisms of nZVI@biochar include reduction, surface complexation, and coprecipitation. The magnetic biochar can also be prepared by

pre-treatment and post-treatment of biomass. In the pre-treatment process, pyrolysis of biomass in the presence of $FeCl_3$ or $FeCl_2$ is performed. However, in the post-treatment precipitation of biochar with $FeSO_4$ and $FeCl_3$ under basic conditions results in immobilization of the iron hydroxides ($Fe(OH)_3$) on biochar.[79] In the literature, the magnetic biochar has been synthesized using different kinds of methods with various biomass materials and magnetic media. The popular methods including co-precipitation, thermal decomposition, and/or reduction and hydrothermal synthesis techniques can all be directed to the synthesis of high-quality magnetic biochar. The iron oxides such as Fe_3O_4 and γ-Fe_2O_3, have been studied largely due to the low cost of raw materials and ease of synthesis.[80] Other than Fe_3O_4, other metal oxides such as CuO, TiO_2, ZnO, MnO_2, Co_3O_4, *etc.* have also been immobilized on biomass and its derivative surfaces and have been extensively explored for their environmental remediation applications.[81]

2.5. Comparative analysis of surface modification techniques

While a wide range of surface modification strategies have been developed for biomass, their effectiveness, scalability, and environmental impact vary significantly. Chemical modifications (*e.g.*, acid/alkali activation and oxidative treatments) are highly effective in introducing functional groups and creating well-developed porosity, which enhances adsorption and catalytic performance. However, these approaches often require strong reagents (H_2SO_4, HNO_3, KOH, *etc.*), generate secondary effluents, and may raise concerns regarding environmental safety and process sustainability.

In contrast, physical methods such as pyrolysis, hydrothermal carbonization, and microwave heating offer greener and more scalable routes, especially at pilot or industrial levels. These methods minimize the use of hazardous chemicals and often produce by-products like bio-oil and syngas that can be valorized. However, their effectiveness in producing high surface areas and tailored functionalities is sometimes limited compared to chemical treatments, often necessitating post-treatment or hybrid approaches.

Biological modifications, employing microbial or enzymatic pretreatments, represent the most eco-friendly strategies, with minimal chemical waste and reduced energy requirements. They can selectively alter lignin, cellulose, or hemicellulose fractions to improve the accessibility of active sites. Yet, their relatively slow kinetics, sensitivity to environmental conditions, and difficulties in scaling beyond laboratory studies restrict their current industrial applicability.

From a sustainability standpoint, the integration of physico-chemical or bio-assisted hybrid approaches may offer the best compromise—combining the efficiency of chemical treatments with the environmental friendliness of biological methods and the scalability of physical routes. Future research should therefore focus on techno-economic analyses and life-cycle assessments (LCA) to evaluate not only the technical performance but also the overall environmental footprint of each modification pathway.

3. Structure of biomass adsorbents

The biomass is mainly categorized into two: lignocellulosic and non-lignocellulosic biomass, having chemical compositions different altogether, with the former being extensively used for its environmental remediation applications. The lignocellulosic biomass mainly consists of cellulose, hemicellulose, silica, and lignin. The complex nature of the lignocellulosic biomass not only provides the structural integrity to the plants, but also contributes to the rigidity and strength of the overall structure. The sources of lignocellulose biomass include wood, agricultural residues, and dedicated energy crops.[13] On the other hand, the non-lignocellulosic biomass includes materials like algae, aquatic plants, animal dung, sewage sludge, and organic waste streams, which contain a diverse array of organic compounds. The composition of non-lignocellulosic biomass includes mainly proteins, lipids, and carbohydrates.[82] The lignocellulosic biomass has a porous structure and high surface area, making it useful in the adsorption processes for the removal of recalcitrant pollutants such as heavy metals, dyes, and organic compounds from water. The abundant hydroxyl and carboxyl groups present in the lignocellulosic biomass facilitate the binding of contaminants through physical as well as chemical interactions.[9] The algal biomass exhibits a high affinity for nutrients, such as nitrogen and phosphorus, thus making it suitable for wastewater treatment applications through processes like nutrient uptake and bio-filtration.[82]

The chemical and physical modifications can be applied to the surface of biomass in order to enhance its properties and potential applications. The physical modifications affect the surface morphology and topography of biomass, resulting in change in the surface area, porosity, and accessibility of active sites.[20] The chemical modification results in the change in composition and the functional groups on the surface of biomass.[83] These modifications can improve certain properties such as hydrophobicity, thermal stability, and compatibility with other materials, thus expanding the range of applications in biocomposites, adsorption, and catalysis.

Biochar, a stable carbon-rich solid product, is obtained through biomass pyrolysis in an environment with limited oxygen. During this process, the hydroxyl, carboxyl, and carbonyl groups present in the biomass are removed, resulting in a modified surface chemistry of biochar with higher carbon content and lower concentration of oxygen-containing functional groups compared to the original biomass.[84] Within biochars, carbon, oxygen, and hydrogen species comprise both inorganic (like HCO_3^-, CO_3^{2-}, metallic oxides, and hydroxides) and organic components (such as C–C, C=C, C–H, –C–O–H, C=O, C–O–C, COOH, and –C_6H_5). The organic component, resembling a skeleton in biochar, originates from cellulose, hemicellulose, and lignin in the biomass, transforming into aliphatic carbon at lower and intermediate pyrolysis temperatures and transitioning to aromatic carbon at higher temperatures[18] (Fig. 4).

The surface chemistry of biochar, encompassing surface functional groups, surface charge, and free radicals, plays a
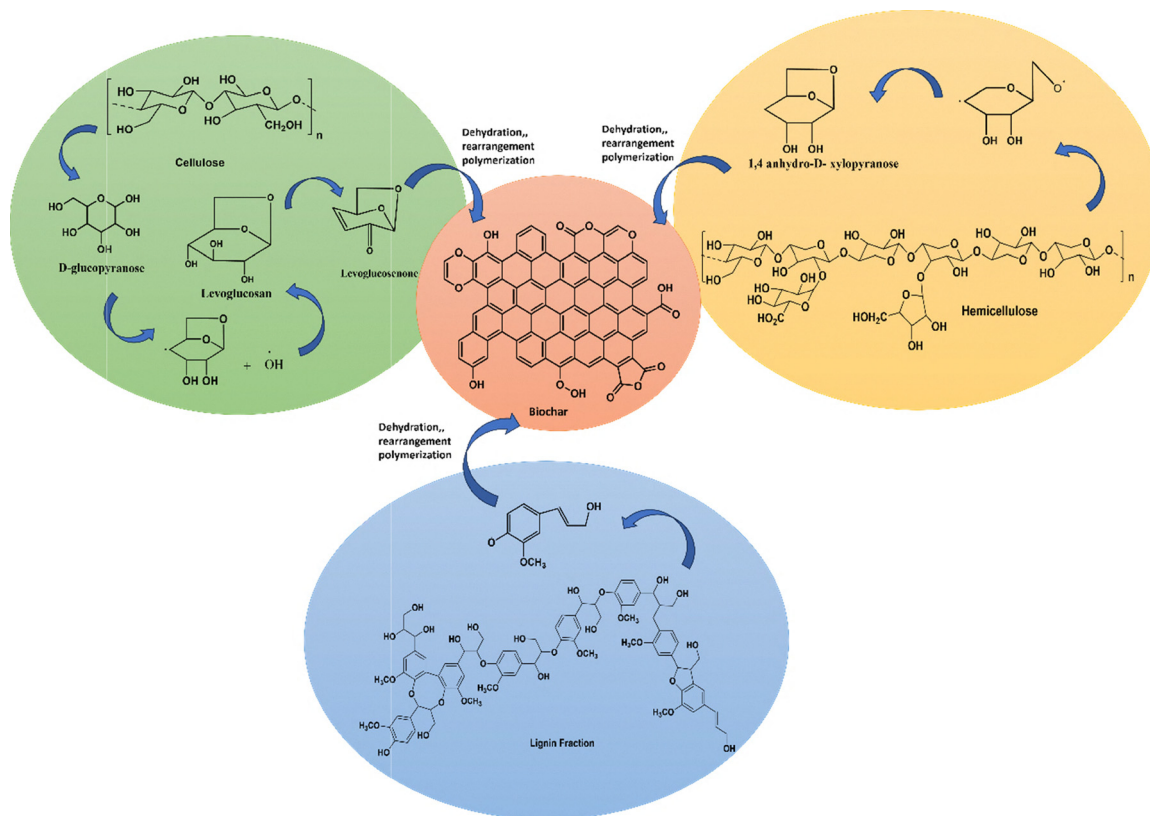
Fig. 4 Scheme for biochar synthesis from lignocellulosic biomass.

crucial role in its interaction with organic and inorganic contaminants. These factors provide significant sites for adsorption and catalytic degradation of pollutants. Different sorption mechanisms, such as partitioning, hydrogen bonding, π–π bonding, electrostatic interaction, and pore-filling, rely on the properties of both biochar and pollutants. The surface negative charge across the natural pH range of 4–12 in biochars originates from the breakdown of functional groups (such as carboxyl moieties) and their aliphatic/aromatic surface.[10] Typically, the biochar surfaces become more negatively charged as the pH of the solution rises above 4. The electrostatic interactions, regulated by the solution, influence the transport of biochar particles and ions. Additionally, biochar displays redox activity due to the presence of electroactive moieties like quinones, phenolic functional groups, polycondensed aromatic sheets, and redox-active metals, capable of accepting/donating or conducting electrons.[80] The electrochemical analyses of the biochar indicate that the redox-active moieties and their electron transfer capacities vary with pyrolysis temperatures, suggesting a correlation between redox properties and biochar structure. In a biochar-mediated p-nitrophenol (PNP) decomposition, approximately 20% of PNP degradation occurs via $^{\bullet}$OH radicals produced from the activation of H_2O_2 by redox-active sites in biochar, while around 80% of PNP degradation involves direct interaction with reactive sites, likely hydroquinones in biochar, through two one-electron transfers, leading to the production of reduced PNP.[85]

Hydrochar is a carbon-rich material produced through hydrothermal carbonization of biomass, which involves heating biomass in water at high pressure and temperature. Its structure typically consists of a network of condensed carbon rings, resulting in a material with high carbon content and significant porosity. The composition of hydrochar includes a mix of carbon, hydrogen, and oxygen, with some residual inorganic minerals depending on the feedstock used. Its properties are characterized by increased stability and reduced volatility compared to the original biomass, making it suitable for applications like water treatment and energy storage. The hydrochar obtained from the physical activation process has poor porosity and surface area compared to the one produced by a chemical activation procedure. The porous structure of hydrochar enhances its surface area, contributing to its effectiveness in adsorbing contaminants and improving its performance in various environmental and industrial applications.[23,24]

Activated carbon is a carbon material derived from organic materials such as agricultural residues, wood, or other plant-based sources through a process of carbonization followed by activation or $vice$ $versa$. Its structure features a network of highly porous carbon, including a range of pore sizes from macropores to micropores, which creates an extensive surface area for adsorption.[86] The composition predominantly consists of carbon, with varying amounts of residual ash, minerals, and potentially some remaining organic matter, depending on the

original biomass and the activation method used. This porous structure enhances the material's ability to adsorb contaminants from gases and liquids, making biomass activated carbon a valuable resource for environmental remediation, water treatment, and other applications requiring efficient adsorption.[28]

The immobilization of metal or metal oxide nanoparticles on biomass and its derived materials results in the formation of metal nanocomposites, commonly referred to as nanostructured biomass. There are various methods for nanocomposite synthesis, such as impregnation, precipitation, *in situ* reduction, and carbothermal reduction.[87] The metal nanoparticles interact with the functional groups on the biomass surface through various mechanisms, including chemical bonding, electrostatic forces, and van der Waals interactions. The functional groups like hydroxyl, carboxyl, and amino groups on the biomass can form bonds with the nanoparticles or attract them due to their charges. These interactions help integrate the nanoparticles into the biomass, influencing how well they are dispersed and attached. Modification of the surface of either the biomass or the nanoparticles can enhance these interactions, ultimately affecting the composite's properties such as strength and reactivity. The unique properties of biomass, such as its porous structure, high surface area, and functional groups stabilize the metal nanoparticles. In addition, the synergistic interactions between the metal nanoparticles and the biomass render the biomass-based metal nanocomposites with enhanced adsorption and catalytic properties.[88]

4. Characterization techniques for biomass and its derived materials

Various characterization techniques or methods are utilized to assess biomass or its nanocomposite materials, including biochar, hydrochars, or activated carbons, tailored to their distinctive chemical, physical, and structural properties.

4.1. Characterization techniques for physical/morphological properties

Biomass and its derived materials have different physical properties such surface area, pore volume, and pore size distribution. The characterization techniques such as microscopy, Brunauer–Emmett–Teller (BET) analysis, transmission electron microscopy (TEM), scanning electron microscopy (SEM), X-ray diffraction (XRD), thermogravimetric analysis (TGA) and differential thermal analysis (DTA) are used to analyze the physical and structural properties of biomass, biochar, activated carbon and metal immobilized nanocomposites.

4.1.1. Brunauer–Emmett–Teller analysis. Depending on the activation method employed (physical or chemical) the BET surface area of biomass undergoes significant changes upon activation. The surface area of untreated biomass is comparatively higher than that of the thermal activated

material, as thermal activation typically leads to a decrease in surface area due to the removal of volatile matter at higher temperature. On the other hand, the chemical activation tends to increase the BET surface area by introducing additional pores and creating a more porous structure. Different types of BET (Brunauer–Emmett–Teller) isotherms type I, II, III, or IV are shown by biomass materials reflecting their diverse structural characteristics and porosities.[89] Type I isotherms are typically observed for the materials with well-defined micropores exhibiting a sharp increase in adsorption at relatively low pressures followed by a plateau, indicating the presence of monolayer adsorption.[90] Type II isotherms are characteristic of materials with non-porous or macroporous structure and display a gradual increase in adsorption upon increasing the relative pressure. The biomass-derived materials with less defined porosity or larger pore sizes may exhibit type II isotherms.[91] Type III isotherms are commonly associated with materials having mesoporous structure and exhibit an inflection point in the adsorption curve, indicating the occurrence of multilayer adsorption on the mesoporous surfaces. This is often observed in activated carbons derived from biomass with a significant mesopore volume. The type IV isotherm indicates hierarchical porosity, displaying both micropores and mesopores. Oginni *et al.* investigated that the activated carbon obtained from Public Miscanthus (PMBC) and Kanlow Switchgrass (KSBC) biochar showed type I and type IV isotherms, respectively[92] (Fig. 5). The activated carbons had pore diameters ranging from 2.01 to 4.15 nm. The activated carbon derived from biomass had larger average pore sizes due to the ordered porous structure of the biochar precursors. This minimized the impact of the activating agent on enhancing the porous structure of the final biochar-derived activated carbons.[92]

4.1.2. Scanning electron microscopy (SEM) and energy dispersive X-ray spectroscopy (EDS). SEM-EDS is an outstanding technique that provides both qualitative morphological and elemental information. The SEM image of biochar and activated carbon shows irregular structures with high heterogeneous surface properties and irregular dense pores. These surface irregularities play an important role in the contaminant removal. The activation processes induced structural changes within the carbon framework, causing it to collapse at high temperatures. The alkali treatment serves as a pore-forming agent, initiating the generation of active vapor or CO/CO_2, which promotes the formation of pores. These pores not only increase the surface area but also provide an abundance of defective sites, facilitating enhanced adsorption and catalytic activities.[93] Shao *et al.* investigated the morphological structure of bamboo and pigeon pea stalks that have a gentle surface with no pores. The biochar prepared at 400 °C and 500 °C from bamboo and pigeon pea stalks had honeycomb-like porous structures. The increase in the pyrolysis temperature to 600 °C causes the pores to crumble and form a channel-like structure.[94] From SEM analysis of eucalyptus biochar (EC) and eucalyptus derived activated carbon (AC) it was confirmed that the former has small irregular shaped particles, whereas
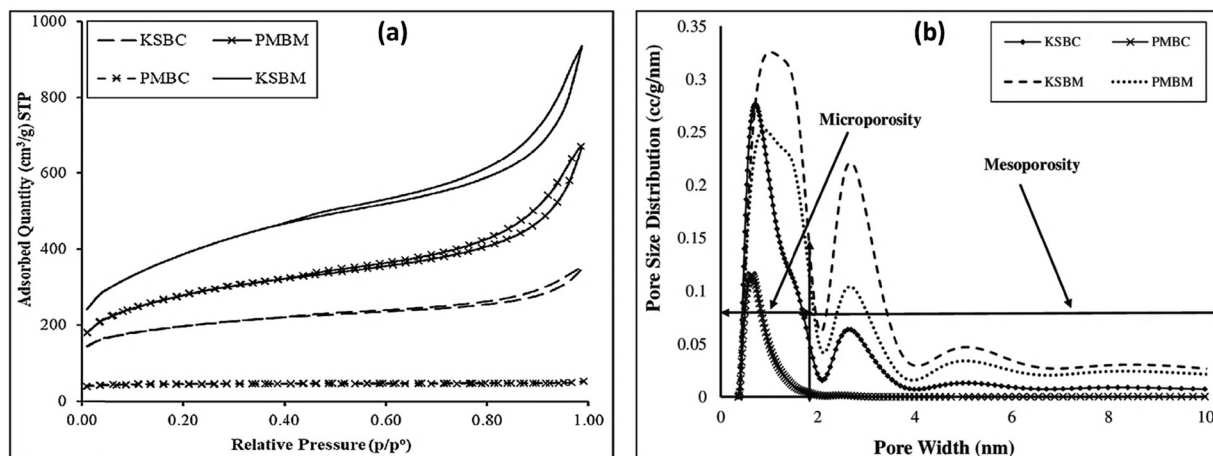
Fig. 5 (a) N$_2$ adsorption/desorption isotherms; and (b) pore size distribution for biochar-derived and biomass-derived activated carbons[92] (reproduced with permission, Elsevier, 2019).

uniform sized particles were observed for the latter. The element composition analysis of activated carbon and biochar displayed carbon as the dominant component (72–83%), and oxygen in smaller amounts (4–23%), along with other trace elements such as P and N in the sample[95] (Fig. 6).

4.1.3. X-ray diffraction analysis. X-ray diffraction (XRD) analysis offers invaluable insights into the structural properties of biomass and its derived materials. The XRD analysis investigates the crystalline structure of biomass constituents such as

cellulose, hemicellulose, and lignin. After pyrolysis, the XRD analysis gives information on the structural properties, confirming the conversion of organic materials into a carbon-rich, porous matrix upon activation of biomass. Gale *et al.* explored the effect of the activation on the structural properties of biomass. The activation of biomass decreases the intensity of cellulosic peaks and the crystallite size. The temperature increase during the activation breaks down the lignocellulosic biomass and generates the turbostratic carbon (t-carbon) with a
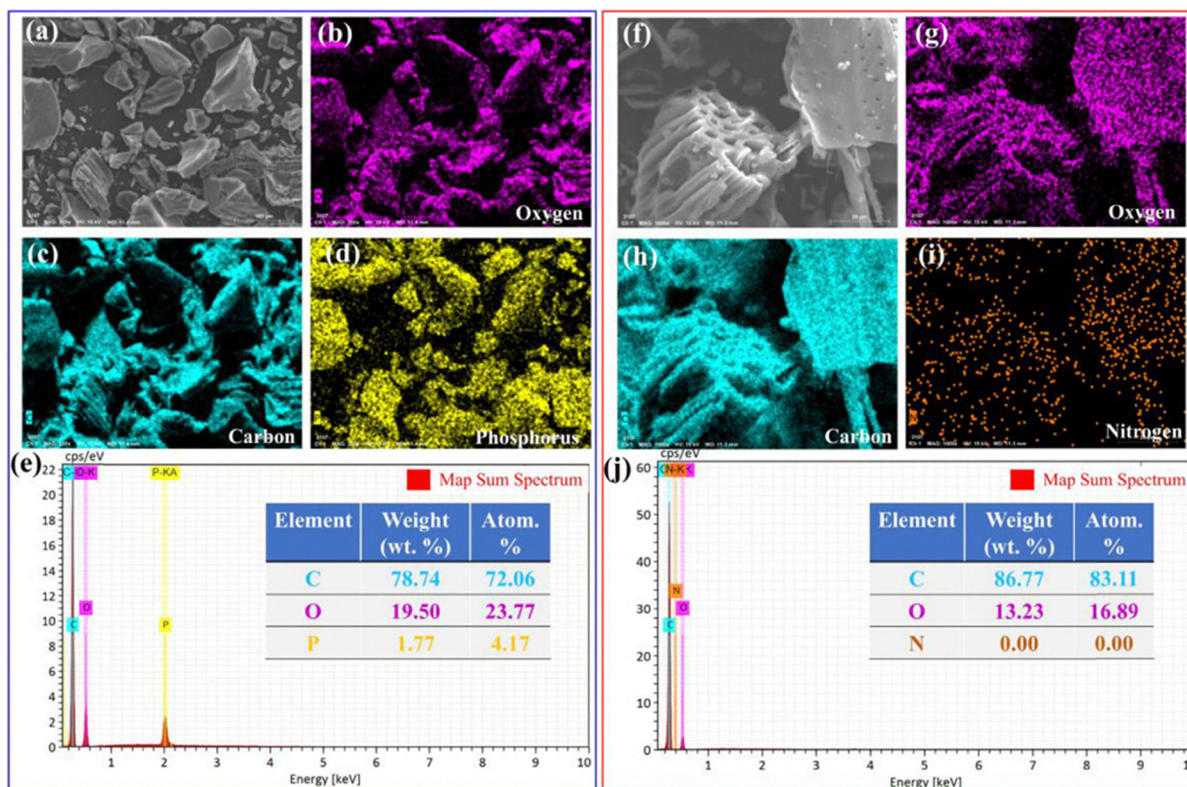

Fig. 6 The elemental mapping and EDS mass spectrum of (a)–(e) eucalyptus activated carbon (AC) and (f)–(j) eucalyptus biochar (EC)[95] (reproduced with permission, Elsevier, 2021).

peak at 26° (2θ), indicating the potential growth of graphene layers.[10] Kaur et al. also investigated the effect of XRD analysis of biomass before and after activation, and they found that significant changes in the phase composition and crystallinity were observed. The untreated biomass showed broad diffraction peaks at 16.2° and 22.1°, indicating the amorphous nature of carbon-containing biomass, attributed to the typical reflection plane (002). However, the XRD patterns after chemical activation of lignocellulosic biomass showed shifted peaks at 16.6° and 23.3°, indicating the presence of crystalline structured graphitic carbons with intense graphitic peaks at 2θ values of 28.2° and 29.4°, which were observed in the XRD pattern of activated biomass, indicating a high degree of crystallinity achieved after the activation process. The XRD analysis of these structural changes provides valuable insights into the transformation of biomass during activation[40] (Fig. 7).

4.1.4. Thermogravimetric analysis (TGA) and differential thermal analysis (DTA). The TGA/DTA analysis explains the thermal behaviour of biomass and its derived materials. In the TGA analysis, the weight percentage change is monitored as a function of temperature or time under controlled pressure.[96] The TGA analysis depicts its thermal stability, pore structure, and surface functional groups. With the help of the degradation stages, the TGA elucidates the key thermal events like dehydration, breakdown of cellulose and lignin and char formation. Further, the DTA analysis provides information regarding endothermic and exothermic reactions, phase transitions and chemical reactions within the materials.[97] The activation of biomass, with pyrolysis or chemical treatment, leads to a notable increase in its thermal stability. The changes on the surface of biomass act as thermal stabilizers and inhibit thermal breakdown reactions and enhance thermal stability.

This enhancement may arise from several factors such as the removal of volatile organic compounds and moisture from the surface of biomass, structural rearrangement with formation of new chemical bonds, creation of a porous structure, generation of new functional groups on the surface of biomass during the activation step, and reduction in its propensity for combustion or decomposition at lower temperature.[27] Further, the immobilization of inorganic materials such as metal/metal oxide nanoparticles on the surface of biomass and its derived materials also enhances the thermal stability of nanocomposites.[98] Maia et al. used physico-chemical activation via KOH treatment followed by pyrolysis to prepare palm fibre biomass derived activated carbon and used it for the adsorptive removal of methylene blue dye. In the TGA analysis, it was observed that the thermal stability of palm fibre biomass derived activated carbon was significantly increased.[95] Kaur et al. investigated the higher thermal stability of the cotton shell activated carbon (CSAC) and its metal nanocomposites compared to the raw CS biomass. The increment in thermal stability is attributed to the formation of different surface groups at specific sites through the interaction of oxygen and oxidized gases, as well as the immobilization of inorganic material on its surface[40] (Fig. 8).

4.2. Characterization techniques for chemical properties

The chemical compositions of cellulose, hemicellulose, and lignin decide the chemical properties of biomass materials, which further depends on the source material and processing methods to obtain the biomass. When the biomass undergoes activation to produce activated carbon, its chemical properties undergo significant changes. The activated carbon obtained via chemical treatment possesses a highly porous structure, which increases its surface area and alters its chemical reactivity. This
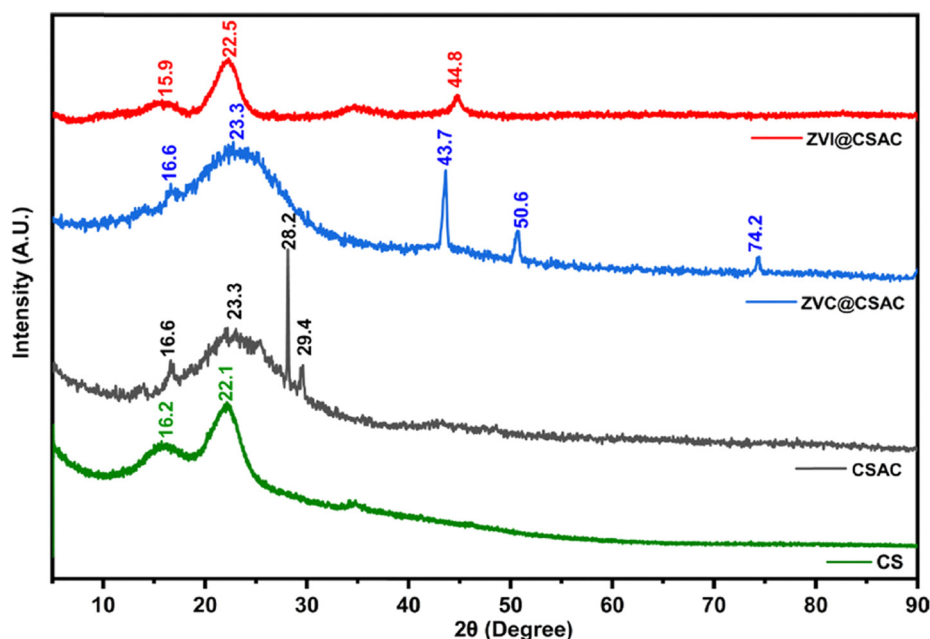

Fig. 7   XRD patterns of biomass (CS), activated carbon (CSAC), and its metal-immobilized nanocomposites[40] (reproduced with permission, Elsevier, 2024).
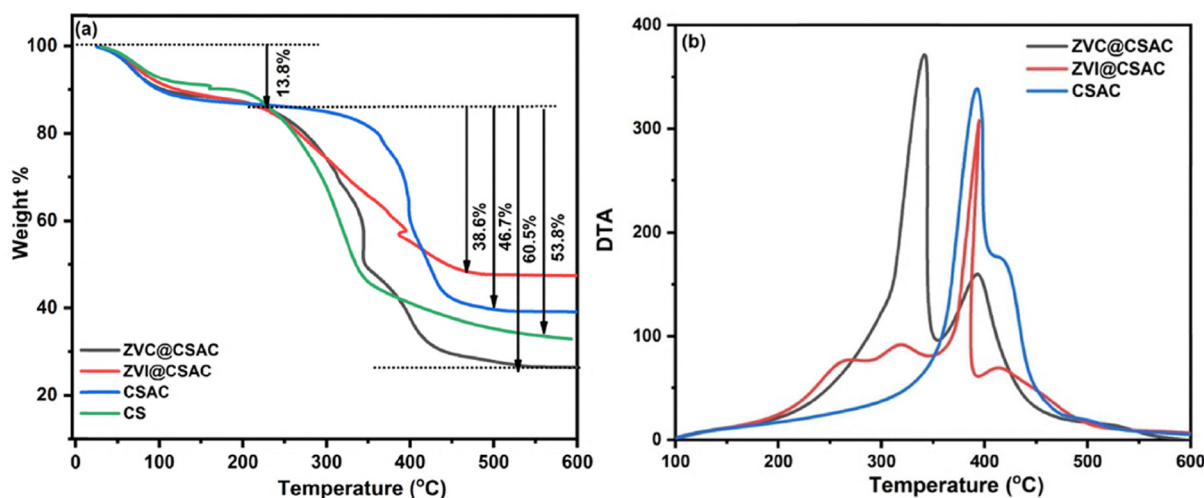
Fig. 8 (a) TGA graph for CS, CSAC, ZVC@CSAC, and ZVI@CSAC; (b) DTA curves for CSAC, ZVC@CSAC, and ZVI@CSAC.[40]

material typically exhibits a high carbon content and a reduced amount of impurities like moisture and volatile organic compounds.[27] The functional groups present in the precursor biomass also have a significant impact on the surface chemistry of activated carbon, deciding its adsorption capabilities and reactivity towards different molecules. These properties render activated carbon a versatile material widely used in various applications, such as water purification, air filtration, and adsorptive removal of contaminants from industrial processes.[82] The characterization techniques used for the evaluation of chemical properties of biomass and its derived materials are discussed below:

4.2.1. Fourier-transform infrared spectroscopic analysis. The Fourier-transform infrared (FTIR) spectroscopic analysis of biomass can provide important information about the changes in the surface functional groups, before and after the activation process. The untreated biomass usually exhibits specific absorption bands that correspond to functional groups such as hydroxyl (–OH), carbonyl (C=O), carboxyl (COOH), and aromatic C=C, which are characteristic of cellulose, hemicellulose, and lignin constituents.[99] The activation can modify these absorption bands, indicating structural transformations. It was observed that thermal activation may lead to dehydration, and thus a decrease in the intensity of the hydroxyl (–OH) peak was common in the FTIR spectrum, while the formation of new oxygen-containing functional groups on the activated surface can produce new bands or shift in existing bands. The chemical activation introduces functional groups from activating agents such as KOH or H_3PO_4, leading to additional peaks or changes in the peak intensities in the FTIR spectra. The disappearance or reduction of specific peaks associated with the organic functional groups suggested the removal of volatile matter or the breakdown of organic compounds during activation. Vunain *et al.* prepared activated carbon from raw baobab fruit shell biomass using an H_3PO_4 chemical activation process. The FTIR spectrum of a raw baobab fruit shell shows strong peaks associated with hydroxyl (–OH) and carbonyl (C=O)

groups of a lignocellulose framework. After chemical activation with H_3PO_4 followed by carbonization, these peaks either disappeared or shifted, with the appearance of peaks associated with the activated carbon[70] (Fig. 9).

4.2.2. X-ray photoelectron spectroscopy analysis. X-ray photoelectron spectroscopy (XPS) is a powerful analytical technique used to provide valuable insights into the chemical composition and surface functionalities of biomass and its activated carbon by measuring the binding energies of electrons emitted from the sample upon exposure to X-ray.[10] The surface elemental composition of biomass including carbon, oxygen, nitrogen, and other trace elements, if present, can be evaluated using XPS analysis. It also provides information about the functional groups such as hydroxyl (–OH), carbonyl (C=O), and carboxyl (–COOH) groups, which are important for defining its reactivity and potential applications. On the other
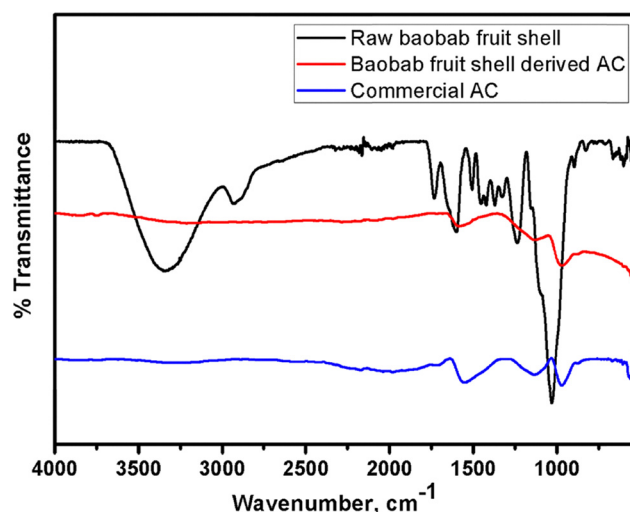

Fig. 9 The FTIR spectra of raw baobab fruit shell biomass and its activated carbon in comparison with commercial activated carbon[70] (reproduced under Creative Commons Attribution (CC BY) license **https://creativecommons.org/licenses/by/4.0/**).
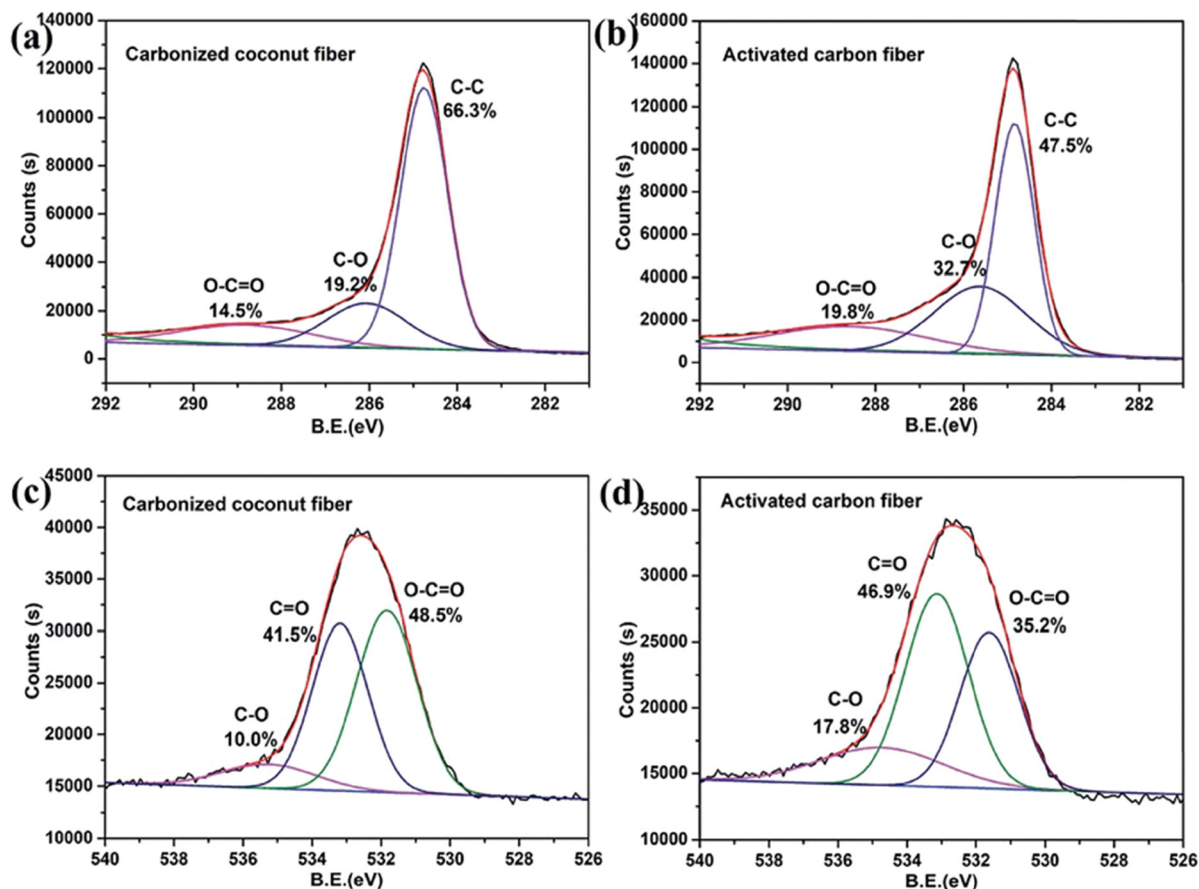

Fig. 10 XPS diagram of C1s and O1s of carbonized coconut fibres and activated carbon fibres. (a) and (b) are the C1s XPS spectra and (c) and (d) are the O1s XPS spectra of the two samples[100] (reproduced under Creative Commons Attribution-NonCommercial 3.0 Unported Licence).

hand, XPS analysis of activated carbon describes the changes in the surface chemistry with the activation process. When compared to the biomass precursor, the activated carbon displayed a higher carbon content with reduced oxygen functionalities during activation. XPS can determine the changes in the elemental composition and functional groups, thus providing significant information about the structure–property relationships of derived activated carbon and its suitability for applications such as adsorption or catalysis.[40] Gale *et al.* explored the elemental analysis and effect of pyrolysis temperature on the oxygen-containing functional groups of biochar materials, prior to and after activation with KOH. The XPS analysis revealed that the activation process results in decreased C–O content of the biochars and activated carbons.[10] Zhang *et al.* compared the elemental compositions of carbonized coconut fibres and the activated carbon prepared after KOH treatment. The KOH activation of coconut fibres results in an increase in oxygen-containing functionalities[100] (Fig. 10).

5. Mechanism involved in contaminant removal

The mechanism of contaminant removal in biomass and its derived materials mainly involves the adsorption process,

wherein the contaminants are physically or chemically bound to the surface of the biomass adsorbents. In biomass, the porous structure and surface functional groups facilitate the adsorption of contaminants from water or air onto the surface through electrostatic forces, van der Waals interactions, or chemical bonding, thus effectively removing them from the surrounding medium.[101] The activated carbons, derived from carbonaceous biomass, possess an extensive surface area and a high degree of microporosity, which enhances their adsorption capacities.[84] Further, the functionalities present on the surface of biomass and its activated carbons may undergo chemical reactions with certain contaminants, or help in the activation of certain oxidizing agents for further aiding in their removal.[102] In this section, a general discussion on the various mechanisms involved in the contaminant removal process by biomass and derived materials has been performed.

5.1. Adsorptive removal

The adsorption mechanism with biomass involves the adherence of contaminant molecules or ions from aqueous solution onto the surface of a solid substrate. When biomass is used as the substrate, its porous structure provides ample surface area for the adsorption to occur.[11] Biomass can be modified to enhance its adsorption properties by treating it with acids or

bases, which can alter its surface chemistry and increase its affinity for specific pollutants or molecules. The acid-modified biomass tends to increase the number of surface acidic functional groups, while base-modified biomass increases basic functional groups, thereby enhancing adsorption capabilities. Materials derived from biomass, such as biochar and activated carbon, exhibit excellent adsorption potential due to their high surface area and porous structure.[28] Biochar, a carbon-rich material obtained from the pyrolysis of biomass, possesses a stable structure and a high surface area and porosity derived from pyrolysis and enhances absorption through π–π interactions and hydrogen bonding, particularly effective for organic pollutants. Activated carbon, produced by the activation of carbonaceous materials, undergoes additional processing to create a highly porous structure with active functional groups, which enhance adsorption properties. Activated carbon, with its extensive microporous and mesoporous structure, facilitates multilayer adsorption through van der Waals forces, π–π interactions, and electrostatic attraction.[101] Understanding these surface mechanisms is crucial for optimizing the design of adsorbents and advancing wastewater treatment technologies for effective contaminant removal. Tran *et al.* suggested the adsorptive removal of paracetamol (PRC), a pharmaceutical contaminant, from the surface of biochar with included pore-filling, Yoshida hydrogen bonding, dipole–dipole interactions, van der Waals forces, and π–π interactions[102] (Fig. 11).

Vo *et al.* investigated the removal mechanism of Cr(VI) onto biochar and activated carbon. The Cr(VI) removal predominantly relies on the adsorption-coupled reduction, whereby the Cr(VI) ions are partially reduced to Cr(III) ions during the adsorption process. The process of chromium adsorption on

biochar and activated carbon is multifaceted, driven primarily by electrostatic forces that attract Cr(III) ions to the surface. This attraction encompasses several mechanisms, including complexation, Cπ–cation interaction, cation exchange, and pore filling[103] (Fig. 12).

5.2. Degradative removal

Biomass-derived materials and nanocomposites offer another promising feature as catalysts in the advanced oxidation processes (AOPs). These materials efficiently generate a spectrum of reactive oxygen species (ROS), including sulfate radicals ($SO_4^{\bullet-}$), hydroxyl radicals ($^{\bullet}OH$), superoxide radicals ($O_2^{\bullet-}$), and singlet oxygen ($^1O_2$), through mechanisms such as Fenton-like reactions or single electron transfer processes.[17] These highly reactive oxygen species play a primary role in the oxidative degradation of diverse recalcitrant contaminants.[40] Further, the surface functional groups present in the biomass-derived materials, such as biochar and activated carbons or immobilized metals, serve as activators for various oxidizing agents like persulfate (PS), peroxymonosulfate (PMS), and hydrogen peroxide (H_2O_2), promoting the generation of radical species and thereby enhancing the oxidative degradation process.[78]

Tang *et al.* investigated two possible pathways involving radical and non-radical processes for the degradation of tetracycline (TC) in the FeO$_x$@N-BC/PMS system (Fig. 13). The N-biochar contains surface graphite N and pyridine N, which increases the electron density and hence facilitates the PMS decomposition by the generation of $^1O_2$ (eqn (1)). Further, the electron pair of pyridine N transfers π-electrons to PMS to generate $SO_4^{\bullet-}$ and $^{\bullet}OH$ (eqn (2) and (3)). The FeO$_x$
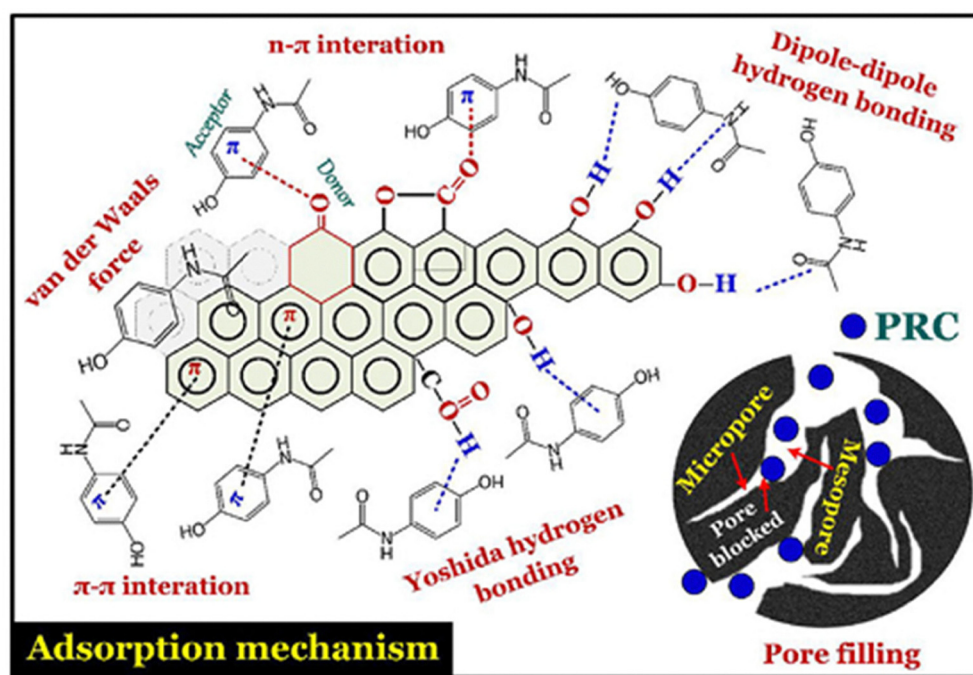

Fig. 11 The schematic of the mechanism of adsorptive removal of paracetamol onto biochar[102] (reproduced with permission, Elsevier, 2020).
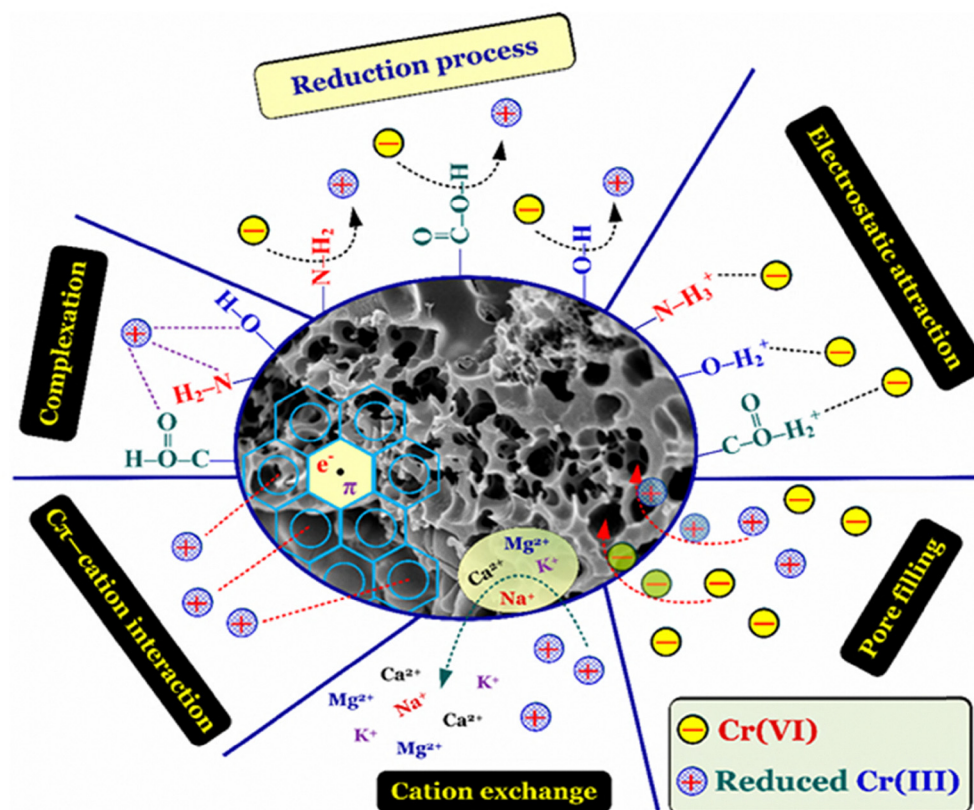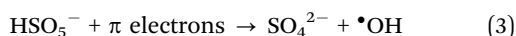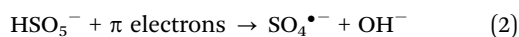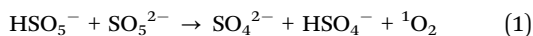
© 2025 The Author(s). Published by the Royal Society of Chemistry

Fig. 12 The schematic of reductive adsorption of Cr(VI) onto biochar and activated carbon[103] (reproduced under Creative Commons Attribution (CC BY) license **https://creativecommons.org/licenses/by/4.0/**).

nanoparticle on the surface of the biochar also activates PMS to generate various reactive species (eqn (4)–(8)). These reactive oxygen species collectively contribute to the degradation of TC in the FeO$_x$@N-BC/PMS system.[99]

Generation of non-radical oxygen species

$$HSO_5^- + SO_5^{2-} \rightarrow SO_4^{2-} + HSO_4^- + {}^1O_2 \quad (1)$$

$$HSO_5^- + \pi \text{ electrons} \rightarrow SO_4^{\bullet-} + OH^- \quad (2)$$

$$HSO_5^- + \pi \text{ electrons} \rightarrow SO_4^{2-} + {}^\bullet OH \quad (3)$$

Generation of radical oxygen species:

$$Fe^0 + O_2 + H^+ \rightarrow Fe^{2+} + H_2O_2 \quad (4)$$

$$Fe^{2+} + HSO_5^- \rightarrow Fe^{3+} + SO_4^{\bullet-} + OH^- \quad (5)$$

$$Fe^{2+} + H_2O_2 \rightarrow Fe^{3+} + {}^\bullet OH + OH^- \quad (6)$$

$$SO_4^{\bullet-} + H_2O \rightarrow SO_4^{2-} + {}^\bullet OH + H^+ \quad (7)$$

$${}^\bullet OH + H_2O_2 \rightarrow H^+ + O_2^{\bullet-} + H_2O \quad (8)$$
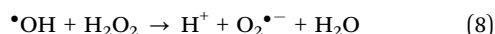
Despite these advances, the catalytic degradation field remains underdeveloped in several aspects. Most current studies emphasize radical-mediated degradation (${}^\bullet OH$ and $SO_4^{\bullet-}$), while non-radical pathways such as ${}^1O_2$ generation, surface-bound electron transfer, and direct oxidation are relatively less explored, despite their potential for greater selectivity and
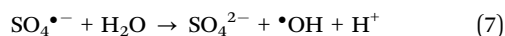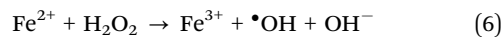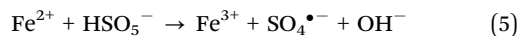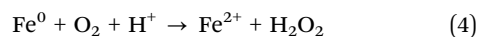
stability under real environmental conditions. In addition, the contribution of redox-active moieties (e.g., quinones, phenolic groups, and graphitic N sites) to catalytic performance remains poorly defined and requires more systematic investigation using advanced in situ spectroscopic and electrochemical techniques. Furthermore, much of the existing research is conducted in simplified laboratory settings, with limited evaluation of catalyst regeneration, long-term stability, or performance in complex wastewater matrices. Addressing these knowledge gaps will be essential for translating biomass-derived catalysts into practical, scalable, and sustainable degradation technologies.

5.3. Synergy between adsorption and degradation mechanisms

In biomass derived nanocomposite materials, the synergy between adsorption efficiencies of biomass derivatives and catalytic efficiencies of metal nanoparticles maximizes the contaminant removal efficiencies. The porous nature of biomass, biochar, and activated carbon in nanocomposites amplifies the surface area, ensuring extensive contact between contaminants and the active sites, where the metal nanoparticle mediated chemical reactions break them down. The synergistic interaction enhances the overall performance of the composite material, leading to improved removal efficiency and degradation rates compared to individual components.
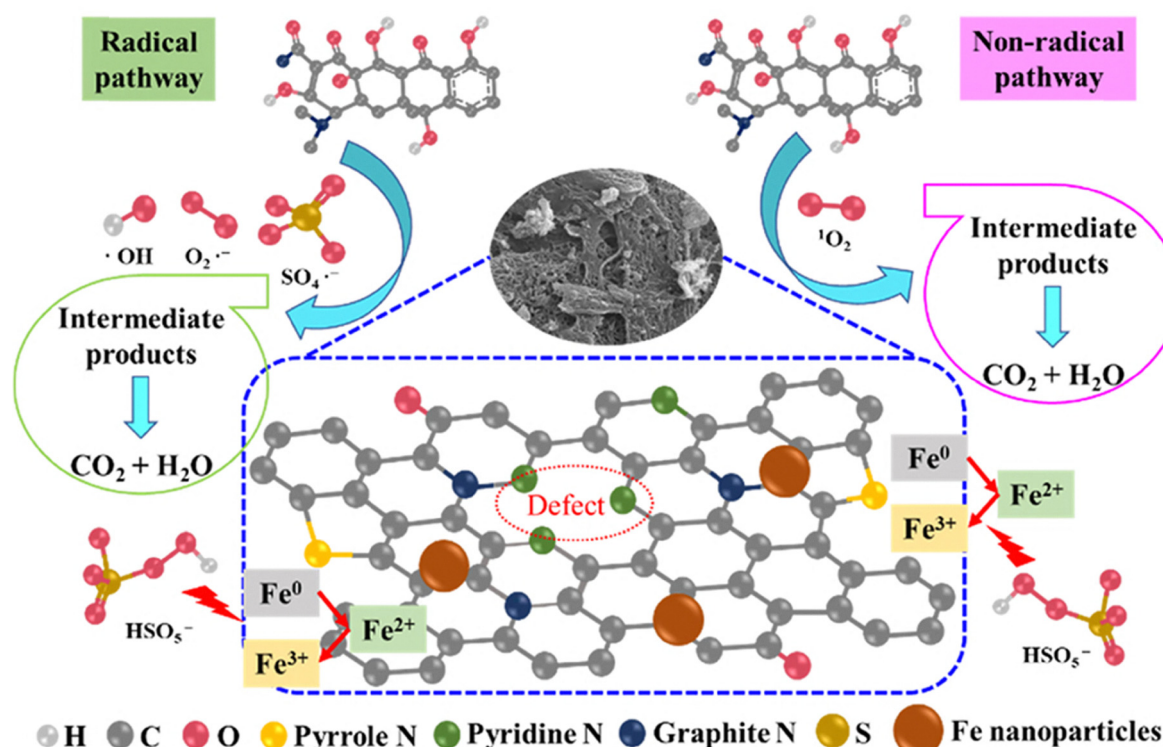
Fig. 13 The mechanism for tetracycline (TC) degradation *via* radical and non-radical pathways in the FeO$_x$@N–BC/PMS system[99] (reproduced with permission, Elsevier, 2023).

Kumar *et al.* investigated the synergistic effect in lignocellulosic biomass and manganese oxide (MnO$_2$) nanoparticles for the removal of crystal violet at a range of pH[88] values (Fig. 14).

6. Environmental remediation application of biomass and its surface modified derivative

Biomass and its surface-modified derivatives find extensive application in environmental remediation processes, serving as versatile and sustainable tools for addressing pollution challenges. Their porous structure, abundant surface functional groups, and diverse chemical compositions make them effective adsorbents for a wide range of contaminants in soil, water, and air. The surface modification techniques, such as chemical activation or carbonization and impregnation with metal nanoparticles, further enhance their adsorption capacity, selectivity, and reusability. These modified biomass materials exhibit improved performance in removing heavy metals, organic pollutants, and even emerging contaminants like pharmaceuticals and personal care products (PPCPs). Further, the biomass-based materials can be utilized in the catalytic degradation of pollutants through advanced oxidation processes, *via* exploiting their catalytic activity and reactive surface sites. In this review section, we will explore the environmental remediation applications, beginning with raw biomass and advancing to surface-modified biomass derivatives and metal-

immobilized nanocomposites. Throughout this discussion, we will examine the diverse mechanisms employed for the removal of various organic/inorganic contaminants.

6.1 Raw biomass as an environmental remediation agent

Raw biomass holds immense potential as an environmental remediation agent due to its ease of availability and eco-friendly nature (Table S1). Its properties, including high surface area and diverse surface functionalities, enable effective adsorption of contaminants from various environmental sources. Further, the biodegradable nature of these raw biomasses ensures a minimal environmental impact.[12]

6.1.1. Organic contaminant removal. The removal of organic pollutants, including pharmaceutical drugs and dyes, is a critical challenge due to their widespread presence and the detrimental effects on the ecosystems as well as human health. The dyes and the pharmaceutical drugs are often introduced into water bodies through wastewater discharge or improper disposal, which can lead to antibiotic resistance, disrupt endocrine systems, and cause adverse health effects in aquatic organisms and humans. Biomass-based remediation approaches emerge as promising strategies in addressing these issues.

Perez-Millan *et al.* studied the removal of reactive blue 19 (RB19) and basic blue 3 (BB3) dyes from water using coconut endocarp (CE) and sugarcane bagasse (SB). The DFT modelling and characterization reveal that the sulfonate group of these dye molecules and the nitrogen present in the phenoxazine
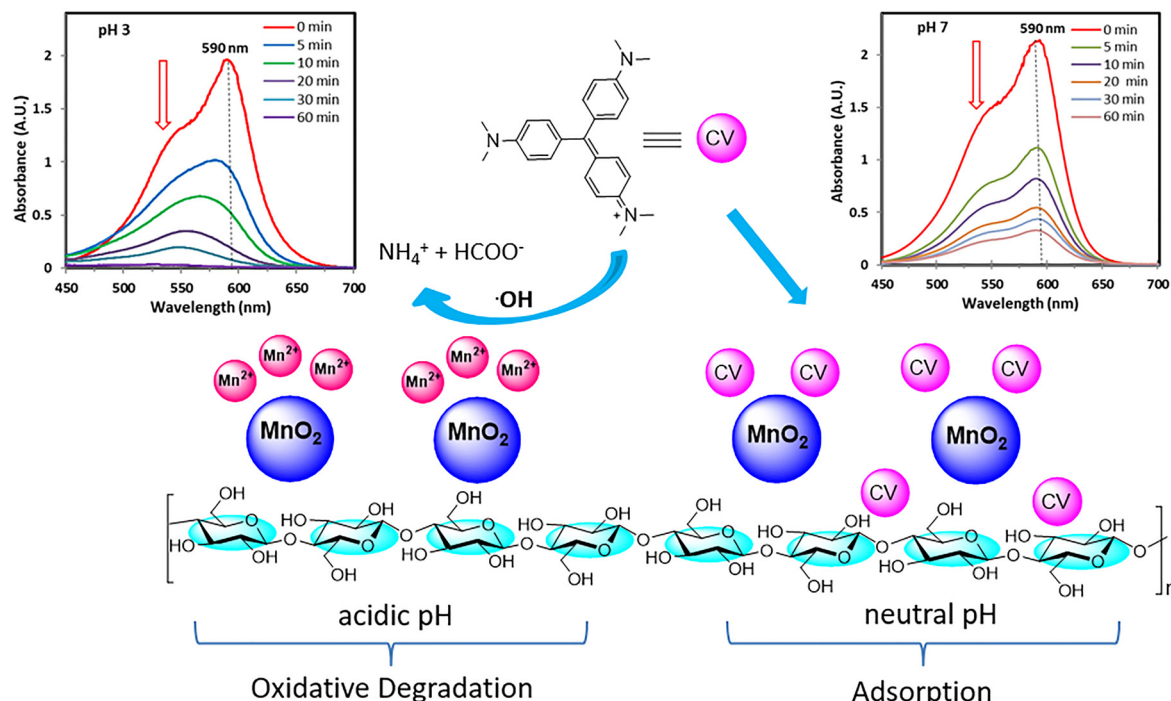
Fig. 14 Synergistic effect originating from the surface adsorptive removal with pistachio biomass (PS), and oxidative degradation with MnO_2 nanoparticles in the MnO_2@PS nanocomposite[88] (reproduced with permission, Springer Nature, 2023).

were found to be the highly reactive areas to interact with the hydroxyl and carboxyl groups of the biomass surface.[104] Kaur *et al.* performed a study on the adsorption of methylene blue dye onto rice husk biomass. The Redlich–Peterson isotherm provides the best fit of adsorption equilibrium data, indicating multilayer adsorption with a non-uniform distribution of adsorption heat and affinities over a heterogeneous surface.[51] The maximum monolayer adsorption capacity was found to be 71.28 mg g^{-1}. The best correlation of kinetics results with pseudo-second-order kinetic models suggests a chemical adsorption process. Kaur *et al.* further explored the utilization of cotton shell (CS) biomass for the adsorption of terbinafine hydrochloride (TBH). The adsorption efficiency of cotton shell biomass for TBH was 47.2 mg g^{-1} under optimal experimental conditions.[105] Yardimici *et al.* investigated the adsorption of methylene blue using cinnamon bark biomass (CB). The best fitting of adsorption data using the Langmuir isotherm shows the monolayer maximum adsorption capacity of 123.25 mg g^{-1}. The experimental results also suggested the adsorption process to be of physical nature.[106] Al-Mokhalelati *et al.* evaluated the adsorption efficiency of sugarcane bagasse for the removal of methylene blue (MB) dye. The best correlation of Langmuir isotherms and Halsey adsorption isotherms with equilibrium data indicates the favourability of multilayer sorption. The thermodynamics study reveals that the adsorption process is spontaneous and endothermic in nature.[107] Tang *et al.* investigated the methylene blue (MB) removal efficiency of walnut-shell biomass. The adsorption of MB onto walnut shell biomass was chemical in nature, as described using the Dubinin–

Radushkevich isotherm model and pseudo-second-order kinetic model. The thermodynamic data indicated that the adsorption was favourable, spontaneous, and exothermic in nature.[108] Uddin *et al.* used mango leaf biomass for the adsorption of MB dye. The Langmuir isotherm describes the best fitting for the experimental equilibrium data with a maximum monolayer adsorption capacity of 156 mg g^{-1}. Further, the removal of MB with mango leaf biomass follows a pseudo-second order kinetics.[109] Deng *et al.* determined the effect of cotton stalk biomass (CS) for the removal of methylene blue dye (MB). The equilibrium adsorption efficiency of methylene blue (MB) onto the cotton shell reached 147.06 mg g^{-1} under optimal experimental conditions. The equilibrium adsorption and kinetics data were best fitted with Langmuir and pseudo-second order models, respectively.[110] Ertas *et al.* studied methylene blue (MB) adsorption using cotton waste (CW), cotton stalk (CS), and cotton dust (CD). The cotton dust was the most effective in MB removal. The CS adsorption data fit both Freundlich ($R^2 = 0.967$) and Langmuir ($R^2 = 0.997$) isotherms, while CW and CD fit Freundlich. The thermodynamic parameters showed positive $\Delta G°$ for CS and negative for CW and CD, with positive $\Delta H°$ and $\Delta S°$ for all sorbents.[111]

6.1.2. Inorganic contaminant removal. Inorganic contamination, particularly heavy metals, poses a significant threat to environmental and human health due to their persistence and toxicity. The biomass can effectively remove heavy metals from aqueous solutions due to its metal-binding capabilities through processes such as adsorption, precipitation, or ion exchange. These eco-friendly approaches not only mitigate pollution, but

also offer a sustainable means of metal recovery and recycling, contributing to both environmental remediation and resource conservation efforts.[112]

Kebir *et al.* studied chromate adsorption onto red peanut skin (RPS) in a fixed-bed column. The optimal conditions were 100 mg L^{-1} Cr(VI) concentration and a 10 cm bed height, with high column adsorption capacity. The Bohart–Adams model ($R^2 > 0.98$) indicated surface diffusion as the rate-limiting step. The RPS demonstrated a Cr(VI) removal capacity of 26.23 mg g^{-1} at pH 5.35, with electrostatic interactions being crucial in the adsorption process.[113] Mahmood-ul-Hassan *et al.* studied heavy metal adsorption (Cd, Cr, and Pb) using banana stalks, corn cob, and sunflower achene. The Langmuir model showed that banana stalks had the highest Pb adsorption (21–60 mg g^{-1}), with the order of sorption capacities being Pb > Cr > Cd.[114] Akram *et al.* used cotton shell biomass for lead (Pb) removal from wastewater, achieving up to 90% efficiency in 90 min with a 1000 mg L^{-1} dose and 1 mg L^{-1} Pb concentration. The Freundlich isotherm model best describes Pb sorption. The SEM analysis revealed a microporous structure with a 45 m^2 g^{-1} BET surface area and 2.3 mm pore size, involving complexation and ion exchange mechanisms.[115] Ye *et al.* studied the adsorptive removal of cadmium (Cd) with rice husk biomass. The equilibrium adsorption data were best fit with the Langmuir isotherm with a Cd(II) adsorption capacity of 73.96 mg g^{-1} at pH 6.5.[53] Cao *et al.* used wheat straw biomass for the adsorptive removal of lead from wastewater. The results indicate that the Pb(II) adsorption capacity at an adsorbent dosage of 0.2 g L^{-1} onto wheat straw biomass was 46.33 mg g^{-1}. The adsorption mechanism involves processes such as ion exchange and precipitation.[50] Banerjee and coworkers investigated the adsorption of Cr(VI) onto a pistachio shell with a fixed bed column. The experimental results indicate that adsorption capacity increases with increase in column bed depth.[116] Ezeonuegbu *et al.* studied sugarcane bagasse for Pb(II) and Ni(II) removal from untreated wastewater. The Freundlich and pseudo-second order models best describe the adsorption isotherms and kinetics for Pb(II) and Ni(II), with capacities of 1.61 mg g^{-1} and 123.46 mg g^{-1}, respectively.[117] Varsihini *et al.* investigated cerium(III) biosorption using prawn carapace (PC) and corn style (CS). The maximum adsorption capacities were 218.3 mg g^{-1} for PC and 180.2 mg g^{-1} for CS. The Freundlich and Langmuir models best fit PC and CS data, respectively, with physisorption indicated and the process found to be endothermic and spontaneous.[118]

6.2 Surface modified biomass as an environmental remediation agent

Surface modification of raw biomass *via* physical, chemical or physicochemical activation processes results in increased removal efficiencies of the biomass. This section of the review will discuss the environmental remediation applications of surface modified biomass with special emphasis on the mechanistic aspects and methodologies used for evaluating the enhanced surface efficacies (Table S2).

6.2.1. Physically modified biomass. Physical modification of biomass includes its conversion to biochar or hydrochar. This conversion process involves various physical modifications such as pyrolysis, size reduction, hydrothermal treatment, *etc.*, intended to improve the quality of the resulting biochar or hydrochar such as surface area, density, stability and purity, and thus to enhance the efficiency of the contaminant removal process.[24] This part of review discusses various literature reports on the use of physically modified biomass for environmental contaminant removal.

Ju *et al.* explored the use of biochar derived from tobacco stalks for removing sulfamethazine (SMT) through a dual approach of adsorption and degradation. The characterization revealed that this biochar had a porous structure with a high specific surface area of 905.6 m^2 g^{-1} and active functional groups on its surface. These features significantly enhanced SMT removal, facilitated by the generation of hydroxyl radicals (•OH) observed in the EPR spectrum, which played a crucial role in the degradation of SMT.[42] Dias *et al.* examined biochars made from pine nut shells for adsorbing methylene blue (MB) dye. They found that pyrolysis temperature influenced the thermal stability and weight loss of the biochar, with remaining mass percentages of 78%, 45%, 41%, 36%, and 32% at temperatures of 221 °C, 309 °C, 350 °C, 420 °C, and 488 °C, respectively. Adsorption experiments showed that biochar produced at lower pyrolysis temperatures had higher removal efficiency, achieving up to 53.9 mg g^{-1}.[119] Liu *et al.* studied shiitake mushroom bran biochar prepared at various pyrolysis temperatures (300 °C, 500 °C, and 700 °C) for tetracycline removal. The research revealed that the surface chemistry of the biochar varied with temperature. The adsorption data for BC300 and BC500 fit the Langmuir isotherm, indicating monolayer adsorption, while BC700 fit the Freundlich isotherm, suggesting heterogeneous adsorption. The kinetic studies indicated that the pseudo second-order model best described the adsorption, signifying chemisorption across all biochar.[43] Qin *et al.* assessed biochar from rape straw, activated with KOH, for tetracycline (TC) removal. This biochar had a specific surface area of 1531 m^2 g^{-1}, abundant oxygen-containing functional groups, and a graphite-like structure. The adsorption data matched both pseudo second-order kinetics and the Freundlich isotherm, indicating a chemisorption process and heterogeneous adsorption. The thermodynamic analysis showed that TC adsorption was spontaneous and endothermic, with hydrogen bonding, electrostatic interactions, and pi–pi interactions contributing to the adsorption mechanism.[44] Tomczyk *et al.* investigated tetracycline removal using sunflower biomass-derived biochar, modified with vitamin C, hydrogen peroxide, and silver nanoparticles. Although modifications decreased the biochar's surface area and pore volume, they increased the presence of acidic and basic functional groups, enhancing electrostatic interactions with tetracycline. The vitamin C-modified biochar demonstrated superior adsorption efficiency compared to other modifications.[45] Chen *et al.* studied tannic acid-modified rice straw biochar for tetracycline removal. The modification increased oxygen-containing

functions on the biochar surface, improving adsorption capacity. Adsorption followed the Freundlich and Elovich models, suggesting physisorption through electrostatic interactions, pi–pi interactions, and hydrogen bonding.[46] Hoslet et al. analysed biochar from food and plant waste for tetracycline removal. Produced via pyrolysis at 300 °C, the biochar achieved an adsorption capacity of 9.45 mg g^{-1} for tetracycline. The kinetic and isotherm models indicated an Elovich kinetics and Freundlich isotherm, reflecting a combination of chemisorption and heterogeneous adsorption.[47] Zhang et al. investigated cow manure biochar for tetracycline removal. Biochar produced at 300 °C, 500 °C, and 700 °C showed differences in surface area, charge, and pore volume. The adsorption mechanism involved electrostatic interactions, hydrogen bonding, pore filling, and pi–pi interactions. Freundlich and pseudo-second-order kinetics models best described the adsorption, suggesting heterogeneous surface properties and chemical adsorption.[48] Chen et al. evaluated the biochar from pomelo peels, activated with KOH, for carbamazepine removal. Characterization indicated that activation temperature affected biochar morphology. Adsorption data fit the pseudo-second-order kinetics and Langmuir isotherm models, suggesting physisorption through intraparticle diffusion. Thermodynamic analysis showed that the adsorption process was spontaneous and exothermic.[49]

Cao and colleagues studied the adsorption of Pb(II) using different wheat straw-based materials: acid-modified wheat straw (WS), wheat straw biochar (WS-BC), and ball-milled wheat straw biochar (WS-BC + BM). They found that pyrolysis and ball milling significantly enhanced Pb(II) removal, with capacities of 46.33 mg L^{-1} for WS, 119.55 mg L^{-1} for WS-BC, and 134.68 mg L^{-1} for WS-BC + BM. Pb(II) removal was primarily driven by ion exchange, precipitation, and complexation with acid functional groups (AFGs). The carbonization and ball milling improved ion exchange and precipitation, but high adsorbent concentrations led to competition between these mechanisms. Further, the acid modification increased Pb(II) complexation, as indicated by FTIR peak shifts showing changes in AFG bond energies.[50]

6.2.2. Chemically modified biomass. Chemical modification of biomass involves changing its chemical composition through various chemical treatments to improve its properties, typically focusing on increasing surface area or porosity. Chemical activation of biomass can involve agents such as mineral acids and oxidants, including HNO_3, H_2O_2, $HClO$, H_2SO_4, H_3PO_4, and HCl, as well as alkalis like $NaOH$, KOH, $LiOH$, Na_2SiO_3, Na_2CO_3, and various oxides. Depending on the type of reagent used, the surface of the biomass may develop either positive or negative charges and thus can be used for the remediation of target contaminants. This section of the review provides a summary of the literature on chemically activated biomass and its applications in environmental remediation.

Kaur et al. studied how varying sodium hydroxide (NaOH) treatment parameters affects the efficiency of rice husk in adsorbing methylene blue (MB) from water. NaOH-treated rice husks were prepared by adjusting NaOH concentration, treatment time, and temperature. The results showed that the higher NaOH concentration, longer treatment duration, and increased temperature improved the adsorption process. The maximum monolayer adsorption capacity for NaOH-treated rice husk was 123.39 mg g^{-1}, compared to 71.28 mg g^{-1} for untreated husk.[51] Yang et al. developed porous biosorbents from hickory wood using a one-step ball milling process with acidic or alkaline treatments. These modifications enhanced the biomass's oxygen-containing functional groups, porous structure, and capacity to remove crystal violet (CV, 476.4 mg g^{-1}) and Congo red (CR, 221.8 mg g^{-1}) dyes from water at neutral pH. The adsorption followed Freundlich isotherm and pseudo second-order kinetic models, indicating surface complexation.[120] Jiang et al. created activated carbon from seaweed biomass (SWAC) via NaOH activation for methylene blue removal, achieving a high specific surface area of 1238.491 mg g^{-1} and a 98.56% MB removal efficiency at 30 °C and pH 5. The high adsorption capacity is linked to graphitic N sites and interactions such as π–π stacking and electrostatic forces.[52] Homagai et al. evaluated chemically modified rice husks for crystal violet removal, finding adsorption capacities of 62.85 mg g^{-1} for charred rice husk and 90.02 mg g^{-1} for xanthate rice husk at pH 10.[121] Al-Mokhalelati et al. examined the sugarcane bagasse (SB) before and after alkaline treatment and observed temperature-dependent MB adsorption increase.[107] Deng et al. examined cotton stalk (CS), cotton stalk treated with sulphuric acid (SCS), and cotton stalk treated with phosphoric acid (PCS) for their effectiveness in removing methylene blue (MB) from aqueous solutions. The study revealed that the porosity of activated materials can be easily regulated by employing different activation agents. The initial pH of the aqueous solution minimally influenced the adsorption capacity of both SCS and PCS, whereas it significantly affected the removal efficiency of CS. The MB adsorption capacity followed the order of SCS > PCS > CS.[110]

Mahmood et al. evaluated the adsorption effectiveness of unmodified and chemically modified banana stalks, corn cobs, and sunflower achenes for cadmium (Cd), chromium (Cr), and lead (Pb) in wastewater. The modifications involved treating the agricultural wastes with sodium hydroxide (NaOH) combined with nitric acid (HNO_3) and sulfuric acid (H_2SO_4) to boost their adsorption capabilities. The results showed that NaOH-modified materials had better adsorption capacity than those modified with acids. The highest adsorption capacities were observed in the order of Pb > Cr > Cd. The enhancement in Pb adsorption capacity was most significant in banana stalks (117%) and corn cobs (62%), while sunflower achenes showed only a 34% increase, possibly due to their higher lignin content. This suggests that chemical modification improved adsorption through increased active binding sites and new functional groups.[114] Ye et al. tested natural and alkali-modified rice husks for Cd(II) removal. The modified rice husks showed enhanced Cd(II) adsorption (125.94 mg g^{-1}) compared to natural rice husks (73.96 mg g^{-1}) due to structural changes from alkali treatment.[53] Yardımcı and Kanmaz studied the use of waste cinnamon bark biomass (CB) and manganese dioxide-immobilized CB (MnO$_2$@CB) for methylene blue (MB) dye

removal. MnO$_2$@CB with a higher surface area (145.2 m^2 g^{-1}) compared to CB (45.59 m^2 g^{-1}) demonstrated better adsorption capacity. The Langmuir isotherm best fitted CB data, while MnO$_2$@CB followed the Freundlich isotherm, with both adsorbents showing kinetics best described by the pseudo-second-order model.[106]

6.2.3. Physico-chemically modified biomass. Physico-chemical modification of biomass involves a combination of physical and chemical treatment processes. The modification led to changes in biomass properties such as increased surface area, enhanced reactivity, improved stability, or altered chemical composition.[10] This section of the review discusses literature on physico-chemically modified biomass and its applications in various environmental remediation efforts.

6.2.3.1. Organic contaminant removal. Yurtay and Kılıç investigated the production of activated carbon (AC) from agricultural residues such as hazelnut shells (HS), rice husks (RH), and corn stalks (CS) using chemical activation with potassium hydroxide (KOH) and carbonization at 950 °C. This study aimed to explore the effectiveness of these ACs in removing metronidazole from aqueous solutions. The BET analysis revealed significant improvements in surface area of hazelnut shell AC (1650 m^2 g^{-1}), rice husk AC (2573 m^2 g^{-1}), and corn stalk AC (2304 m^2 g^{-1}) due to chemical activation. The adsorption isotherms showed that both HS-AC and RH-AC best fit the Langmuir model, while CS-AC was best described by the Freundlich model. The kinetic studies indicated that the pseudo-second-order model was the most accurate for metronidazole adsorption. Thermodynamic analysis confirmed that the adsorption process was exothermic and spontaneous.[54] Bouzidi *et al.* examined the adsorption of ibuprofen (IBP) and paracetamol (PCM) using activated carbon derived from *Erythrina speciosa* tree pods activated with zinc chloride (ZnCl$_2$). The AC displayed a high BET surface area of 795.1 m^2 g^{-1}. The double-layer model (DLM) suggested multi-molecular adsorption for both IBP and PCM, indicating the simultaneous accommodation of each functional group on the adsorbent's surface. The energy evaluation indicated that the adsorption was predominantly physical.[55] Astuti *et al.* developed activated carbon from pineapple leaves, cocoa shells, and coconut shells using microwave heating and ZnCl$_2$ activation. This method created a template effect that resulted in uniformly distributed pores. The specific surface area and porosity were enhanced, with the average pore sizes being 2.41 nm for coconut shell AC, 1.75 nm for cocoa shell AC, and 1.79 nm for pineapple crown leaf AC. All four activated carbons showed the best fit with the Langmuir isotherm for methyl violet adsorption.[122] Kandasamy and colleagues evaluated the effectiveness of carbons derived from goat and sheep dung, activated with KOH and ZnCl$_2$ using a hydrothermal method, for methylene blue dye removal. The KOH-activated carbon from goat dung achieved a 99.6% removal rate with a maximum adsorption capacity of 24.81 mg g^{-1}. Adsorption equilibrium data best fit the Freundlich model for ZnCl$_2$-activated carbon, the Langmuir model for KOH-activated carbon, and the Dubinin–Radushkevich model for hydrothermally carbonized carbon. The pseudo-second-order model described the kinetic data well, indicating a chemisorption process.[56] Cui *et al.* employed a bamboo-derived activated carbon aerogel (BACA) for tetracycline hydrochloride (TCH) removal. Synthesized through KOH activation of a bamboo cellulose aerogel, BACA demonstrated a strong fit with the Langmuir isotherm and pseudo-second-order kinetics, indicating monolayer adsorption and chemisorption. Thermodynamic analysis suggested that the adsorption process was spontaneous and endothermic.[57]

Al Sarjidi *et al.* explored the removal of various emerging pollutants such as diclofenac, amoxicillin, carbamazepine, and ciprofloxacin using activated carbon derived from pomegranate peels, with laccase immobilization (LMPP). When compared to unloaded pomegranate peel-derived AC (MPP), LMPP demonstrated superior pollutant removal efficiency. The adsorption process followed the Langmuir isotherm and first-order kinetics, also characterized as spontaneous and endothermic.[123] Zhang *et al.* synthesized amorphous activated carbon from sesame straw using KOH and Ca(OH)$_2$ co-activation. The activated carbon exhibited a surface area of 935 m^2 g^{-1} and high adsorption capacities for ofloxacin, ciprofloxacin, and enrofloxacin. The kinetic and adsorption data indicated heterogeneous and multilayer adsorption, with the pseudo-second-order and Sips models providing the best fits. The DFT calculations revealed hydrogen bonding, electrostatic interactions, and π–π interactions as key mechanisms in drug removal.[58] Srinivasan *et al.* evaluated activated carbon from *Thevetia neriifolia* Juss wood for adsorbing direct orange 102 dye (DO102). The adsorption capacity increased with temperature, suggesting an endothermic process. The pseudo-second-order model provided a more accurate fit compared to the pseudo-first-order model, and the Langmuir model best described the adsorption with capacities ranging from 9.44 mg g^{-1} to 33 mg g^{-1}.[60] Yusop *et al.* studied the adsorptive removal of methylene blue using activated carbon derived from Acacia wood (AWAC). The AWAC exhibited a BET surface area of 1045.56 m^2 g^{-1} and a mesopore surface area of 689.77 m^2 g^{-1}. The adsorption followed the Langmuir isotherm and pseudo-second-order kinetics, with film diffusion being the main process. The Langmuir monolayer capacity was 338.29 mg g^{-1}, and the process was exothermic.[60] Piriya and colleagues investigated malachite green adsorption on zinc chloride-activated carbon from coconut. The activation process increased surface area to 544.66 m^2 g^{-1} and adsorption capacity to 39.683 mg g^{-1}. The Freundlich isotherm and intraparticle diffusion model best described the data. The coconut shell AC showed effective dye removal from industrial effluents, suggesting it as a viable alternative to commercial activated carbon.[41]

Baloo *et al.* compared activated carbons from empty fruit bunches (EFB) and mesocarp fibers (MF) of oil palm for removing methylene blue (MB) and Acid Orange 10 (AO10). The MF AC had a higher BET surface area (552.7222 m^2 g^{-1}) compared to EFB (35.6328 m^2 g^{-1}). The adsorption of dyes followed the pseudo-second-order kinetic model, with the Langmuir model better representing MB adsorption for

MF.[124] Abatal *et al.* created a carbonaceous material from *Haematoxylum campechianum* bark using phosphoric acid activation and thermal treatment at 500 °C. This material, with a mixed graphitized/amorphous phase, showed high adsorption capacities for phenol, 4-chlorophenol, and 4-nitrophenol. The Langmuir model provided the best fit, with a maximum phenol adsorption capacity of 94.09 mg g^{-1}.[61] Geczo *et al.* derived activated carbon from cashew nut shells using H_3PO_4 activation. The study highlighted the importance of acidic groups in acetaminophen removal, showing that highly acidic groups facilitated hydrolysis while lower concentrations led to physisorption.[33] Yang *et al.* utilized one-step H_3PO_4 activation to produce porous carbon from corn straw for tetracycline removal. The AC showed a high surface area of 463.89 m^2 g^{-1} and demonstrated excellent adsorption performance. Both pseudo-second-order and Langmuir models fit the data well, with the process being endothermic and spontaneous.[34] Abo El Naga *et al.* examined sugar cane bagasse-derived activated carbon (SCG-AC) for diclofenac sodium removal. The SCG-AC, produced *via* $ZnCl_2$ activation, showed good fits with the Langmuir and pseudo-second-order models. The pH influenced the adsorption mechanism, with hydrophobic interactions dominating at low pH and electrostatic/hydrogen bonding at moderate pH.[62]

El Mouchtari *et al.* developed a bio-composite material for removing pharmaceuticals from water. This composite, combining activated carbon from *Argania Spinosa* nutshells and commercial TiO_2, demonstrated high efficacy for diclofenac, carbamazepine, and sulfamethoxazole removal through adsorption and photodegradation.[125] Darweesh and Ahmed synthesized granular activated carbon from *Phoenix dactylifera* L. stones using microwave-assisted KOH activation. This material exhibited a high levofloxacin adsorption capacity of 100.38 mg g^{-1}. The adsorption process was influenced by initial levofloxacin concentration and flow rate, with the Thomas and Yoon–Nelson models providing better fits than Adams-Bohart.[126] Jung *et al.* produced granular activated carbon from spent coffee grounds using calcium-alginate beads. This material effectively removed acid orange 7 (AO7) and methylene blue (MB) from water, with adsorption controlled by pore diffusion. The carbon showed high capacity and was effective in both environmental and economic terms.[127]

6.2.3.2. Inorganic contaminant removal. Elewa and colleagues studied activated carbons (AC) from rice husk for removing Fe(III) and Mn(II) from aqueous solutions. The AC was produced at 700 °C in an electric furnace with activation with NaOH (AC-1), acetic acid (AC-2), phosphoric acid (AC-3), and without chemical activation (AC-4). The AC-4 showed superior efficiency compared to the other. The adsorption followed pseudo-second-order kinetics and Langmuir isotherm, with an endothermic process.[128] Huang *et al.* prepared N, P co-doped activated carbon from cabbage waste using H_3PO_4 activation *via* a hydrothermal method. The carbon, with a high BET surface area (1400 m^2 g^{-1}), showed over 97.5% efficiency in adsorbing antibiotics within 10 min, with adsorption being a

chemical process.[63] Neolaka and colleagues synthesized an activated carbon mesopore adsorbent (ACMA) from Kesambi wood for Pb(II) removal. The characterization analysis confirmed the presence of oxygenated functional groups with carbon and oxygen as predominant elements, a rough surface with amorphous structure, low crystallinity, and mesoporous size. The adsorption followed the pseudo second-order model and Langmuir isotherm signifying a homogeneously energetic adsorbent surface. Thermodynamic studies suggest processes being exothermic and spontaneous.[64] Kharrazi and colleagues studied adsorbent carbons from Elm tree sawdust treated with various chemicals to remove Pb(II) and Cr(VI) from water. Acid treatment enhanced Cr(VI) absorption, while alkali treatment improved Pb(II) adsorption, with a pseudo-second-order model best describing the process. Treatment with $MgCl_2$ resulted in a mesoporous AC capable of absorbing Pb(II) up to 1430 mg g^{-1}.[65] Thompson *et al.* found H_3PO_4-activated biomass (groundnut shell, yam peels, and cassava peels) as a cost-effective alternative for Pb^{2+} removal from wastewater. The process was endothermic, rapid, and best fit the pseudo second-order model. The optimal temperature for ion removal from yam peels and groundnut shells was identified as 60 °C, while temperature exerted no discernible effect on the adsorption process of cassava peels.[66] Wang *et al.* studied Cr(VI) adsorption on coconut shell-derived Granular Activated Carbon (GAC), finding a redox reaction that forms a Cr_2O_3 layer on GAC, limiting Cr(VI) uptake. It was suggested that nanoscale AC or porous nanoscale AC pellets could offer promising solutions for effective Cr(VI) water treatment applications.[129] Salomón–Negrete and colleagues developed avocado-based adsorbents for fluoride removal through pyrolysis, finding that pyrolyzed adsorbents outperformed CO_2-activated ones. Fluoride adsorption was influenced by carbonization temperature and involved silicon-based ligand exchange and electrostatic interactions.[130] Sajjad *et al.* synthesized activated carbon from pistachio wood waste using NH_4NO_3 activation, showing it has a higher surface area with well-developed pores for better Hg^{2+} adsorption than commercial carbon, making it a cost-effective, efficient adsorbent for hazardous metals.[67] Norouzi *et al.* converted Date Press Cake into activated carbon using NaOH, achieving a high surface area (2025.9 m^2 g^{-1}) and Cr(VI) adsorption capacity (282.8 mg g^{-1}), best described by Elovich and Redlich–Peterson models.[68] Gebrewold and colleagues evaluated chemically modified rice husk and corn cob activated carbon for fluoride adsorption. They found that Langmuir and pseudo-second-order models best fit the data, with adsorption influenced by intraparticle and surface diffusion.[69] Vunain *et al.* found that activated carbon from baobab fruit shells, chemically activated with phosphoric acid was more economical compared to commercially available activated carbon, and efficiently removes Cu^{2+} ions from aqueous solution.[70] Thamarai *et al.* investigated Pb(II) removal using physically modified (PMSB) and chemically modified seaweed biosorbents (CMSB). Optimal conditions were 303 K, pH 5.0, and dosages of 2.5 g L^{-1} (PMSB) and 1 g L^{-1} (CMSB), with contact times of 80 and 40 min. Maximum adsorption capacities were 149.8 mg g^{-1} (PMSB)

and 175.5 mg g^{-1} (CMSB).[131] Further, the Cd(II) removal was also compared using CMSB and PMSB. The CMSB (19.682 m^2 g^{-1}) and PMSB (14.803 m^2 g^{-1}) showed optimal adsorption at 303 K, pH 6.0, with dosages of 1 g L^{-1} and 2.5 g L^{-1}. The maximum capacities reached 181.6 mg g^{-1} (PMSB) and 151.2 mg g^{-1} (CMSB), following Langmuir isotherm and pseudo-second-order kinetics.[132]

The free radicals, generated during the charring process, also play a crucial role in biochar's surface chemistry. The surface free radicals can react with certain chemical substances, like hydrogen peroxide and persulfate, thereby facilitating the degradation of organic contaminants.[38] This mechanism, primarily driven by electrochemical analysis, indicates that high-temperature-pyrolysis-derived biochar possesses electron-accepting capabilities mediated by free radicals. The biochar not only facilitates the degradation or transformation of pollutants by serving as a catalyst for electron transfer, but can also directly react with pollutants, significantly impacting their environmental fate. Although a limited relevant literature is available, surface redox-active moieties predominantly contribute to biochar's redox activity. These moieties activate certain oxidants to produce reactive radicals like $^{\bullet}$OH and SO$_4^{\bullet-}$ and can also directly engage with pollutants through non-radical pathways.[99]

Zhou et al. created biochar from α-cellulose and sodium lignosulfonate via microwave pyrolysis, achieving 99.9% oxytetracycline degradation in 15 min. The removal pathway was based on a non-free radical pathway involving ^{1}O$_2$ as the main active species responsible for OTC removal, which was promoted by enriched thiophene S and C=O groups. The enrichment of carbon vacancies further improved the removal of pollutant through direct electron transfer that accelerated the PMS activation.[133] Xu et al. studied poplar flour (PF) and walnut shell flour (WSF) biochar, finding that higher pyrolysis temperatures improved their performance in activating peroxymonosulfate (PMS) for diclofenac (DCF) removal. Poplar biochar (PB) outperformed walnut shell biochar (WSB) due to better porosity, functional groups, and conductivity. The non-radical mechanism, including singlet oxygen (^{1}O$_2$) and electron transfer, was key to DCF degradation.[71] Dong et al. investigated N-doped biochar (N-biochar) from soybean biomass for atrazine removal via enhanced catalytic ozonation. The key factors included delocalized π-electrons and functional groups that generated reactive oxygen species (ROS) like hydroxyl radicals ($^{\bullet}$OH) and singlet oxygen (^{1}O$_2$).[72] Zeng et al. studied plant-based biochar (PBC) for tetracycline (TC) degradation via peroxymonosulfate (PMS) activation, noting a large surface area (725 m^2 g^{-1}) and effective pyrrolic-N in enhancing PMS activation and degrading TC in a non-radical reaction pathway.[134] Hou et al. synthesized graphene/biochar composites for persulfate (PS) activation and phenol degradation, with non-radical pathways and π–π* EDA interactions playing crucial roles.[135] Dai et al. studied periodate-based advanced oxidation for BPA degradation using wheat straw-derived biochar. A metastable C–PI* intermediate was identified as the primary oxidant, with BPA donating electrons. The DFT calculations confirmed strong van der Waals interactions between PI and biochar with an observed synergistic effect, whereby an adsorption takes place on the biochar surface, while the PI facilitates the degradation of BPA.[136] Wang and Chen synthesized a nitrogen-doped biochar from pomelo peel, achieving 95% sulfamethoxazole removal in 30 min via PMS activation, with high activity due to graphitic and pyrrolic N, carbonyl groups, and a large surface area (738 m^2 g^{-1}).[137] Gao et al. investigated BPA degradation using ferric chloride-modified rice husk biochar activated by PMS. With 1.0 g L^{-1} catalyst and 1.6 g L^{-1} PMS, over 97% of 20 mg L^{-1} BPA was removed in 150 min, involving SO$_4^{\bullet-}$, $^{\bullet}$OH, O$_2^{\bullet-}$, and ^{1}O$_2$.[138] Hu et al. studied tetracycline hydrochloride (TCH) degradation using biochar from passion fruit shells pyrolyzed at 900 °C under N$_2$. The metal-free biochar activated PMS, achieving 90.9% TCH removal via singlet oxygen-mediated oxidation and non-radical pathways, including direct electron transfer and O$_2^{\bullet-}$/^{1}O$_2$ generation.[139] Cai et al. studied pyrrolic N-rich biochar from waste bean dregs for BPA removal, finding that N-biochar/PDS was most effective under neutral and acidic conditions. The ESR and quenching tests showed that SO$_4^{\bullet-}$, $^{\bullet}$OH, and ^{1}O$_2$ had minimal impact. The DFT results revealed enhanced electron donation and charge density in N-biochar, improving PDS activation and ROS formation.[140] Xu et al. developed a cost-effective N-doped biochar from sawdust via single-step calcination. The biochar, with high graphitic and pyridinic nitrogen, activates PMS for degrading BPA, phenol, acetaminophen, and sulfamethoxazole. The EPR and quenching tests identified ROS, especially singlet oxygen, as key in degradation.[141] Ding et al. studied nitrogen and sulphur-doped rice straw biochar for metolachlor degradation using PMS. N-doping improved PMS interaction, while S-doping disrupted charge balance. The DFT study showed that hydroxyl radicals and singlet oxygen were crucial, with HPLC-TOF-MS revealing the degradation pathways through hydroxylation, hydrolytic dechlorination, N-dealkylation, dehydroxylation, demethylation, and amide bond cleavage mechanisms.[142] Li et al. used biomass-derived activated carbon (BAC) for sulfamethoxazole removal with PDS. The BAC–PDS complex facilitated electron transfer, with EPR detecting ROS like $^{\bullet}$OH, SO$_4^{\bullet-}$, and ^{1}O$_2$. In real water, common anions had minimal impact on SMX degradation, providing insights into ROS generation.[143]

6.2.4. Nanostructured biomass. The immobilization of metal or metal oxide nanoparticles on the surface of the biomass and its derived materials such as biochar, hydrochar and activated carbon holds significant importance for various applications, particularly in the fields of environmental remediation and catalysis. This process involves the deposition of nanoparticles onto the surface of these carbonaceous materials through various methods such as carbothermal reduction, hydrothermal methods, etc.[15] The biomass derived materials have ample surface area and functional groups for the immobilization of nanoparticles, facilitating strong interactions and stability. The metal or metal oxide nanoparticles, such as iron, copper, silver, titanium dioxide, manganese oxide, etc. can be selectively deposited onto the surface of biomass derived

materials to impart specific properties or functionalities.[40] For instance, metal nanoparticles immobilized on activated carbon can serve as highly efficient catalysts for organic transformations, while metal oxide nanoparticles supported on biochar can act as effective adsorbents for pollutant removal in water treatment applications. The immobilization of nanoparticles on the carbonaceous materials not only enhances their stability and reusability but also expands their range of applications, contributing to the development of sustainable and efficient technologies for various environmental and industrial challenges (Table S3).[88] The incorporation of nanoparticles onto biomass or its carbon-rich derivatives significantly alters their physicochemical properties, thereby enhancing their remediation performance. Nanostructuring contributes to the following: (a) increased surface area and hierarchical porosity provide abundant active sites for pollutant binding, while functional groups on nanoparticles (*e.g.*, –OH, –O–, and metal oxides) strengthen interactions through hydrogen bonding, electrostatic attraction, or π–π stacking; (b) metal and metal oxide nanoparticles act as catalytic centers, activating oxidants such as H_2O_2, persulfate, or PMS, and generating reactive oxygen species (ROS) such as $^{\bullet}OH$, $SO_4^{\bullet-}$, $O_2^{\bullet-}$, and $^1O_2$. The porous biomass matrix supports nanoparticle dispersion and prevents agglomeration, ensuring sustained catalytic activity; (c) biomass facilitates pre-concentration of pollutants onto its surface, while immobilized nanoparticles drive catalytic degradation, leading to faster and more complete removal compared to either mechanism alone; (d) carbonized biomass with graphitic domains can act as an electron shuttle, accelerating redox reactions at nanoparticle sites and enhancing pollutant breakdown.

6.2.4.1. Raw biomass immobilized with metal/metal oxide nanoparticles. Kaur *et al.* studied the adsorption of terbinafine hydrochloride (TBH) using cotton shell powder (CS), nano zerovalent copper (nZVC), and zerovalent copper on CS (ZVC@CS). ZVC@CS effectively concentrated or removed TBH under acidic conditions (pH < 5) through hydrophobic and electrostatic interactions. Analysis revealed external mass transport as the limiting step for TBH adsorption, with ZVC@CS achieving a q_{max} of 285.3 mg g^{-1}, better than other adsorbents.[105] Kumar *et al.* also studied how pistachio shell biomass combined with nano-MnO$_2$ (nMPP) affects crystal violet (CV) removal. The adsorption capacity of the pistachio shell works synergistically with oxidative degradation efficacy of MnO$_2$ to enhance CV removal. Under acidic conditions, oxidative CV degradation occurs *via* $^{\bullet}OH$ radicals from nMPP, while neutral pH conditions show CV adsorption. This combination shows promise for organic contaminant remediation in water.[88] Kumar *et al.* evaluated the nanocomposite of pistachio shell powder combined with nano-zerovalent copper for the chromium remediation. The immobilized nano-copper (ZVC@PS) showed superior Cr(VI) adsorption (110.9 mg g^{-1}) compared to pistachio shell powder alone (27.95 mg g^{-1}). XPS confirmed the presence of the synergistic effect from Cr(VI) adsorption and reduction to Cr(III), enhancing remediation

efficiency.[144] Kaur *et al.* explored a synergistic approach combining pistachio shell powder adsorption with ZVI or ZVC in Fenton-like and PMS activation processes to enhance tetracycline (TCH) degradation. ZVI@PS-PMS showed superior performance with high contaminant removal, faster degradation (0.34 min^{-1}), and 86% COD removal, due to effective adsorption, catalysis, and PMS activation for advanced oxidation[145] (Table S4).

6.2.4.2 Surface modified biomass immobilized with metal/metal oxide nanoparticles. Surface-modified biomass immobilized with metal/metal oxide nanoparticles offers a promising approach for environmental remediation, combining the high surface area and reactivity of nanoparticles with the renewable, sustainable properties of biomass to enhance pollutant removal and treatment efficiency (Table 2). Further, the catalytic efficiencies of these metal/metal oxide nanoparticles in advanced oxidation processes significantly enhance the overall pollutant removal processes (Table 3).

6.2.4.2.1. Adsorptive removal. Sutradhar *et al.* synthesized biochar from pre-roasted sunflower seed shells (SFS) and peanut shells (PNS) using direct pyrolysis and assessed their effectiveness for textile dye removal from wastewater. FTIR and XRD analyses showed degradation of cellulosic and lignin components, and XPS indicated a 13.8% increase in C–C/C=C in SFS and 22.6% in PNS biochar, reflecting polyaromatic structure condensation. The PNS biochar demonstrated superior dye removal efficiency, enhanced by pyridinic-N, graphitic-N, hydrogen bonding, and electrostatic interactions.[146] Qu *et al.* evaluated the rice straw-derived biochar (BC) for ciprofloxacin (CIP) removal from water, finding a maximum Langmuir adsorption capacity of 747.64 mg g^{-1} at pH 5. The adsorption involved C=O groups facilitating electrostatic, π–π, and hydrogen bond interactions. TiO$_2$ is incorporated to create a Ti–RSB composite with enhanced photocatalytic performance and CIP removal efficiency across pH 5–9, owing to improved biochar surface functionality.[147] Sen synthesized a magnetic bamboo charcoal iron oxide nanocomposite for removing the cationic methylene blue (MB) dye from synthetic wastewater. The pseudo-second-order model described batch adsorption kinetics well. Both Freundlich and Langmuir isotherms fit the equilibrium data, with a maximum capacity of 111.11 mg g^{-1}. The composite's 80.25% desorption efficiency suggests its potential for treating industrial dye effluents.[148] Nascimento *et al.* assessed magnetic nanohybrids of sugar cane straw biochar and Fe$_3$O$_4$ (Fe$_3$O$_4$@BC) for removing congo red (CR) and indigo carmine (IC) dyes. The adsorption process following pseudo-second-order and Elovich models involved chemisorption and was best described by the Sips model, with endothermic and favourable thermodynamics.[149]

Dai *et al.* studied the impact of modification and magnetization on rice straw-derived biochar for tetracycline (TC) removal. Enhanced surface area and pore volume improved hydrogen bonding and pore-filling effects, achieving an adsorption capacity of 98.33 mg g^{-1}.[150] Hao *et al.* investigated hazelnut shell biomass-derived biochar with zerovalent iron (ZVI@HS) for

Table 2 Surface modified biomass nanocomposites as environmental remediating agents

Nanocomposite	Contaminant	Optimized conditions				% Removal	Ref.
		pH	Dose (g L^{-1})	Conc. (g L^{-1})	Time (min)		
Fe@BC	Methylene blue	10	0.4	0.02	120	80.25	148 and 158
Fe$_3$O$_4$@BC	Congo red	7	0.2	0.01	1440	72	149
Fe$_3$O$_4$@BC	Indigo carmine	10	0.2	0.01	1440	27	
Fe-BC	Tetracycline	3–10	1.2	0.05	60	98.3	150
ZVI@HS	Oxytetracycline	6.5	4	0.4	60	96.7	151
ZVI@HS	Chlortetracycline	6.5	4	0.4	60	95.5	
ZVI@HS	Tetracycline	6.5	4	0.4	60	95	
Fe/Pd@RS	1,2,4-Trichlorobenzene	5.58	0.16	0.01	2880	98.8	159
ZVI@PH	Chromium	4.4	1	0.3	6000	100	156
ZVI@PH	Trichloroethene	4.4	1	0.3	6000	100	
Pd/Fe@CS	Trichlorobenzene	3.7–10.3	0.1	0.1	1440	93	160
Co/Fe@MB	Cefotaxime	6	0.5	0.02	380	99.46	161
Fe@PSd	Sulfamethoxazole	4.5	0.004	0.02	1440	55.6	162
Ag/Fe@MB	Cefotaxime	6.1	1	0.04	90	91.3	163
Ni/Fe@WS	1,1,1-Trichloroethane	6	1	0.2	180	99.3	164
ZVI@RS	2,4-Dinitrotoluene	7.4	4	0.04	1440	40–50	165
ZVI@RS	4-Chlorophenol	7.4	4	0.052	1440	40–50	
Ni/Fe@SB	Decabromodiphenyl	6	2	0.002	10	91.2	166
nZVI/Pd@Si-RS	Chromium	4	0.01	0.05	480	95.9	157
nZVI@BC	Uranium	6	2	0.02	120	99.9%	158
Fe–Mn–Zn–Cu@BC	Thiamethoxam	3	0.4	0.05	20	100	167
ZVI@BC	Cadmium	6	2	0.1	480	96.2	168
ZVI@BC	Oxytetracycline	4	1.5	0.1	480	98.8	
Ag–SiO$_2$@AC	Copper	5.5	1	0.01	200	97	152
Ag–SiO$_2$@AC	Cadmium	5.5	1	0.01	200	100	
Ag–SiO$_2$@AC	Lead	5.5	1	0.01	200	95	
Ag–SiO$_2$@AC	Zinc	5.5	1	0.01	200	99	
ZVI@CS	Methyl orange	7	0.0005	0.2	60	97.9	169
TiO$_2$@AC	Phenol red	4.3	0.04	0.046	8.2	100	153
TiO$_2$@AC	Congo red	4.3	0.04	0.015	8.2	100	
Fe@AC	Methylene blue	4	0.4	0.1	30	100	154
ZVI@AC	Arsenic	7	2	0.1	90	99	170
ZnO@AC	Orange G	7	0.4	0.05	30	92	155
ZnO@AC	Rhodamine B	7	0.4	0.05	30	99	

removing oxytetracycline, chlortetracycline, and tetracycline. The adsorption process followed Langmuir isotherm and pseudo-second-order kinetics, with up to 95% removal efficiency, indicating spontaneous and endothermic processes.[151] Nyirenda et al. used sulphuric acid to create activated carbon from maize cobs and then deposited silver on silica nanoparticles to form the Ag–SiO$_2$@AC nanocomposite. This composite efficiently removed Pb^{2+}, Cd^{2+}, Cu^{2+}, and Zn^{2+} from solutions, with maximum adsorption capacities of 81.30, 87.72, 84.75, and 81.97 mg g^{-1}, respectively. The adsorption process was spontaneous, endothermic, and physical in nature.[152] Masoudian and colleagues efficiently removed Congo Red and Phenol Red dyes from water using TiO$_2$ nanoparticles on activated carbon from watermelon rind. The dye removal followed the Langmuir equation and second-order kinetics.[153] Altıntığ et al. created magnetic activated carbon (Fe@AC) from a ZnCl$_2$-activated corn shell, showing high methylene blue adsorption (357.1 mg g^{-1}) with fast uptake, endothermic process, and good reusability up to four cycles.[154] Saini et al. prepared zinc oxide-loaded activated carbon (ZnO@AC) via hydrothermal synthesis to remove Orange G (OG) and rhodamine B (Rh-B) dyes. The Langmuir model best fit the adsorption isotherms, with capacities of 153.8 mg g^{-1} for OG and 128.2 mg g^{-1} for Rh-B. The adsorption

followed the pseudo-second-order model, and thermodynamic studies indicated spontaneous and endothermic removal of dyes.[155]

Liu et al. evaluated magnetic zerovalent iron-supported biochar from peanut hull for chromium(VI) and trichloroethane (TCE) removal. The mechanisms included pore-filling, hydrophobic partitioning, and reductive degradation. The XPS showed Cr(VI) reduction to Cr(III) and a redox reaction with a decrease in the Fe^0 peak, suggesting effective, cost-efficient water treatment.[156] Qian et al. conducted an investigation into the reduction and adsorption of hexavalent chromium using a combination of palladium (Pd) and silicon-rich biochar derived from rape straw, supported by nanoscale zerovalent iron (nZVI). The presence of silicon and Pd facilitated the reduction of Cr(VI), attributed to the Fe^0 crystallinity within the structures of nZVI.[157] Zhang et al. investigated the adsorption and reduction of uranium using biochar-supported zerovalent iron (ZVI@BC) prepared through an environmentally friendly carbothermal reduction process. The maximum adsorption capacity reached 55.58 mg g^{-1}, with the Langmuir isotherm providing the best fit. Moreover, X-ray photoelectron spectroscopy (XPS) spectra obtained after adsorption revealed simultaneous occurrences of adsorption and reduction, as both U(IV) and U(VI) were detected in the spectra.

Table 3 Surface modified biomass nanocomposite mediated advanced oxidation processes for environmental contaminant removal

Nanocomposite	Oxidizing agent	Contaminant	Optimized conditions					Ref.
			pH	Dose (g L^{-1})	Conc. (g L^{-1})	Time (min)	% Removal	
ZVC@CSAC	PMS	Rhodamine B	3	0.05	0.01	60	87.6	40
ZVC@CSAC	PMS	Crystal violet	3	0.05	0.01	10	99.8	
ZVI@CSAC	PMS	Rhodamine B	3	0.05	0.01	60	84.1	
ZVI@CSAC	PMS	Crystal violet	3	0.05	0.01	60	98.3	
FeO$_x$@N–BC	PMS	Tetracycline	6.6	0.2	0.1	10	91.8	99
Cu@BC	PS	Tetracycline	4	0.5	0.12	270	93.6	199
Fe@BC	PDS	Acid orange 7	6	1	0.05	20	98	171
CuO-Biochar	PS	Bisphenol	3.84	0.1	0.01	40	93	172
Fe–N–P@BC	PDS	Sulfadiazine	6.1	0.2	0.01	60	97.2	173
MRBC, Fe@BC	PDS	Levofloxacin	7	1.6	0.01	30	88.59	174
Fe–N–BC	PS	Oxytetracycline	7	0.1	0.01	20	98	175
Fe–BC	PMS	Bisphenol A	7.26	0.5	0.002	30	100	176
ZnFe$_2$O$_4$@BC	H$_2$O$_2$	Methylene blue	3	1	0.1	60	100	177
CuO-Biochar	PDS	Phenacetin	4.26	0.3	0.01	30	100	178
nZVI@BC	PDS	Oxytetracycline	2	0.35	0.2	240	90.7	179
RSBC-FeS	H$_2$O$_2$	Oxytetracycline	2	0.35	0.2	240	79.35	180
Co$_3$O$_4$–MnO$_2$@BC	PMS	Sulfadiazine	5–9	0.1	0.025	10	100	181
FeS$_2$@BC	H$_2$O$_2$	Ciprofloxacin	3	1.5	0.03	20	96.8	182
Fe–Mo@N–BC	PMS	Orange II	4.74	0.1	0.03	40	100	183
Co$_3$O$_4$@BC	PMS	Tetracycline hydrochloride	4.6	0.1	0.04	20	90	184
Fe–Ce@N–BC	PMS	Metronidazole	5.74	0.75	0.01	60	97.5	185
Fe$_3$O$_4$@NCNTs-BC	PS	Sulfamethoxazole	7	0.4	0.01	40	100	186
Co@RBC	PMS	Levofloxacin	4.5	0.2	0.01	15	100	187
Fe-BC	PMS	Perfluorooctanoic acid	6.4	1	0.002	120	99	189
Magnetic BC	PS	Tetracycline hydrochloride	5.7	1	0.02	120	99	190
ZVI-Biochar	PS	Atrazine	4	0.175	0.025	30	73.47	191
Co@BC	PMS	Atrazine	5.3	0.010	0.002	10	100	192
CuO-Biochar	PMS	Methylene blue	7	0.2	0.032	30	99.68	193
CuO-Biochar	PMS	Acid orange 7	7	0.2	0.035	30	100	
CuO-Biochar	PMS	Rhodamine B,	7	0.2	0.048	30	100	
CuO-Biochar	PMS	Atrazine	7	0.2	0.022	30	100	
CuO-Biochar	PMS	Ciprofloxacin	7	0.2	0.033	30	78.27	
Fe–Mg@BC	PS	Sulfamethazine	3	2	0.03	30	99	194
ZVI@BC	PMS	Bisphenol A	8.2	0.15	0.02	5	100	196
ZVI@BC	H$_2$O$_2$	Sulfamethoxazole	5	0.1	0.0025	120	99	195
ZVI-biochar	PS	Phenol	7	0.3	0.094	330	97	198
MnFe$_2$O$_4$-biochar	H$_2$O$_2$	Tetracycline	5.5	0.5	0.04	120	95	200
nZVI-Biochar	H$_2$O$_2$	Ciprofloxacin	3	0.4	0.1	60	70	201
Co$_3$O$_4$-Biochar	PMS	Ofloxacin	7	0.2	0.019	60	98.9	203
nZVI-Biochar	H$_2$O$_2$	Sulfamethazine	3	1.2	0.01	720	74.04	204
ZVI-Biochar	PS	Sulfadiazine	3	0.2	0.02	10	100	205
MnO$_x$@AC	PMS	Ciprofloxacin	2.7	0.5	0.01	60	95.3	206
FeO$_x$-cherry stones	PMS	Bisphenol A	7	0.1	0.02	5	100	207
CoFe$_2$O$_4$@SAC	PMS	Norfloxacin	5–9	0.1	0.01	60	98	208
FeTiO$_2$/AC	H$_2$O$_2$	Malachite green	4	1	0.1	45	97	209
ZVI@AC	PS	Amoxicillin	2–9	1	0.1	10	99	210
AC/g-C$_3$N$_4$	PMS	Atrazine	3	1	0.005	120	100	211
CO-AC	PS	Ciprofloxacin	7	0.75	0.017	120	100	212
MAC	H$_2$O$_2$	Acid orange 10	3	0.2	0.1	30	93.9	213
Fe@N-C	PMS	Sulfamethoxazole	5.6	0.05	0.01	40	95.2	214
Co$_3$O$_4$@N-AC	PMS	Sulfamethoxazole	7	0.015	0.025	5	100	215

6.2.4.2.2. Catalytic removal. Shang *et al.* tested biochar-supported nanoscale zero-valent iron (nZVI) and palladium (Pd) composites for removing 1,2,4-trichlorobenzene (1,2,4-TCB). The modified biochar achieved up to 98.8% removal, primarily through Fe/Pd nanoparticle reduction and biochar adsorption.[159] Han *et al.* elucidated the impact of Pd/Fe supported by biochar on the elimination of 1,2,4-trichlorobenzene (1,2,4-TCB). A method involving both Pd/Fe electrochemical dechlorination and biochar adsorption is employed to eradicate trichlorobenzene.[160] Wu *et al.* studied cefotaxime degradation using Co/Fe bimetallic nanoparticles supported on modified biochar. The composite efficiently removed cefotaxime (CFX) through adsorption and degradation, with Co/Fe nanoparticles breaking down adsorbed CFX. The β-lactam ring instability of CFX under strong reducing agents was analysed *via* HPLC-ESI-MS.[161] Reguyal and Sarmah assessed the magnetic biochar (Fe@PSd) from pine sawdust (PSd) for sulfamethoxazole (SMX) removal. The SMX sorption was pH-dependent, with hydrophobic and π–π electron interactions significantly influencing the process due to SMX's aromatic and heterocyclic structures.[162] Wu *et al.* investigated the degradation and adsorption of cephalexin (CLX) using Ag/Fe bimetallic

nanoparticles supported on modified biochar. Ag/Fe@MB effectively removed CLX through reduction and adsorption, with degradation products analysed by LC–MS.[163]

Li et al. evaluated the reductive degradation of 1,1,1-trichloroethane (1,1,1-TCA) using biochar-supported Ni/Fe bimetallic nanoparticles. Nickel assisted zero-valent iron (ZVI) corrosion and thus generated atomic hydrogen that forms hydride-like species, enhancing 1,1,1-TCA reduction. Inorganic ions had minimal effects, but NO_3^- and humic acid significantly inhibited degradation.[164] Oh et al. used rice straw biochar-supported zerovalent iron for removing nitro explosives and halogenated phenols from contaminated water. XPS showed no change in Fe^0 redox properties after co-pyrolysis. The biochar facilitated contaminant reduction through Fe^0 was proved more efficient than direct Fe^0 reduction due to enhanced electron transfer mediated by biochar's surface functional groups.[165] Yi et al. examined decabromodiphenyl ether degradation using biochar-supported Ni/Fe (BC@Ni/Fe) nanoparticles. BC@Ni/Fe showed a higher removal efficiency than Ni/Fe alone, with stepwise debromination as the primary mechanism, complemented by the adsorption process.[166] Li et al. used biochar-supported Fe@BC to activate persulfate (PDS) for degrading Acid Orange 7. The maximum removal (98%) occurred in 20 min under optimal conditions (50 mg L^{-1} AO7, 1 g L^{-1} catalyst, 20 mM PMS, and pH 6). The process involves electron transfer and a non-radical pathway, primarily generating singlet oxygen ($^1O_2$) for degradation.[171] Qu et al. assessed the efficiency of CuO-supported biochar (CuO@BC) for activating persulfate (PS) to degrade bisphenol A (BPA). The free radical and ESR analyses showed involvement of $^•OH$, $SO_4^{•-}$, $O_2^{•-}$, and $^1O_2$ in the degradation process. The CuO@BC-PS system reduced BPA toxicity to a significant extent, with no toxicity observed for the CuO@BC composite.[172]

Chai et al. used a multi-metal loaded heterogeneous Fenton catalyst (M@BC) for thiamethoxam (THX) removal, synthesized by pyrolyzing rice straw biomass rich in Fe, Cu, Mn, and Zn. This mesoporous biochar effectively generated hydroxyl radicals ($^•OH$) for complete THX degradation (100%). DFT studies helped in identifying the regions with a high Fukui index for $O_2^{•-}$ and $^•OH$ attack.[167] Seo et al. investigated seaweed biomass-derived biochar's catalytic properties for sulfadiazine (SDZ) removal. The adsorption process involves both physical and chemical mechanisms. Pyrolysis enriched the biochar with N, P, and Fe, enhancing SDZ degradation through peroxydisulfate (PDS) activation. The electron spin resonance (ESR) confirmed reactive oxygen species (ROS) generation, including radicals ($O_2^{•-}$, $SO_4^{•-}$, and $^•OH$) and non-radicals ($^1O_2$), with non-radical mechanisms dominating, highlighting electron transfer pathways.[173] Yang et al. evaluated a modified red mud biochar catalyst (MRBC, Fe@BC) for levofloxacin (LFX) degradation in water. MRBC synthesized via acid pretreatment and pyrolysis at 700 °C effectively activated peroxydisulfate (PDS), achieving 88.59% LFX removal in 30 min with minimal Fe leaching (0.049 mg L^{-1}). The high performance of the catalyst was due to the synergy of red mud and biomass, generating reactive oxygen species (ROS) through Fe(II) and

PDS activation. The quenching experiments and DMPOX presence in EPR confirmed that $SO_4^{•-}$ and $^•OH$ were key to LFX degradation.[174] Tian et al. used Fe–N biochar from waste chestnut shells, doped with iron and nitrogen (Fe–N–BC), to activate persulfate (PS) for 98% oxytetracycline (OTC) degradation in 20 min. The process, dominated by direct electron transfer and $^1O_2$ generation, benefited from Fe–N structure altering electron distribution, enhancing the efficiency and preventing iron ion leaching.[175] An oxytetracycline removal study was also evaluated using rice husk-derived biochar (BC), hydrochar (HC), and raw husk (RH) as supports for zerovalent iron nanocomposites in PMS-activated AOPs. ZVI@BC achieved 98.3% removal due to enhanced surface defects and ROS generation. Mechanisms were validated via scavenger tests, DFT analysis, and HRMS intermediate identification.[218]

Tian et al. studied biochar-supported zerovalent iron (ZVI@BC) for adsorbing Cd(II) and degrading oxytetracycline (OTC). The immobilization of zerovalent iron on the biochar in ZVI@BC improved electron transfer and its oxidation efficiency. The Cd(II) adsorption was monolayer chemisorption, involving electrostatic interactions, ion exchange, and complex formation, while OTC adsorption was multilayer chemisorption. The ESR identified hydroxyl radicals ($^•OH$) as key in OTC degradation, with LC–MS revealing dealkylation, deamination, and dehydroxylation as main degradation steps.[168] Tang et al. synthesized nitrogen-doped corn cob biochar and immobilized it with mixed valence iron (FeO$_x$@N–BC) for tetracycline degradation via PMS activation. Nitrogen doping prevents Fe^0 nanoparticle agglomeration, enhancing electron transfer and PMS activation. The ESR analysis showed reactive oxygen species, with singlet oxygen ($^1O_2$) as dominant in tetracycline removal.[99] Shi et al. studied N-doped biochar composite catalysts for Bisphenol A (BPA) degradation using peroxymonosulfate (PMS) activation. Fe$_3$C/biochar, synthesized by pyrolyzing wood powder with ferric ferrocyanide, effectively degraded 0.05 mM BPA in 30 min with 0.5 g L^{-1} catalyst. The system generated radicals, high-valent iron-oxo, and non-radical species using both Fe$_3$C and N-doped biochar. Fe$_3$C activates PMS efficiently and thus minimizes Fe ion leaching and sludge formation.[176] Leichtweis et al. used ZnFe$_2$O$_4$-supported biochar from coffee grounds for methylene blue dye degradation using H$_2$O$_2$ activation. The composite achieved 100% dye removal compared to pure ZnFe$_2$O$_4$ (∼37%). The high efficiency was attributed to biochar's phenolic, hydroxyl, and carboxylic groups. The radical tests identified h^+, $O_2^{•-}$, and $^•OH$ as the reactive species involved in dye degradation.[177]

Li et al. developed copper oxide-modified rice straw biochar (CuO@BC) for phenacetin (PNT) degradation using peroxydisulfate (PDS). CuO@BC showed effective PNT decomposition, with EPR analysis identifying reactive oxygen species ($SO_4^{•-}$, $^•OH$, $O_2^{•-}$, and $^1O_2$) as key in the process. Scavenger experiments revealed that $^1O_2$ and $O_2^{•-}$ played a key role in PNT removal.[178] Yang et al. synthesized zerovalent iron-supported biochar (nZVI@BC) at 1000 °C, used for peroxydisulfate (PDS) activation to degrade oxytetracycline (OTC). TOC results

showed effective CO_2 conversion, while ESR and quenching identified $SO_4^{\bullet-}$, $^{\bullet}OH$, and $^1O_2$ as key reactive species in OTC degradation.[179] Yang et al. used FeS-modified rape straw (RS-FeS) and its biochar (RSBC-FeS) for oxytetracycline (OTC) removal via H_2O_2 activation. The maximum removal capacities were 635.66 mg g^{-1} (RS-FeS) and 827.80 mg g^{-1} (RSBC-FeS), with degradation rates of 70.14% and 79.35%, respectively. The process involved both radical ($SO_4^{\bullet-}$, $^{\bullet}OH$, and $O_2^{\bullet-}$) and non-radical ($^1O_2$) pathways, including hydroxylation, dehydration, quinonization, demethylation, decarbonylation, alcohol oxidation, and ring cleavage.[180] Jiang et al. studied Co_3O_4–MnO_2 nanoparticles on rice straw biochar (BC) for peroxymonosulfate (PMS) activation to remove sulfadiazine (SDZ). Nearly 100% SDZ degradation was achieved in 10 min, primarily via singlet oxygen ($^1O_2$) and sulfate radicals ($SO_4^{\bullet-}$).[181] Sang et al. developed a catalyst from natural pyrite (FeS_2) and rice straw biochar (BC) for ciprofloxacin (CIP) degradation, using a grinding and calcination method. The $FeS_2@BC$ system achieved 96.8% CIP degradation in 20 min. The catalyst efficacy originates from both free radicals and adsorption processes. The ESR and quenching experiments identified hydroxyl ($^{\bullet}OH$), superoxide ($O_2^{\bullet-}$), and sulfate ($SO_4^{\bullet-}$) radicals, with $^{\bullet}OH$ being the most effective. The HCO_3^- significantly impacted CIP degradation, while Cl^-, NO_3^-, and SO_4^{2-} had no effect.[182] Yao et al. studied the effectiveness of bimetallic Fe and Mo immobilized on nitrogen-doped biochar (Fe–Mo@N-BC) for degrading Orange II. They found that N-doping enhanced metal stability and dispersion. In the PMS activation process, Fe–Mo nanoparticles transfer electrons to PMS, generating significant ROS. The Fe/Mo bimetallic system facilitates Fe^{3+}/Fe^{2+} and Mo^{6+}/Mo^{4+} redox cycles, accelerating PMS activation and organic degradation. The EPR and radical quenching experiments identified $SO_4^{\bullet-}$, $^{\bullet}OH$, and $^1O_2$ as key ROS in the process.[183] Xiong et al. synthesized Co_3O_4 composites on biochar from rape straw for tetracycline hydrochloride (TCH) degradation via peroxymonosulfate (PMS) activation. The $Co_3O_4@BC$ catalyst achieved 90% TCH removal in 20 min, utilizing both radical ($SO_4^{\bullet-}$, $^{\bullet}OH$, and $O_2^{\bullet-}$) and non-radical pathways. The DFT calculations showed an electric field at the Co_3O_4–BC interface, enhancing electron transfer and the Co^{2+}/Co^{3+} redox cycle, improving degradation efficiency.[184] Xiao et al. developed bimetallic iron and cerium embedded in nitrogen-enriched porous biochar (Fe–Ce@N-BC) for metronidazole (MNZ) removal via PMS activation. MNZ degradation reached 97.5% in 60 min. The nitrogen-enriched biochar increased surface area and porosity, enhancing PMS activation. Fe–Ce oxide nanocrystals acted as activation centres, facilitating both radical and non-radical degradation pathways.[185]

Liu et al. studied $Fe_3O_4@NCNTs$-BC, a nitrogen-doped magnetic carbon nanotube-bridged biochar catalyst, which effectively activates persulfate (PS) for sulfamethoxazole (SMX) degradation. The quenching and ESR results showed that superoxide radicals ($O_2^{\bullet-}$) and direct electron transfer dominate in the process. The $Fe_3O_4@NCNTs$-BC/PMS/SMX system decomposes HSO_5^- to generate active radicals, while carbon–PDS* complexes extract electrons from SMX.[186] Liu et al.

explained the excellent PMS activation with a cobalt nanoparticle supported biochar (Co@BC) catalyst for levofloxacin (LVF) degradation. The Co@BC-PMS activation process showed that superoxide $^1O_2$ non-radicals and the electron transfer mechanisms played the dominant role in LVF degradation, as evidenced by quenching experiments, electron paramagnetic resonance (EPR) and density functional theory (DFT) calculations.[187] Chen et al. investigated printing and dyeing sludge (PADS) biochar as a peroxymonosulfate (PMS) activator for bisphenol A (BPA) removal. Prepared by pyrolysis at 800 °C for 1.5 h, the biochar achieved 99% BPA removal in 20 min. The radical trapping experiments indicated that the non-radical pathway, dominated by singlet oxygen ($^1O_2$), was crucial for degradation, with CO, graphite nitrogen, and pyridine nitrogen identified as active sites for PMS activation.[188] Fu et al. used iron-doped sludge biochar to activate peroxymonosulfate (PMS) for degrading perfluorooctanoic acid (PFA). In the Fe-BC/PMS system, singlet oxygen ($^1O_2$) was generated, facilitated by quinone and pyridinic-N groups. The DFT calculations indicated that PFA degradation followed a non-radical pathway with $^1O_2$ as the main reactive species.[189]

Huang et al. investigated the persulfate activation (PS) with magnetic rape straw biochar catalyst for the degradation of tetracycline hydrochloride (TCH) from water. The magnetic biochar mediated PS activation generates reactive oxygen species such as $SO_4^{\bullet-}$, $^{\bullet}OH$, and $O_2^{\bullet-}$ as confirmed by ESR analysis. The sulfate radical ($SO_4^{\bullet-}$) and superoxide radical ($O_2^{\bullet-}$) were observed as the dominant reactive oxygen species for the degradation of TCH.[190] Jiang et al. studied a zero-valent iron and biochar composite (ZVI@BC) activated by persulfate (PS) for atrazine degradation. The EPR and quenching experiments revealed $SO_4^{\bullet-}$ and $^{\bullet}OH$ as the primary radicals responsible for degradation. The analysis of iron corrosion products and XPS suggested that ZVI@BC-PS activates PS, generating these radicals and altering iron's valence state, which degrades atrazine. The GC–MS and LC–MS identified degradation pathways including alkyl oxidation, dealkylation, dechlorination-hydroxylation, etc.[191] Liu et al. studied biochar from wheat straw immobilized with cobalt (Co@BC) for activating PMS to degrade atrazine (ATZ). The biochar enhanced Co@BC efficiency by donating electrons to generate superoxide radicals ($O_2^{\bullet-}$), converting Co(III) to Co(II). The radical scavenging and EPR analysis revealed $SO_4^{\bullet-}$ as the dominant reactive species in ATZ degradation.[192] Li et al. developed a biochar-supported copper oxide composite (CuO@BC) to activate peroxymonosulfate (PMS) for removing methylene blue, acid Orange 7, rhodamine B, atrazine, and ciprofloxacin from saline wastewater. The biochar enhanced CuO stability and catalytic activity. The EPR analysis confirmed singlet oxygen ($^1O_2$) as the primary reactive species, with sulfate radicals ($SO_4^{\bullet-}$) and hydroxyl radicals ($^{\bullet}OH$) also contributing to degradation of pollutants.[193]

Qin et al. studied the impact of bimetallic (Fe–MgO) supported biochar on persulfate (PS) activation for sulfamethazine (SMT) degradation. Nearly 99% SMT degradation was achieved with Fe–MgO@BC-PS activation. The Fe–MgO@BC composite activated PS by leveraging Fe^{2+}, and biochar's hydroxyl and

carboxyl groups, producing $SO_4^{\bullet-}$ radicals. The SMT degradation mechanism involved dehydrogenation, bond cracking, and unsaturated bond addition.[194] Zhang et al. studied ZVI@BC-H_2O_2 activation for sulfamethoxazole (SMX) degradation. They achieved 99% SMX degradation in 2 h with Fe-impregnated biochar, which enhanced H_2O_2 activation. The EPR results showed that H_2O_2 generated hydroxyl radicals ($^{\bullet}OH$) through interactions with C–OH on biochar. Both radical and non-radical processes contributed to SMX degradation.[195] Jiang et al. studied zerovalent iron (ZVI) immobilized biochar for persulfate (PMS) activation to degrade bisphenol A (BPA). The complete BPA removal was achieved in 5 min. The quenching and EPR experiments revealed that $SO_4^{\bullet-}$ was the primary radical, crucial for BPA degradation. Additionally, carbon-based materials activated PMS's O–O bond, enabling both radical-mediated and non-radical degradation mechanisms.[196] Nguyen et al. explored cobalt-impregnated spent coffee ground biochar (Co-SCG) for tetracycline (TC) removal. Co-SCG showed high adsorption and catalytic activity, with $SO_4^{\bullet-}$ identified as the key radical in TC degradation via EPR analysis.[197] Nguyen and Oh studied how biochar enhances phenol degradation in Fe^0-persulfate systems. Their research shows that Fe^0 combined with biochar and persulfate significantly boosts oxidation of contaminants. The radicals generated by electron transfer from Fe^0 to persulfate involved $SO_4^{\bullet-}$ and $^{\bullet}OH$ radicals to degrade phenol, with hydroxyl radicals being dominant as confirmed by EPR and quenching experiments.[198]

Chen et al. developed an in situ method for tetracycline (TC) removal using biochar (BC) adsorption and persulfate (PS) oxidation in the Cu@BC-PS system. The process, driven by Cu^{1+}, effectively degrades TC across various pH levels and high COD concentrations. The XPS, EPR, and quenching studies show that Cu^{1+} on biochar activates PS, with $SO_4^{\bullet-}$ and $^{\bullet}OH$ as key radicals. Cu^{2+} and TC adsorption is the rate-limiting step.[199] Lia et al. developed magnetically separable $MnFe_2O_4$ nanoparticles and $MnFe_2O_4$/biochar composites to activate hydrogen peroxide (H_2O_2) for tetracycline (TC) degradation. The SEM analysis showed that spherical $MnFe_2O_4$ was effectively loaded on biochar. The $^{\bullet}OH$ radicals confirmed by quenching and ESR experiments drive the TC degradation. The XPS revealed Fe and Mn ions in H_2O_2 activation, while biochar prevents $MnFe_2O_4$ aggregation and scavenges excess hydroxyl radicals.[200] Mao et al. studied biochar-supported nanoscale zero-valent iron (nZVI@BC) with hydrogen peroxide (H_2O_2) for removing organic contaminants, focusing on ciprofloxacin degradation. Their research showed that hydroxyl radicals ($^{\bullet}OH$) were key in oxidation. The theoretical calculations indicated that hydrogen atom abstraction (HAA) contributed 92.3% to the second-order rate constants (k) for ciprofloxacin oxidation.[201] Fu et al. investigated graphitized hierarchical porous biochar from corn parts and synthesized $MnFe_2O_4$/BC composites for organic pollutant degradation via peroxymonosulfate (PMS) activation. The EPR and quenching studies revealed three degradation pathways: radical-induced oxidation by $SO_4^{\bullet-}$ and $^{\bullet}OH$, non-radical oxidation by $^1O_2$ from PMS decomposition, and electron

transfer from organic compounds to PMS via graphitization structures.[202]

Chen et al. studied Co_3O_4 rice straw-derived biochar (BC-Co_3O_4) for peroxymonosulfate (PMS) activation, achieving high efficiency in degrading ofloxacin (OFX). The radical scavenging and EPR analysis showed that $SO_4^{\bullet-}$ and $^{\bullet}OH$ radicals were involved, with enhanced degradation under neutral to weak basic conditions and reduced effectiveness at extreme pH.[203] Deng and colleagues studied biochar-supported nanoscale zero-valent iron (nZVI@BC) for sulfamethazine removal using a H_2O_2-activated Fenton-like reaction. The nZVI decomposed H_2O_2 into hydroxyl radicals, while biochar adsorbed sulfamethazine, activated H_2O_2, and prevented nZVI aggregation, thus enhancing sulfamethazine removal efficacy.[204] Ma and colleagues developed ZVI@BC via co-pyrolysis of K_2FeO_4 and bamboo biomass, creating a material with a high surface area. The study found that lower pH, higher temperature, and Cl^- ions improved sulfadiazine degradation, while CO_3^{2-} and HPO_4^{2-} impeded it. The free radicals and non-free radicals, particularly $^1O_2$, played significant roles in the degradation process.[205]

Zhang and Wang synthesized nanoscale zerovalent iron on activated carbon from coconut shells (nZVI@AC) using a pulse electrodeposition method, which was simpler and cheaper than traditional methods. nZVI@AC achieved 97.94% removal of methyl orange from water by breaking its azo bonds.[169] Kaur and colleagues used Ficus religiosa bark extract to immobilize zerovalent copper (ZVC@CSAC) and zerovalent iron (ZVI@CSAC) on cotton shell activated carbon (CSAC) for activating peroxymonosulfate (PMS) to degrade rhodamine B (Rh B) and crystal violet (CV) dyes. ZVI@CSAC proved more effective than ZVC@CSAC in dye removal. The DFT optimizations and HRMS analysis outlined the degradation pathways. The solution toxicity tests showed that intermediates were less toxic than the original dyes.[40] Chen et al. investigated MnO_x loaded on activated carbon (MnO_x/AC) for activating PMS to degrade ciprofloxacin. MnO_x/AC showed excellent performance and reusability, with activated carbon enhancing the effectiveness of MnO_x. The redox cycles among Mn(II, III, and IV) species produced reactive oxygen species, predominantly singlet oxygen (63.75%). The PMS adsorption on MnO_x/AC was crucial for ciprofloxacin degradation under acidic conditions. The LC–MS analysis identified seven intermediates to propose the degradation pathway.[206]

Li et al. developed a composite material, BAC/FeO_x, combining FeO_x nanoparticles with biomass activated carbon for bisphenol A (BPA) remediation via sulfate radical-based advanced oxidation processes (AOPs). BAC/FeO_x efficiently degrades BPA by activating peroxydisulfate (PDS) and the process was influenced by BAC/FeO_x dosage and PDS concentration, showing versatility across pH levels and temperatures. The ESR and quenching experiments confirmed the involvement of $SO_4^{\bullet-}$ and $^{\bullet}OH$ radicals as key species in the degradation process.[207] Yang et al. synthesized $CoFe_2O_4$@SAC nanocomposites from the sludge activated carbon via a simple hydrothermal method. These nanocomposites effectively

degraded norfloxacin (NOR) by activating peroxymonosulfate (PMS) and showed over 90% NOR removal after five cycles. The study explored the effects of Cl^-, HCO_3^-, and NO_3^- on the catalysis and identified $SO_4^{\bullet-}$ and $^\bullet OH$ radicals as key to NOR degradation, with XPS revealing redox couples Co^{3+}/Co^{2+} and Fe^{3+}/Fe^{2+} in PMS activation.[208] Loo et al. synthesized Fe–TiO_2@AC from oil palm empty fruit bunches via the sol–gel method. The Fe–TiO_2 particles were well-dispersed on the AC support, retaining their anatase phase. The high surface area and porous structure of AC improved the adsorption process, while the enhanced electrostatic interactions and reduced recombination rates, combined with Fe doping, boosted the photocatalytic activity. Fe–TiO_2@AC achieved 97% dye removal after 45 min of light irradiation.[209]

Zhao and colleagues found that activated carbon-supported iron (Fe@AC) is a highly effective catalyst for amoxicillin (AMO) degradation using persulfate (PS). The complete AMO breakdown occurred within 10 min, with improved efficiency at higher catalyst dosages and PS concentrations. The process followed pseudo-first-order kinetics, with an activation energy of 28.11 kJ mol^{-1}. The ESR analysis identified hydroxyl and sulfate radicals, with surface-adsorbed hydroxyl radicals crucial for the degradation of AMO. The Fe@AC-PS system also significantly reduced the toxicity of degraded AMO, highlighting its practical application potential.[210] Dangwang Dikdim et al. developed a composite, AC/g-C_3N_4, for photocatalytic atrazine degradation under visible light with PMS. Incorporating AC effectively mitigated electron–hole recombination and enhanced the photocatalytic activity of graphitic carbon nitride. Reactive radical trapping experiments and EPR analysis revealed that sulfate and hydroxyl radicals played crucial roles in atrazine degradation during the reaction process.[211]

Erdem and Erdem studied ciprofloxacin degradation in water using a persulfate activation process with an activated carbon-supported cobalt catalyst (Co@AC). The synthesized Co@AC activated persulfate to generate $SO_4^{\bullet-}$ and $^\bullet OH$ radicals, with $SO_4^{\bullet-}$ being more effective. The kinetic analysis showed pseudo-first-order kinetics with an activation energy of 62.69 kJ mol^{-1}.[212] Nguyen et al. prepared magnetic activated carbon (MAC) using one-pot pyrolysis of lotus seedpod waste with $ZnCl_2$ and $FeCl_3$ coactivation. This MAC, with a high surface area (S_{BET} = 1080 m^2 g^{-1}) and pore volume (V_{total} = 0.51 cm^3 g^{-1}), effectively activated H_2O_2 for removing Acid Orange 10, outperforming MAC prepared from single activation using $FeCl_3$ only.[213] Li et al. found that nZVI supported on biomass-derived porous carbon (nZVI@AC) removed As(III) from water more effectively and quickly than nZVI@BC and pure nZVI. The adsorption kinetics followed the pseudo-second-order model, and the Langmuir model described isotherms. The removal involved electrostatic interaction, oxidation, and complexation processes.[170] Wang et al. used an affordable single-atom iron catalyst (Fe@N–C) on nitrogen-doped porous carbon to degrade sulfamethoxazole in water. The DFT calculations identified nitrogen and oxygen coordination to iron as the active site for PMS activation. The quenching experiments and ESR analysis showed that Fe@N–C enhanced

singlet oxygen ($^1O_2$) production, contributing 78.77% to the degradation.[214] Chen et al. synthesized Co_3O_4@N-doped porous carbon (Co_3O_4@NPC/rGO) using self-assembly and pyrolysis-oxidation, with graphene oxide and bimetallic zeolite imidazolate frameworks as precursors. The composite efficiently activates peroxymonosulfate across various pH levels, degrading sulfamethoxazole in 5 min via both radical and non-radical pathways.[215]

6.3. Reusability and stability of modified biomass materials

In practical environmental remediation, the reusability and stability of biomass-derived materials are just as critical as their initial adsorption or catalytic efficiency. Materials that quickly lose activity or suffer structural degradation during repeated use have limited applicability in real-world scenarios. Thus, systematic evaluation and enhancement of their long-term durability are indispensable for advancing their practical deployment.

6.3.1. Regeneration and cycling performance.
Many modified biomass adsorbents exhibit significant regeneration potential through simple desorption techniques such as washing with dilute acids, bases, or organic solvents. For instance, alkali-activated rice husk biochar has retained more than 80% of its dye removal efficiency over five adsorption–desorption cycles,[40] while iron-immobilized biochars showed consistent Cr(VI) removal performance across multiple cycles.[216] The regeneration capacity largely depends on the stability of functional groups introduced during surface modification and the resilience of the porous network to repeated sorption–desorption stresses.

6.3.2. Thermal and structural stability.
The thermal stability of biomass-derived adsorbents is strongly influenced by the activation or nanostructuring technique employed. Pyrolysis-derived biochars demonstrate higher carbonization and improved resistance to thermal degradation, while hydrothermal carbonization often results in hydrochars with moderate stability but abundant oxygenated groups. Further enhancement is achieved by immobilization of metal or metal oxide nanoparticles (e.g., Fe_3O_4, TiO_2, and ZnO), which not only provide catalytic activity but also prevent collapse of pore structures at elevated temperatures.[16] Thermogravimetric analyses have confirmed that chemically activated carbons and nanocomposites display improved decomposition resistance compared to raw biomass.[217]

6.3.3. Chemical stability under operational conditions.
In real wastewater systems, pH fluctuations, high ionic strengths, and competing contaminants may compromise material performance. Acid-modified biochars, for example, may leach functional groups under highly alkaline conditions, whereas nanoparticle-loaded composites risk metal leaching into the environment.[218] Stabilization strategies such as covalent cross-linking, polymer coating, or strong electrostatic immobilization of nanoparticles can significantly improve long-term chemical resistance.[14] However, comprehensive studies under variable real-world conditions remain limited.

6.3.4. Strategies for enhancing reusability and durability. Surface functionalization with stable moieties (*e.g.*, amine and sulfonic acid groups), hybridization with inorganic supports (clays, silica, and zeolites), and carbonization under optimized conditions have proven effective in improving reusability.[215] Additionally, coupling adsorption with catalytic degradation (as in biochar–metal oxide nanocomposites) reduces fouling of active sites, thereby extending material lifetime. Developing multifunctional composites that combine adsorption, photocatalysis, and redox reactivity represents a promising path toward enhanced stability.[14]

6.4. Economic viability and scalability of biomass modification techniques

Although biomass itself is an abundant and low-cost feedstock, the economic feasibility of its modified derivatives depends heavily on the activation and nanostructuring techniques employed. While many studies emphasize material performance, fewer critically assess the cost and scalability of these treatments, which are crucial for large-scale deployment.

6.4.1. Cost implications of modification techniques. Chemical activation methods (*e.g.*, acid/alkali treatment and use of oxidative agents) can substantially improve porosity and functional group density, but they also incur significant costs from reagent consumption, high-temperature processing, and post-treatment washing to remove residues. Additionally, chemical processes generate secondary waste streams requiring careful disposal, which further adds to operational costs.[218] In contrast, physical methods such as pyrolysis, hydrothermal carbonization, or microwave heating are generally more cost-efficient and scalable, though they may yield materials with lower surface functionalization unless combined with post-modification steps.[217]

6.4.2. Scalability considerations. From a scalability perspective, physical methods hold greater promise for industrial adoption due to their simpler setups, compatibility with bulk biomass feedstocks, and potential to integrate with existing waste-to-energy infrastructure. Hydrothermal carbonization, for instance, eliminates the need for biomass drying and operates under moderate conditions, making it suitable for continuous-flow systems.[219] On the other hand, nanostructuring with metal/metal oxide nanoparticles, although effective for enhancing catalytic and adsorption performance, raises concerns regarding raw material costs, potential leaching, and complex synthesis protocols that may hinder scale-up.[218]

6.4.3. Strategies for improving economic feasibility. Hybrid approaches that combine low-cost physical methods with selective chemical or biological modifications may offer a more balanced trade-off between performance and cost. Valorization of process by-products (*e.g.*, bio-oil, syngas from pyrolysis) could further offset treatment costs.[22] Moreover, implementing circular economy principles such as reusing spent adsorbents in energy recovery or soil amendment could enhance the overall economic and environmental sustainability.

6.5. Real-world and pilot-scale applications of surface-modified and nanostructured biomass in environmental remediation

While laboratory-scale investigations dominate the literature, several pilot-scale and field applications highlight the feasibility of biomass-derived materials in real environmental systems. For example, granular walnut shell biochar layered into sand-based constructed wetlands effectively neutralized acidity and removed multiple heavy metals from simulated mining-impacted water, while enhancing plant growth and regulating microbial communities.[220] In another study, alkali-activated rice husk biochar was tested in a textile wastewater treatment plant and demonstrated > 80% dye removal efficiency, with stable regeneration performance over multiple cycles.[221] Similarly, hydrothermally carbonized sewage sludge was applied at a field scale to immobilize heavy metals in contaminated soils, thus reducing metal leaching.[222] Further, a pilot-scale biochar-amended sand filtration system was evaluated for drinking water treatment, which showed significant removal of natural and heavy metals.[223]

These case studies demonstrate that surface-modified biomass can be engineered into scalable remediation systems such as packed-bed reactors, constructed wetlands, and filtration units. Nevertheless, challenges remain in ensuring long-term stability, regeneration, and economic viability.

7. Future perspectives

In the future, the modified surface of biomass, its carbon-rich derivatives, and metal nanocomposites hold significant potential for enhancing environmental remediation applications, particularly through persulfate (PMS) activation. Advanced material synthesis techniques will be crucial for fine-tuning catalytic efficiency and durability, as well as for deepening mechanistic understanding of pollutant degradation pathways. Such mechanistic insights can guide the rational development of surface-modified materials tailored for specific environmental challenges. Equally important will be the scaling-up of production methods and their integration into practical remediation strategies, which requires innovation in reactor design, cost-effectiveness analysis, and techno-economic feasibility studies. The exploration of multifunctional materials and prioritization of sustainability in both synthesis and application will further improve adaptability and long-term effectiveness across diverse environmental matrices.

Looking forward, artificial intelligence (AI) and machine learning (ML) are expected to play transformative roles in accelerating material design and process optimization. AI-guided computational approaches can predict pollutant–surface interactions, identify optimal modification strategies, and reduce reliance on trial-and-error experimentation. Similarly, ML-driven process control can optimize operating conditions in pilot and full-scale systems, enabling real-time adjustments that enhance efficiency and lower costs.

Another emerging direction is the integration of biomass valorization into circular economy frameworks. Agricultural

residues, forestry by-products, and municipal wastes can be transformed into functional remediation materials, turning waste streams into value-added resources. Closed-loop strategies, where spent adsorbents are regenerated, reused, or repurposed into new products, will be critical for sustainable deployment. Combining advanced characterization techniques with AI/ML will also enable deeper insights into adsorption and catalytic mechanisms, thereby guiding the rational design of next-generation nanostructured biomass composites. Collectively, these future directions suggest a paradigm shift from conventional modification approaches toward digitally optimized, multifunctional, and circular bio-based remediation technologies, which hold promise for addressing global pollution challenges in a sustainable and scalable manner.

8. Conclusion

The tailored surface modified biomass and its carbon-rich derivatives offer tremendous potential for enhanced environmental remediation applications. The innovative surface modification techniques, such as chemical functionalization and nanoparticle deposition on biomass materials, can be engineered to exhibit superior adsorption and degradation capacities, selectivity, and stability for various environmental remediation processes. These modified biomaterials not only demonstrate remarkable efficiency for the removal of contaminants, but also present several advantages, including cost-effectiveness, biodegradability, and sustainability. The conversion of biomass into the carbon-rich derivatives, such as biochar and activated carbon, not only mitigates waste, but also creates valuable materials with exceptional adsorption properties and pore structures. These carbonaceous materials serve as effective sorbents for a wide range of contaminants, including inorganic and organic materials. Further immobilization of metal nanocomposites presents a powerful approach for enhanced environmental remediation applications, particularly in the activation of persulfate (PMS) for pollutant degradation. The synergistic interactions between biomass-derived carbon matrices and metal nanoparticles result in enhanced catalytic activity, stability, and selectivity, thereby offering promising solutions for addressing complex environmental challenges. The incorporation of metal nanoparticles onto biomass-derived carbon substrates not only enhances the surface area and porosity, but also facilitates electron transfer and reactive species generation, leading to efficient activation of PMS and subsequent degradation of various contaminants. The surface modification of biomass allows for precise control over surface chemistry and functional groups, further optimizing the performance of these composites for specific contaminant removal.

Author contributions

All authors have made significant contributions to the formulation and composition of this review article. Conceptualization: Sandeep Kumar, Parminder Kaur, Chou-Yi Hsu, Mohammed Ahmed Mustafa, Jyoti Rani, Jasmeen Kaur, Sandeep Kaushal; methodology: Sandeep Kumar, Parminder Kaur, Chou-Yi Hsu, Mohammed Ahmed Mustafa, Sandeep Kaushal; writing – original draft: Sandeep Kumar, Parminder Kaur, Chou-Yi Hsu, Mohammed Ahmed Mustafa, Jyoti Rani, Jasmeen Kaur, Sandeep Kaushal; visualization: Sandeep Kumar, Parminder Kaur, Chou-Yi Hsu, Mohammed Ahmed Mustafa, Sandeep Kaushal; supervision: Sandeep Kumar, Sandeep Kaushal.

Conflicts of interest

The authors declare no conflict of interest.

Abbreviations

MW	Microwave assisted
HTC	Hydrothermal carbonization
nZVI	Nanoscale zerovalent iron
BET	Brunauer–Emmett–Teller
TEM	Transmission electron microscopy
SEM	Scanning electron microscopy
XRD	X-Ray diffraction
TGA	Thermogravimetric analysis
DTA	Differential thermal analysis
EDS	Energy dispersive X-ray spectroscopy
FTIR	Fourier-transform infrared spectroscopy
XPS	X-ray photoelectron spectroscopy
EPR	Electron paramagnetic resonance
AC	Activated carbon
BC	Biochar
N-BC	Nitrogen-doped biochar
PS	Persulfate
PMS	Peroxymonosulfate
PDS	Peroxydisulfate
PI	Periodate
DFT	Density functional theory
GC–MS	Gas chromatography-mass spectrometry
LC–MS	Liquid chromatography-mass spectrometry
HRMS	High-resolution mass spectrometry

Data availability

No new data were created or analyzed in this study. Data sharing is not applicable to this article as it is a review of the existing literature.

Supplementary information (SI) is available. See DOI: **https://doi.org/10.1039/d5ma00494b**.

Acknowledgements

References

1 M. Fantini, Biomass Availability, Potential and Characteristics, in *Biorefineries*, ed. M. Rabaçal, A. F. Ferreira, C. A. M. Silva and M. Costa, Springer International Publishing, Cham, 2017, (Lecture Notes in Energy; vol. 57), pp. 21–54, DOI: **10.1007/978-3-319-48288-0_2**.

2 L. Amjith and B. Bavanish, A review on biomass and wind as renewable energy for sustainable environment, *Chemosphere*, 2022, **293**, 133579.

3 R. Phiri, S. Mavinkere Rangappa and S. Siengchin, Agrowaste for renewable and sustainable green production: A review, *J. Cleaner Prod.*, 2024, **434**, 139989.

4 A. Bhuyan and M. Ahmaruzzaman, Recent advances in new generation nanocomposite materials for adsorption of pharmaceuticals from aqueous environment, *Environ. Sci. Pollut. Res.*, 2023, **30**(14), 39377–39417.

5 M. Antar, D. Lyu, M. Nazari, A. Shah, X. Zhou and D. L. Smith, Biomass for a sustainable bioeconomy: An overview of world biomass production and utilization, *Renewable Sustainable Energy Rev.*, 2021, **139**, 110691.

6 C. Wan, G. Q. Shen and S. Choi, Waste Management Strategies for Sustainable Development, in *Encyclopedia of Sustainability in Higher Education*, ed. W. Leal Filho, Springer International Publishing, Cham, 2019, p. 1–9. Available from: **https://link.springer.com/10.1007/978-3-319-63951-2_194-1**.

7 S. Mishra, L. Cheng and A. Maiti, The utilization of agro-biomass/byproducts for effective bio-removal of dyes from dyeing wastewater: A comprehensive review, *J. Environ. Chem. Eng.*, 2021, **9**(1), 104901.

8 M. Mujtaba, L. Fernandes Fraceto, M. Fazeli, S. Mukherjee, S. M. Savassa and G. Araujo De Medeiros, *et al.*, Lignocellulosic biomass from agricultural waste to the circular economy: a review with focus on biofuels, biocomposites and bioplastics, *J. Cleaner Prod.*, 2023, **402**, 136815.

9 Y. Zhou, L. Zhang and Z. Cheng, Removal of organic pollutants from aqueous solution using agricultural wastes: A review, *J. Mol. Liq.*, 2015, **212**, 739–762.

10 M. Gale, T. Nguyen, M. Moreno and K. L. Gilliard-AbdulAziz, Physiochemical Properties of Biochar and Activated Carbon from Biomass Residue: Influence of Process Conditions to Adsorbent Properties, *ACS Omega*, 2021, **6**(15), 10224–10233.

11 A. Nayak, B. Bhushan and S. Kotnala, Fundamentals and mechanism of adsorption, *Sustainable Technologies for Remediation of Emerging Pollutants from Aqueous Environment*, 2024, pp. 29–62. Available from: **https://linkinghub.elsevier.com/retrieve/pii/B9780443186189000024**.

12 S. Kainth, P. Sharma and O. P. Pandey, Green sorbents from agricultural wastes: A review of sustainable adsorption materials, *Appl. Surf. Sci. Adv.*, 2024, **19**, 100562.

13 S. Wu, W. Shi, K. Li, J. Cai and L. Chen, Recent advances on sustainable bio-based materials for water treatment: Fabrication, modification and application, *J. Environ. Chem. Eng.*, 2022, **10**(6), 108921.

14 H. Han, M. K. Rafiq, T. Zhou, R. Xu, O. Mašek and X. Li, A critical review of clay-based composites with enhanced adsorption performance for metal and organic pollutants, *J. Hazard. Mater.*, 2019, **369**, 780–796.

15 M. Singh, Engineered Biochar-Based Nanocomposites: A Sustainable Solution for Smart Agriculture, in *Biochar-Based Nanocomposites for Contaminant Management*, ed. D. Mishra, R. Singh and P. Khare, Springer International Publishing, Cham, 2023, pp. 119–31. (Advances in Science, Technology & Innovation). Available from: **https://link.springer.com/10.1007/978-3-031-28873-9_10**.

16 S. Kumar, P. Kaur, R. S. Brar and J. N. Babu, Nanoscale zerovalent copper (nZVC) catalyzed environmental remediation of organic and inorganic contaminants: A review, *Heliyon*, 2022, **8**(8), e10140. Available from: **https://linkinghub.elsevier.com/retrieve/pii/S2405844022014281**.

17 J. Rani, T. Goyal, A. Kaur, S. Ganesan, A. K. Sharma and A. S. Chauhan, *et al.*, Bimetallic nanoparticles as pioneering eco-friendly catalysts for remediation of pharmaceuticals and personal care products (PPCPs), *Nanoscale Adv.*, 2025, **7**(11), 3160–3188, DOI: **10.1039/D5NA00151J**. Available from: .

18 P. Zhang, W. Duan, H. Peng, B. Pan and B. Xing, Functional Biochar and Its Balanced Design, *ACS Environ. Au*, 2022, **2**(2), 115–127.

19 S. M. Abegunde, K. S. Idowu, O. M. Adejuwon and T. Adeyemi-Adejolu, A review on the influence of chemical modification on the performance of adsorbents, *Resour. Environ. Sustain.*, 2020, **1**, 100001.

20 M. Eldhose, R. Roy, C. George and A. Joseph, Physical Modification of Biomass, in *Handbook of Biomass*, ed. S. Thomas, M. Hosur, D. Pasquini and C. Jose Chirayil, Springer Nature, Singapore, 2023, pp. 1–20. Available from: **https://link.springer.com/10.1007/978-981-19-6772-6_17-1**.

21 A. R. Mankar, A. Pandey, A. Modak and K. K. Pant, Pretreatment of lignocellulosic biomass: A review on recent advances, *Bioresour. Technol.*, 2021, **334**, 125235.

22 A. N. Amenaghawon, C. L. Anyalewechi, C. O. Okieimen and H. S. Kusuma, Biomass pyrolysis technologies for value-added products: a state-of-the-art review, *Environ. Dev. Sustain.*, 2021, **23**(10), 14324–14378.

23 H. S. Kambo and A. Dutta, A comparative review of biochar and hydrochar in terms of production, physico-chemical properties and applications, *Renewable Sustainable Energy Rev.*, 2015, **45**, 359–378.

24 S. Masoumi, V. B. Borugadda, S. Nanda and A. K. Dalai, Hydrochar: A Review on Its Production Technologies and Applications, *Catalysts*, 2021, **11**(8), 939.

25 J. A. Menéndez, A. Arenillas, B. Fidalgo, Y. Fernández, L. Zubizarreta and E. G. Calvo, *et al.*, Microwave heating processes involving carbon materials, *Fuel Process. Technol.*, 2010, **91**(1), 1–8.

26 W. Ao, J. Fu, X. Mao, Q. Kang, C. Ran and Y. Liu, *et al.*, Microwave assisted preparation of activated carbon from biomass: A review, *Renewable Sustainable Energy Rev.*, 2018, **92**, 958–979.

27 İ. Demiral, C. Samdan and H. Demiral, Enrichment of the surface functional groups of activated carbon by modification method, *Surf. Interfaces*, 2021, **22**, 100873.

28 Z. Heidarinejad, M. H. Dehghani, M. Heidari, G. Javedan, I. Ali and M. Sillanpää, Methods for preparation and activation of activated carbon: a review, *Environ. Chem. Lett.*, 2020, **18**(2), 393–415.

29 J. Pallarés, A. González-Cencerrado and I. Arauzo, Production and characterization of activated carbon from barley straw by physical activation with carbon dioxide and steam, *Biomass Bioenergy*, 2018, **115**, 64–73.

30 A. E. Ogungbenro, D. V. Quang, K. A. Al-Ali, L. F. Vega and M. R. M. Abu-Zahra, Synthesis and characterization of activated carbon from biomass date seeds for carbon dioxide adsorption, *J. Environ. Chem. Eng.*, 2020, **8**(5), 104257.

31 L. Suárez and T. A. Centeno, Unravelling the volumetric performance of activated carbons from biomass wastes in supercapacitors, *J. Power Sources*, 2020, **448**, 227413.

32 J. Baek, H. M. Lee, K. H. An and B. J. Kim, Preparation and characterization of highly mesoporous activated short carbon fibers from kenaf precursors, *Carbon Lett.*, 2019, **29**(4), 393–399.

33 A. Geczo, D. A. Giannakoudakis, K. Triantafyllidis, M. R. Elshaer, E. Rodríguez-Aguado and S. Bashkova, Mechanistic insights into acetaminophen removal on cashew nut shell biomass-derived activated carbons, *Environ. Sci. Pollut. Res.*, 2021, **28**(42), 58969–58982.

34 Q. Yang, P. Wu, J. Liu, S. Rehman, Z. Ahmed and B. Ruan, *et al.*, Batch interaction of emerging tetracycline contaminant with novel phosphoric acid activated corn straw porous carbon: Adsorption rate and nature of mechanism, *Environ. Res.*, 2020, **181**, 108899.

35 X. Gao, L. Wu, Z. Li, Q. Xu, W. Tian and R. Wang, Preparation and characterization of high surface area activated carbon from pine wood sawdust by fast activation with H_3PO_4 in a spouted bed, *J. Mater. Cycles Waste Manage.*, 2018, **20**(2), 925–936.

36 Y. Liu, B. Huang, X. Lin and Z. Xie, Biomass-derived hierarchical porous carbons: boosting the energy density of supercapacitors *via* an ionothermal approach, *J. Mater. Chem. A*, 2017, **5**(25), 13009–13018.

37 M. Demir, S. K. Saraswat and R. B. Gupta, Hierarchical nitrogen-doped porous carbon derived from lecithin for high-performance supercapacitors, *RSC Adv.*, 2017, **7**(67), 42430–42442.

38 X. Xing, W. Jiang, S. Li, X. Zhang and W. Wang, Preparation and analysis of straw activated carbon synergetic catalyzed by $ZnCl_2$–H_3PO_4 through hydrothermal carbonization combined with ultrasonic assisted immersion pyrolysis, *Waste Manage.*, 2019, **89**, 64–72.

39 A. K. Dey and Md Ahmaruzzaman, Recent Advances in Nano-metal Oxide-Biochar Composites for Efficient Removal of Environmental Contaminants, *Rev. Environ. Contam. Toxicol.*, 2023, **261**(1), 6.

40 P. Kaur, S. Kumar, J. Rani, J. Singh, S. Kaushal and K. Hussain, *et al.*, Rationally tailored synergy between adsorption efficiency of cotton shell activated carbon and PMS activation *via* biogenic Fe0 or Cu0 for effective mitigation of triphenylmethane dyes, *Sep. Purif. Technol.*, 2024, **342**, 127010.

41 R. Sangeetha Piriya, R. M. Jayabalakrishnan, M. Maheswari, K. Boomiraj and S. Oumabady, Coconut shell derived $ZnCl_2$ activated carbon for malachite green dye removal, *Water Sci. Technol.*, 2021, **83**(5), 1167–1182.

42 M. Ju, P. Rao, L. Yan, D. Gu, G. Li and Q. Chen, *et al.*, Synergistic adsorption and degradation of sulfamethazine by tobacco stalk-derived activated biochar: Preparation, mechanism insight and application, *J. Environ. Chem. Eng.*, 2023, **11**(3), 110265.

43 X. Liu, Z. Shao, Y. Wang, Y. Liu, S. Wang and F. Gao, *et al.*, New use for Lentinus edodes bran biochar for tetracycline removal, *Environ. Res.*, 2023, **216**, 114651.

44 Y. Qin, B. Chai, C. Wang, J. Yan, G. Fan and G. Song, Removal of tetracycline onto KOH-activated biochar derived from rape straw: Affecting factors, mechanisms and reusability inspection, *Colloids Surf., A*, 2022, **640**, 128466.

45 A. Tomczyk and K. Szewczuk-Karpisz, Effect of Biochar Modification by Vitamin C, Hydrogen Peroxide or Silver Nanoparticles on Its Physicochemistry and Tetracycline Removal, *Materials*, 2022, **15**(15), 5379.

46 J. Chen, H. Li, J. Li, F. Chen, J. Lan and H. Hou, Efficient removal of tetracycline from water by tannic acid-modified rice straw-derived biochar:Kinetics and mechanisms, *J. Mol. Liq.*, 2021, **340**, 117237.

47 J. Hoslett, H. Ghazal, E. Katsou and H. Jouhara, The removal of tetracycline from water using biochar produced from agricultural discarded material, *Sci. Total Environ.*, 2021, **751**, 141755.

48 P. Zhang, Y. Li, Y. Cao and L. Han, Characteristics of tetracycline adsorption by cow manure biochar prepared at different pyrolysis temperatures, *Bioresour. Technol.*, 2019, **285**, 121348.

49 D. Chen, S. Xie, C. Chen, H. Quan, L. Hua and X. Luo, *et al.*, Activated biochar derived from pomelo peel as a high-capacity sorbent for removal of carbamazepine from aqueous solution, *RSC Adv.*, 2017, **7**(87), 54969–54979.

50 Y. Cao, W. Xiao, G. Shen, G. Ji, Y. Zhang and C. Gao, *et al.*, Carbonization and ball milling on the enhancement of Pb(II) adsorption by wheat straw: Competitive effects of ion exchange and precipitation, *Bioresour. Technol.*, 2019, **273**, 70–76.

51 P. Kaur, Kalpana, S. Kumar, A. Kumar and A. Kumar, Effect of various sodium hydroxide treatment parameters on the adsorption efficiency of rice husk for removal of methylene blue from water, *Emergent Mater.*, 2023, **6**(6), 1809–1824.

52 D. Jiang, H. Li, X. Cheng, Q. Ling, H. Chen and B. Barati, *et al.*, A mechanism study of methylene blue adsorption on seaweed biomass derived carbon: From macroscopic to microscopic scale, *Process Saf. Environ. Prot.*, 2023, **172**, 1132–1143.

53 H. Ye, Q. Zhu and D. Du, Adsorptive removal of Cd(II) from aqueous solution using natural and modified rice husk, *Bioresour. Technol.*, 2010, **101**(14), 5175–5179.

54 A. Yurtay and M. Kılıç, Biomass-based activated carbon by flash heating as a novel preparation route and its application in high efficiency adsorption of metronidazole, *Diamond Relat. Mater.*, 2023, **131**, 109603.

55 M. Bouzidi, L. Sellaoui, M. Mohamed, D. S. P. Franco, A. Erto and M. Badawi, A comprehensive study on paracetamol and ibuprofen adsorption onto biomass-derived activated carbon through experimental and theoretical assessments, *J. Mol. Liq.*, 2023, **376**, 121457.

56 S. Kandasamy, N. Madhusoodanan, P. Senthilkumar, V. Muneeswaran, N. Manickam and V. R. Myneni, Adsorption of methylene blue dye by animal dung biomass–derived activated carbon: optimization, isotherms and kinetic studies, *Biomass Convers. Biorefin.*, 2023, 1–15, DOI: 10.1007/s13399-023-04710-y.

57 C. Cui, M. Yang, J. Zhai, W. Bai, L. Dai and L. Liu, *et al.*, Bamboo cellulose–derived activated carbon aerogel with controllable mesoporous structure as an effective adsorbent for tetracycline hydrochloride, *Environ. Sci. Pollut. Res.*, 2022, **30**(5), 12558–12570.

58 Y. Zhang, L. Cheng and Y. Ji, A novel amorphous porous biochar for adsorption of antibiotics: Adsorption mechanism analysis *via* experiment coupled with theoretical calculations, *Chem. Eng. Res. Des.*, 2022, **186**, 362–373.

59 P. Srinivasan, A. John Bosco, R. Kalaivizhi, J. Arockia Selvi and P. Sivakumar, Adsorption isotherm and kinetic study of Direct Orange 102 dyes on TNJ activated carbon, *Mater. Today: Proc.*, 2021, **34**, 389–394.

60 M. F. M. Yusop, M. A. Ahmad, N. A. Rosli and M. E. A. Manaf, Adsorption of cationic methylene blue dye using microwave-assisted activated carbon derived from acacia wood: Optimization and batch studies, *Arabian J. Chem.*, 2021, **14**(6), 103122.

61 M. Abatal, I. Anastopoulos, D. A. Giannakoudakis and M. T. Olguin, Carbonaceous material obtained from bark biomass as adsorbent of phenolic compounds from aqueous solutions, *J. Environ. Chem. Eng.*, 2020, **8**(3), 103784.

62 A. O. Abo El Naga, M. El Saied, S. A. Shaban and F. Y. El Kady, Fast removal of diclofenac sodium from aqueous solution using sugar cane bagasse-derived activated carbon, *J. Mol. Liq.*, 2019, **285**, 9–19.

63 K. Huang, S. Yang, X. Liu, C. Zhu, F. Qi and K. Wang, *et al.*, Adsorption of antibiotics from wastewater by cabbage-based N, P co-doped mesoporous carbon materials, *J. Cleaner Prod.*, 2023, **391**, 136174.

64 Y. A. B. Neolaka, Y. Lawa, J. Naat, A. A. P. Riwu, H. Darmokoesoemo and B. A. Widyaningrum, *et al.*, Indonesian Kesambi wood (Schleichera oleosa) activated with pyrolysis and H$_2$SO$_4$ combination methods to produce mesoporous activated carbon for Pb(II) adsorption from aqueous solution, *Environ. Technol. Innovation*, 2021, **24**, 101997.

65 S. M. Kharrazi, M. Soleimani, M. Jokar, T. Richards, A. Pettersson and N. Mirghaffari, Pretreatment of lignocellulosic waste as a precursor for synthesis of high porous activated carbon and its application for Pb(II) and Cr(VI) adsorption from aqueous solutions, *Int. J. Biol. Macromol.*, 2021, **180**, 299–310.

66 C. O. Thompson, A. O. Ndukwe and C. O. Asadu, Application of activated biomass waste as an adsorbent for the removal of lead(II) ion from wastewater, *Emerging Contam.*, 2020, **6**, 259–267.

67 S. A. Sajjadi, A. Mohammadzadeh, H. N. Tran, I. Anastopoulos, G. L. Dotto and Z. R. Lopičić, *et al.*, Efficient mercury removal from wastewater by pistachio wood wastes-derived activated carbon prepared by chemical activation using a novel activating agent, *J. Environ. Manage.*, 2018, **223**, 1001–1009.

68 S. Norouzi, M. Heidari, V. Alipour, O. Rahmanian, M. Fazlzadeh and F. Mohammadi-moghadam, *et al.*, Preparation, characterization and Cr(VI) adsorption evaluation of NaOH-activated carbon produced from Date Press Cake; an agro-industrial waste, *Bioresour. Technol.*, 2018, **258**, 48–56.

69 B. D. Gebrewold, P. Kijjanapanich, E. R. Rene, P. N. L. Lens and A. P. Annachhatre, Fluoride removal from groundwater using chemically modified rice husk and corn cob activated carbon, *Environ. Technol.*, 2019, **40**(22), 2913–2927.

70 E. Vunain, D. Kenneth and T. Biswick, Synthesis and characterization of low-cost activated carbon prepared from Malawian baobab fruit shells by H$_3$PO$_4$ activation for removal of Cu(II) ions: equilibrium and kinetics studies, *Appl. Water Sci.*, 2017, **7**(8), 4301–4319.

71 L. Xu, Z. Ye, Y. Pan, Y. Zhang, H. Gong and X. Mei, *et al.*, Effect of lignocellulosic biomass composition on the performance of biochar for the activation of peroxymonosulfate to degrade diclofenac, *Sep. Purif. Technol.*, 2023, **311**, 123312.

72 S. Dong, X. Shen, Q. Guo, H. Cheng, S. Giannakis and Z. He, *et al.*, Valorization of soybean plant wastes in preparation of N-doped biochar for catalytic ozonation of organic contaminants: Atrazine degradation performance and mechanistic considerations, *Chem. Eng. J.*, 2023, **472**, 145153.

73 R. Kumar Mishra, B. Singh and B. Acharya, A comprehensive review on activated carbon from pyrolysis of lignocellulosic biomass: An application for energy and the environment, *Carbon Resour. Convers.*, 2024, **7**(4), 100228.

74 S. Mishra and R. K. Upadhyay, Review on biomass gasification: Gasifiers, gasifying mediums, and operational parameters, *Mater. Sci. Energy Technol.*, 2021, **4**, 329–340.

75 C. Jiang, G. A. Yakaboylu, T. Yumak, J. W. Zondlo, E. M. Sabolsky and J. Wang, Activated carbons prepared by indirect and direct CO$_2$ activation of lignocellulosic biomass for supercapacitor electrodes, *Renewable Energy*, 2020, **155**, 38–52.

76 A. E. Ogungbenro, D. V. Quang, K. A. Al-Ali, L. F. Vega and M. R. M. Abu-Zahra, Synthesis and characterization of

activated carbon from biomass date seeds for carbon dioxide adsorption, *J. Environ. Chem. Eng.*, 2020, **8**(5), 104257. Available from: https://linkinghub.elsevier.com/retrieve/pii/S2213343720306060.

77 Y. Zhong, Y. Wang, Y. Ji, X. Zhang and X. Wang, Biomass carbon-based composites for adsorption/photocatalysis degradation of VOCs: A comprehensive review, *Colloid Interface Sci Commun.*, 2023, **57**, 100749.

78 M. Mazarji, M. T. Bayero, T. Minkina, S. Sushkova, S. Mandzhieva and T. V. Bauer, *et al.*, Nanomaterials in biochar: Review of their effectiveness in remediating heavy metal-contaminated soils, *Sci. Total Environ.*, 2023, **880**, 163330.

79 L. Lu, W. Yu, Y. Wang, K. Zhang, X. Zhu and Y. Zhang, *et al.*, Application of biochar-based materials in environmental remediation: from multi-level structures to specific devices, *BioChar*, 2020, **2**(1), 1–31.

80 M. S. Chavali and M. P. Nikolova, Metal oxide nanoparticles and their applications in nanotechnology, *SN Appl. Sci.*, 2019, **1**(6), 607.

81 F. H. Isikgor and C. R. Becer, Lignocellulosic biomass: a sustainable platform for the production of bio-based chemicals and polymers, *Polym. Chem.*, 2015, **6**(25), 4497–4559.

82 A. M. Joseph, Chemical Modifications of Biomass, in *Handbook of Biomass*, ed. S. Thomas, M. Hosur, D. Pasquini and C. Jose Chirayil, Springer Nature, Singapore, 2023, pp. 1–29. Available from: https://link.springer.com/10.1007/978-981-19-6772-6_18-1.

83 P. R. Yaashikaa, P. S. Kumar, S. Varjani and A. Saravanan, A critical review on the biochar production techniques, characterization, stability and applications for circular bioeconomy, *Biotechnol. Rep.*, 2020, **28**, e00570.

84 A. V. Rane, K. Kanny, V. K. Abitha and S. Thomas, Methods for Synthesis of Nanoparticles and Fabrication of Nanocomposites, *Synth. Inorg. Nanomater.*, 2018, 121–139. Available from: https://linkinghub.elsevier.com/retrieve/pii/B9780081019757000051.

85 P. Zhang, P. J. Zhang, S. Feng, H. Li, J. Li and W. Du, *et al.*, The mechanism of p-nitrophenol degradation by dissolved organic matter derived from biochar, *Sci. Total Environ.*, 2023, **868**, 161693.

86 P. Kaur, S. Kumar, J. Rani, J. N. Babu and S. Mittal, Comparison of surface adsorption efficacies of eco-sustainable agro/animal biomass-derived activated carbon for the removal of rhodamine B and hexavalent chromium, *Environ. Sci. Pollut. Res.*, 2024, **31**(39), 52371–52390, DOI: 10.1007/s11356-024-34686-9. Available from: .

87 G. Sargazi, D. Afzali, A. Mostafavi, A. Shadman, B. Rezaee and P. Zarrintaj, *et al.*, Chitosan/polyvinyl alcohol nanofibrous membranes: towards green super-adsorbents for toxic gases, *Heliyon*, 2019, **5**(4), e01527.

88 S. Kumar, R. S. Brar, S. Saha, A. Dahiya, Kalpana and J. N. Babu, Synergistic effect of eco-friendly pistachio shell biomass on nano-MnO$_2$ for crystal violet removal: kinetic and equilibrium studies, *Int. J. Environ. Sci. Technol.*, 2023, **20**(5), 5123–5140.

89 K. S. W. Sing, Physisorption of nitrogen by porous materials, *J. Porous Mater.*, 1995, **2**(1), 5–8.

90 J. Bedia, M. Peñas-Garzón, A. Gómez-Avilés, J. Rodriguez and C. Belver, A Review on the Synthesis and Characterization of Biomass-Derived Carbons for Adsorption of Emerging Contaminants from Water, *C*, 2018, **4**(4), 63.

91 C. Schlumberger and M. Thommes, Characterization of Hierarchically Ordered Porous Materials by Physisorption and Mercury Porosimetry—A Tutorial Review, *Adv. Mater. Interfaces*, 2021, **8**(4), 2002181.

92 O. Oginni, K. Singh, G. Oporto, B. Dawson-Andoh, L. McDonald and E. Sabolsky, Effect of one-step and two-step H$_3$PO$_4$ activation on activated carbon characteristics, *Bioresour. Technol. Rep.*, 2019, **8**, 100307.

93 A. V. Girão, G. Caputo and M. C. Ferro, Application of Scanning Electron Microscopy–Energy Dispersive X-Ray Spectroscopy (SEM-EDS), *Compr. Anal. Chem.*, 2017, **75**, 153–168. Available from: https://linkinghub.elsevier.com/retrieve/pii/S0166526X16301519.

94 Y. Shao, J. Li, X. Fang, Z. Yang, Y. Qu and M. Yang, *et al.*, Chemical modification of bamboo activated carbon surface and its adsorption property of simultaneous removal of phosphate and nitrate, *Chemosphere*, 2022, **287**, 132118.

95 L. S. Maia, A. I. C. Da Silva, E. S. Carneiro, F. M. Monticelli, F. R. Pinhati and D. R. Mulinari, Activated Carbon From Palm Fibres Used as an Adsorbent for Methylene Blue Removal, *J. Polym. Environ.*, 2021, **29**(4), 1162–1175.

96 Y. Chen, Z. Wang, S. Lin, Y. Qin and X. Huang, A review on biomass thermal-oxidative decomposition data and machine learning prediction of thermal analysis, *Clean Mater.*, 2023, **9**, 100206.

97 R. R. Nair, M. M. Mondal, S. V. Srinivasan and D. Weichgrebe, Biochar Synthesis from Mineral- and Ash-Rich Waste Biomass, Part 1: Investigation of Thermal Decomposition Mechanism during Slow Pyrolysis, *Materials*, 2022, **15**(12), 4130.

98 K. Akhtar, F. Ali, S. Sohni, T. Kamal, A. M. Asiri and E. M. Bakhsh, *et al.*, Lignocellulosic biomass supported metal nanoparticles for the catalytic reduction of organic pollutants, *Environ. Sci. Pollut. Res.*, 2020, **27**(1), 823–836.

99 Q. Tang, X. Meng, W. Bao, Y. Fan, Y. Gao and Y. Sun, *et al.*, Synergistic activation of peroxymonosulfate by nitrogen-doped biochar loaded with mixed-valence iron nanoparticles for tetracycline degradation, *Colloids Surf., A*, 2023, **669**, 131490.

100 L. Zhang, L. y Tu, Y. Liang, Q. Chen, Z. s Li and C. h Li, *et al.*, Coconut-based activated carbon fibers for efficient adsorption of various organic dyes, *RSC Adv.*, 2018, **8**(74), 42280–42291.

101 X. Liu, Q. Li, Y. Zhang, F. Zhong, X. Ding and Z. Yu, Synthesis of micro-mesoporous hierarchical structure of coal-based activated carbon and its effect on methane adsorption, *Fuel*, 2024, **365**, 131239.

102 H. N. Tran, F. Tomul, N. Thi Hoang Ha, D. T. Nguyen, E. C. Lima and G. T. Le, *et al.*, Innovative spherical biochar for pharmaceutical removal from water: Insight into

adsorption mechanism, *J. Hazard. Mater.*, 2020, **394**, 122255.

103 A. T. Vo, V. P. Nguyen, A. Ouakouak, A. Nieva, B. T. Doma and H. N. Tran, *et al.*, Efficient Removal of Cr(vi) from Water by Biochar and Activated Carbon Prepared through Hydrothermal Carbonization and Pyrolysis: Adsorption-Coupled Reduction Mechanism, *Water*, 2019, **11**(6), 1164.

104 T. M. Pérez-Millán, D. I. Mendoza-Castillo, I. A. Aguayo-Villarreal, C. K. Rojas-Mayorga, F. Villanueva-Mejía and A. Bonilla-Petriciolet, Application of DFT and Response Surface Models to analyze the adsorption process of basic blue 3 and reactive blue 19 dyes on sugarcane bagasse and coconut endocarp biomass, *J. Mol. Struct.*, 2023, **1287**, 135658.

105 P. Kaur, K. Hussain, A. Kumar, J. Singh, J. Nagendra Babu and S. Kumar, Evaluation of synergistic adsorption approach for terbinafine removal by cotton shell powder immobilized zerovalent copper: Adsorption kinetics and DFT simulation, *Environ. Nanotechnol., Monit. Manage.*, 2023, **20**, 100875.

106 B. Yardımcı and N. Kanmaz, An effective-green strategy of methylene blue adsorption: Sustainable and low-cost waste cinnamon bark biomass enhanced *via* MnO₂, *J. Environ. Chem. Eng.*, 2023, **11**(3), 110254.

107 K. Al-Mokhalelati, I. Al-Bakri and N. Al Shibeh Al Wattar, Adsorption of methylene blue onto sugarcane bagasse-based adsorbent materials, *J. Phys. Org. Chem.*, 2021, **34**(7), e4193.

108 R. Tang, C. Dai, C. Li, W. Liu, S. Gao and C. Wang, Removal of Methylene Blue from Aqueous Solution Using Agricultural Residue Walnut Shell: Equilibrium, Kinetic, and Thermodynamic Studies, *J. Chem.*, 2017, **2017**, 1–10.

109 M. J. Uddin, R. E. Ampiaw and W. Lee, Adsorptive removal of dyes from wastewater using a metal-organic framework: A review, *Chemosphere*, 2021, **284**, 131314.

110 H. Deng, J. Lu, G. Li, G. Zhang and X. Wang, Adsorption of methylene blue on adsorbent materials produced from cotton stalk, *Chem. Eng. J.*, 2011, **172**(1), 326–334.

111 M. Ertaş, B. Acemioğlu, M. H. Alma and M. Usta, Removal of methylene blue from aqueous solution using cotton stalk, cotton waste and cotton dust, *J. Hazard. Mater.*, 2010, **183**(1–3), 421–427.

112 A. Ali Redha, Removal of heavy metals from aqueous media by biosorption, *Arab. J. Basic Appl. Sci.*, 2020, **27**(1), 183–193.

113 M. Kebir, H. Tahraoui, M. Chabani, M. Trari, N. Noureddine and A. A. Assadi, *et al.*, Water Cleaning by a Continuous Fixed-Bed Column for Cr(vi) Eco-Adsorption with Green Adsorbent-Based Biomass: An Experimental Modeling Study, *Processes*, 2023, **11**(2), 363.

114 M. Mahmood-ul-Hassan, V. Suthor, E. Rafique and M. Yasin, Removal of Cd, Cr, and Pb from aqueous solution by unmodified and modified agricultural wastes, *Environ. Monit. Assess.*, 2015, **187**(2), 19.

115 M. Akram, B. Khan, M. Imran, I. Ahmad, H. Ajaz and M. Tahir, *et al.*, Biosorption of lead by cotton shells powder: Characterization and equilibrium modeling study, *Int. J. Phytorem.*, 2019, **21**(2), 138–144.

116 M. Banerjee, N. Bar, R. K. Basu and S. K. Das, Removal of Cr(vi) from Its Aqueous Solution Using Green Adsorbent Pistachio Shell: a Fixed Bed Column Study and GA-ANN Modeling, *Water Conserv. Sci. Eng.*, 2018, **3**(1), 19–31.

117 B. A. Ezeonuegbu, D. A. Machido, C. M. Z. Whong, W. S. Japhet, A. Alexiou and S. T. Elazab, *et al.*, Agricultural waste of sugarcane bagasse as efficient adsorbent for lead and nickel removal from untreated wastewater: Biosorption, equilibrium isotherms, kinetics and desorption studies, *Biotechnol. Rep.*, 2021, **30**, e00614.

118 C. J. S. Varsihini, D. Das and N. Das, Optimization of parameters for cerium(iii) biosorption onto biowaste materials of animal and plant origin using 5-level Box-Behnken design: Equilibrium, kinetic, thermodynamic and regeneration studies, *J. Rare Earths*, 2014, **32**(8), 745–758.

119 S. L. P. Dias, C. L. Neto, V. G. Ferreira, J. C. P. Vaghetti, G. B. Machado and O. Bianchi, Exploring the thermal degradation of pine nut shells: a study on biochar production and its efficacy in cationic dye adsorption from water, *Biomass Convers. Biorefin.*, 2024, **15**(4), 5975–5995, DOI: **10.1007/s13399-024-05470-z**.

120 X. Yang, L. Wang, X. Shao, J. Tong, J. Zhou and Y. Feng, *et al.*, Characteristics and aqueous dye removal ability of novel biosorbents derived from acidic and alkaline one-step ball milling of hickory wood, *Chemosphere*, 2022, **309**, 136610.

121 P. L. Homagai, R. Poudel, S. Poudel and A. Bhattarai, Adsorption and removal of crystal violet dye from aqueous solution by modified rice husk, *Heliyon*, 2022, **8**(4), e09261.

122 W. Astuti, T. Sulistyaningsih, D. Prastiyanto, Rusiyanto, Lanjar and F. I. Riayanti, *et al.*, Influence of lignocellulosic composition in biomass waste on the microstructure and dye adsorption characteristics of microwave-assisted ZnCl₂ activated carbon, *Biomass Convers. Biorefin.*, 2023, **14**, 16681–16697, DOI: **10.1007/s13399-023-04281-y**.

123 O. J. Al-sareji, M. Meiczinger, R. A. Al-Juboori, R. A. Grmasha, M. Andredaki and V. Somogyi, *et al.*, Efficient removal of pharmaceutical contaminants from water and wastewater using immobilized laccase on activated carbon derived from pomegranate peels, *Sci. Rep.*, 2023, **13**(1), 11933.

124 L. Baloo, M. H. Isa, N. B. Sapari, A. H. Jagaba, L. J. Wei and S. Yavari, *et al.*, Adsorptive removal of methylene blue and acid orange 10 dyes from aqueous solutions using oil palm wastes-derived activated carbons, *Alexandria Eng. J.*, 2021, **60**(6), 5611–5629.

125 E. M. El Mouchtari, C. Daou, S. Rafqah, F. Najjar, H. Anane and A. Piram, *et al.*, TiO₂ and activated carbon of Argania Spinosa tree nutshells composites for the adsorption photocatalysis removal of pharmaceuticals from aqueous solution, *J. Photochem. Photobiol., A*, 2020, **388**, 112183.

126 T. M. Darweesh and M. J. Ahmed, Batch and fixed bed adsorption of levofloxacin on granular activated carbon from date (*Phoenix dactylifera L.*) stones by KOH chemical activation, *Environ. Toxicol. Pharmacol.*, 2017, **50**, 159–166.

127 K. W. Jung, B. H. Choi, M. J. Hwang, T. U. Jeong and K. H. Ahn, Fabrication of granular activated carbons derived from spent coffee grounds by entrapment in calcium alginate beads for adsorption of acid orange 7 and methylene blue, *Bioresour. Technol.*, 2016, **219**, 185–195.

128 A. M. Elewa, A. A. Amer, M. F. Attallah, H. A. Gad, Z. A. M. Al-Ahmed and I. A. Ahmed, Chemically Activated Carbon Based on Biomass for Adsorption of Fe(III) and Mn(II) Ions from Aqueous Solution, *Materials*, 2023, **16**(3), 1251.

129 Y. Wang, C. Peng, E. Padilla-Ortega, A. Robledo-Cabrera and A. López-Valdivieso, Cr(VI) adsorption on activated carbon: Mechanisms, modeling and limitations in water treatment, *J. Environ. Chem. Eng.*, 2020, **8**(4), 104031.

130 M. Á. Salomón-Negrete, H. E. Reynel-Ávila, D. I. Mendoza-Castillo, A. Bonilla-Petriciolet and C. J. Duran-Valle, Water defluoridation with avocado-based adsorbents: Synthesis, physicochemical characterization and thermodynamic studies, *J. Mol. Liq.*, 2018, **254**, 188–197.

131 P. Thamarai, S. Karishma, V. C. Deivayanai, A. Saravanan and P. R. Yaashikaa, Theoretical and Experimental Analysis of Pb(II) Ion Adsorption Using Surface Modified Macroalgal Biosorbents: Modelling and Desorption Study, *Ind. Eng. Chem. Res.*, 2024, **63**(49), 21505–21518, DOI: **10.1021/acs.iecr.4c02591**. Available from: .

132 P. Thamarai, V. C. Deivayanai, P. Swaminaathan, S. Karishma and A. S. Vickram, *et al.*, Experimental investigation of Cd(II) ion adsorption on surface-modified mixed seaweed Biosorbent: A study on analytical interpretation and thermodynamics, *Environ. Res.*, 2024, **260**, 119670. Available from: **https://linkinghub.elsevier.com/retrieve/pii/S0013935124015755**.

133 Q. Zhou, L. Qin, H. Liu, D. Zhao, M. Yang and B. Sun, *et al.*, Microwave assisted biomass derived carbon aerogel for highly efficient oxytetracycline hydrochloride degradation: Singlet oxygen mechanism and C vacancies accelerated electron transfer, *Chem. Eng. J.*, 2024, **487**, 150370.

134 S. Zeng, K. Li, X. Xu, J. Zhang and Y. Xue, Efficiently catalytic degradation of tetracycline *via* persulfate activation with plant-based biochars: Insight into endogenous mineral self-template effect and pyrolysis catalysis, *Chemosphere*, 2023, **337**, 139309.

135 X. Hou, H. Dong, Y. Li, J. Xiao, Q. Dong and S. Xiang, *et al.*, Activation of persulfate by graphene/biochar composites for phenol degradation: Performance and nonradical dominated reaction mechanism, *J. Environ. Chem. Eng.*, 2023, **11**(2), 109348.

136 J. Dai, Z. Wang, K. Chen, D. Ding, S. Yang and T. Cai, Applying a novel advanced oxidation process of biochar activated periodate for the efficient degradation of bisphenol A: Two nonradical pathways, *Chem. Eng. J.*, 2023, **453**, 139889.

137 W. Wang and M. Chen, Catalytic degradation of sulfamethoxazole by peroxymonosulfate activation system composed of nitrogen-doped biochar from pomelo peel: Important roles of defects and nitrogen, and detoxification of intermediates, *J. Colloid Interface Sci.*, 2022, **613**, 57–70.

138 Y. Gao, Y. Chen, T. Song, R. Su and J. Luo, Activated peroxymonosulfate with ferric chloride-modified biochar to degrade bisphenol A: Characteristics, influencing factors, reaction mechanism and reuse performance, *Sep. Purif. Technol.*, 2022, **300**, 121857.

139 Y. Hu, D. Chen, R. Zhang, Y. Ding, Z. Ren and M. Fu, *et al.*, Singlet oxygen-dominated activation of peroxymonosulfate by passion fruit shell derived biochar for catalytic degradation of tetracycline through a non-radical oxidation pathway, *J. Hazard. Mater.*, 2021, **419**, 126495.

140 S. Cai, Q. Zhang, Z. Wang, S. Hua, D. Ding and T. Cai, *et al.*, Pyrrolic N-rich biochar without exogenous nitrogen doping as a functional material for bisphenol A removal: Performance and mechanism, *Appl. Catal., B*, 2021, **291**, 120093.

141 L. Xu, C. Wu, P. Liu, X. Bai, X. Du and P. Jin, *et al.*, Peroxymonosulfate activation by nitrogen-doped biochar from sawdust for the efficient degradation of organic pollutants, *Chem. Eng. J.*, 2020, **387**, 124065.

142 D. Ding, S. Yang, X. Qian, L. Chen and T. Cai, Nitrogen-doping positively whilst sulfur-doping negatively affect the catalytic activity of biochar for the degradation of organic contaminant, *Appl. Catal., B*, 2020, **263**, 118348.

143 Y. Li, J. Yang, M. Zhang, Z. Yang, K. Shih and G. G. Ying, *et al.*, Coupled Adsorption and Surface-Bound Radical-Mediated Oxidation on Biomass-Derived Porous Carbon: A Selective Approach for Sulfamethoxazole Removal, *Chem. Eng. J.*, 2023, **452**, 139484.

144 S. Kumar, R. S. Brar, J. N. Babu, A. Dahiya, S. Saha and A. Kumar, Synergistic effect of pistachio shell powder and nano-zerovalent copper for chromium remediation from aqueous solution, *Environ. Sci. Pollut. Res.*, 2021, **28**(44), 63422–63436.

145 P. Kaur, A. Kumar, J. N. Babu and S. Kumar, Tetracycline removal *via* three-way synergy between pistachio shell powder, zerovalent copper or iron, and peroxymonosulfate activation, *J. Hazard. Mater. Adv.*, 2023, **12**, 100385.

146 S. Sutradhar, A. Mondal, F. Kuehne, O. Krueger, S. K. Rakshit and K. Kang, Comparison of Oil-Seed Shell Biomass-Based Biochar for the Removal of Anionic Dyes—Characterization and Adsorption Efficiency Studies, *Plants*, 2024, **13**(6), 820.

147 K. Qu, L. Huang, S. Hu, C. Liu, Q. Yang and L. Liu, *et al.*, TiO$_2$ supported on rice straw biochar as an adsorptive and photocatalytic composite for the efficient removal of ciprofloxacin in aqueous matrices, *J. Environ. Chem. Eng.*, 2023, **11**(2), 109430.

148 T. K. Sen, Application of Synthesized Biomass Bamboo Charcoal–Iron Oxide ''BC/Fe'' Nanocomposite Adsorbents in the Removal of Cationic Methylene Blue Dye Contaminants from Wastewater by Adsorption, *Sustainability*, 2023, **15**(11), 8841.

149 R. K. Do Nascimento, B. S. Damasceno, A. N. De Melo, P. H. M. De Farias, J. V. F. L. Cavalcanti and D. C. S. Sales, *et al.*, Hybrid nanomaterial from pyrolyzed biomass and

Fe₃O₄ magnetic nanoparticles for the adsorption of textile dyes, *Cellulose*, 2023, **30**(4), 2483–2501.

150 J. Dai, X. Meng, Y. Zhang and Y. Huang, Effects of modification and magnetization of rice straw derived biochar on adsorption of tetracycline from water, *Bioresour. Technol.*, 2020, **311**, 123455.

151 D. Hao, Y. Chen, Y. Zhang and N. You, Nanocomposites of zero-valent iron@biochar derived from agricultural wastes for adsorptive removal of tetracyclines, *Chemosphere*, 2021, **284**, 131342.

152 J. Nyirenda, G. Kalaba and O. Munyati, Synthesis and characterization of an activated carbon-supported silver-silica nanocomposite for adsorption of heavy metal ions from water, *Results Eng.*, 2022, **15**, 100553.

153 N. Masoudian, M. Rajabi and M. Ghaedi, Titanium oxide nanoparticles loaded onto activated carbon prepared from bio-waste watermelon rind for the efficient ultrasonic-assisted adsorption of congo red and phenol red dyes from wastewaters, *Polyhedron*, 2019, **173**, 114105.

154 E. Altıntıg, H. Altundag, M. Tuzen and A. Sarı, Effective removal of methylene blue from aqueous solutions using magnetic loaded activated carbon as novel adsorbent, *Chem. Eng. Res. Des.*, 2017, **122**, 151–163.

155 J. Saini, V. K. Garg, R. K. Gupta and N. Kataria, Removal of Orange G and Rhodamine B dyes from aqueous system using hydrothermally synthesized zinc oxide loaded activated carbon (ZnO-AC), *J. Environ. Chem. Eng.*, 2017, **5**(1), 884–892.

156 Y. Liu, S. P. Sohi, S. Liu, J. Guan, J. Zhou and J. Chen, Adsorption and reductive degradation of Cr(vi) and TCE by a simply synthesized zero valent iron magnetic biochar, *J. Environ. Manage.*, 2019, **235**, 276–281.

157 L. Qian, S. Liu, W. Zhang, Y. Chen, D. Ouyang and L. Han, *et al.*, Enhanced reduction and adsorption of hexavalent chromium by palladium and silicon rich biochar supported nanoscale zero-valent iron, *J. Colloid Interface Sci.*, 2019, **533**, 428–436.

158 H. Zhang, Y. Ruan, A. Liang, K. Shih, Z. Diao and M. Su, *et al.*, Carbothermal reduction for preparing nZVI/BC to extract uranium: Insight into the iron species dependent uranium adsorption behavior, *J. Cleaner Prod.*, 2019, **239**, 117873.

159 X. Shang, L. Yang, D. Ouyang, B. Zhang, W. Zhang and M. Gu, *et al.*, Enhanced removal of 1,2,4-trichlorobenzene by modified biochar supported nanoscale zero-valent iron and palladium, *Chemosphere*, 2020, **249**, 126518.

160 L. Han, J. Yan, L. Qian, W. Zhang and M. Chen, Multifunctional Pd/Fe-biochar composites for the complete removal of trichlorobenzene and its degradation products, *J. Environ. Manage.*, 2019, **245**, 238–244.

161 H. Wu, Q. Feng, P. Lu, M. Chen and H. Yang, Degradation mechanisms of cefotaxime using biochar supported Co/Fe bimetallic nanoparticles, *Environ. Sci.: Water Res. Technol.*, 2018, **4**(7), 964–975.

162 F. Reguyal and A. K. Sarmah, Adsorption of sulfamethoxazole by magnetic biochar: Effects of pH, ionic strength,

163 natural organic matter and 17α-ethinylestradiol, *Sci. Total Environ.*, 2018, **628–629**, 722–730.

163 H. Wu, Q. Feng, H. Yang, E. Alam, B. Gao and D. Gu, Modified biochar supported Ag/Fe nanoparticles used for removal of cephalexin in solution: Characterization, kinetics and mechanisms, *Colloids Surf., A*, 2017, **517**, 63–71.

164 H. Li, Y. F. Qiu, X. L. Wang, J. Yang, Y. J. Yu, Y. Q. Chen and Y. D. Liu, Biochar supported Ni/Fe bimetallic nanoparticles to remove 1,1,1-trichloroethane under various reaction conditions, *Chemosphere*, 2017, **169**, 534–541.

165 S. Y. Oh, Y. D. Seo, K. S. Ryu, D. J. Park and S. H. Lee, Redox and catalytic properties of biochar-coated zero-valent iron for the removal of nitro explosives and halogenated phenols, *Environ. Sci.:Processes Impacts*, 2017, **19**(5), 711–719.

166 Y. Yi, J. Wu, Y. Wei, Z. Fang and E. P. Tsang, The key role of biochar in the rapid removal of decabromodiphenyl ether from aqueous solution by biochar-supported Ni/Fe bimetallic nanoparticles, *J. Nanopart. Res.*, 2017, **19**(7), 245.

167 Y. Chai, M. Bai, A. Chen, X. Xu, Z. Tong and J. Yuan, *et al.*, Upcycling contaminated biomass into metal-supported heterogeneous catalyst for electro-Fenton degradation of thiamethoxam: Preparation, mechanisms, and implications, *Chem. Eng. J.*, 2023, **453**, 139814.

168 H. Tian, S. Peng, L. Zhao, Y. Chen and K. Cui, Simultaneous adsorption of Cd(ii) and degradation of OTC by activated biochar with ferrate: Efficiency and mechanism, *J. Hazard. Mater.*, 2023, **447**, 130711.

169 B. Zhang and D. Wang, Preparation of Biomass Activated Carbon Supported Nanoscale Zero-Valent Iron (nZVI) and Its Application in Decolorization of Methyl Orange from Aqueous Solution, *Water*, 2019, **11**(8), 1671.

170 X. Li, C. Wang, X. Chen, D. Li and Q. Jin, Enhanced oxidation and removal of As(iii) from water using biomass-derived porous carbon-supported nZVI with high iron utilization and fast adsorption, *J. Environ. Chem. Eng.*, 2023, **11**(1), 109038.

171 Z. Li, S. Deng, Q. An, B. Zhao, Z. Yang and B. Xu, *et al.*, Enhanced activation of persulfate by modified red mud biochar for degradation of dye pollutant: Resource utilization and non-radical activation, *J. Environ. Manage.*, 2024, **353**, 120181.

172 H. Qu, L. Chen, F. Yang, J. Zhu, C. Qi and G. Peng, Synthesis of an Environmentally Friendly Modified Mulberry Branch-Derived Biochar Composite: High Degradation Efficiency of BPA and Mitigation of Toxicity in Silkworm Larvae, *Int. J. Mol. Sci.*, 2023, **24**(4), 3609.

173 G. Seo, S. Annamalai and W. S. Shin, Enhancement of peroxydisulfate activation by inherent nature of Fe–N–P/C biochar derived from Capsosiphon fulvescens as a green biomass material for organic pollutants degradation, *Chem. Eng. J.*, 2023, **475**, 146445.

174 Z. Yang, Q. An, S. Deng, B. Xu, Z. Li and S. Deng, *et al.*, Efficient activation of peroxydisulfate by modified red mud biochar derived from waste corn straw for levofloxacin

degradation: Efficiencies and mechanisms, *J. Environ. Chem. Eng.*, 2023, **11**(6), 111609.

175 H. Tian, K. Cui, S. Sun, J. Liu and M. Cui, Sequential doping of exogenous iron and nitrogen to prepare Fe–N structured biochar to enhance the activity of OTC degradation, *Sep. Purif. Technol.*, 2023, **322**, 124249.

176 J. Shi, B. Dai, X. Shen, L. Xu, Y. Zhang and L. Gan, Wood induced preparation of Fe$_3$C decorated biochar for peroxymonosulfate activation towards bisphenol a degradation with low ion leaching, *J. Environ. Manage.*, 2023, **340**, 117978.

177 J. Leichtweis, N. Welter, Y. Vieira, T. R. Storck, B. Clasen and S. Silvestri, *et al.*, Use of a new ZnFe$_2$O$_4$/biochar composite for degradation and ecotoxicity assessment of effluent containing methylene blue dye, *J. Photochem. Photobiol., A*, 2023, **440**, 114676.

178 W. Li, B. Liu, Z. Wang, K. Wang, Y. Lan and L. Zhou, Efficient activation of peroxydisulfate (PDS) by rice straw biochar modified by copper oxide (RSBC-CuO) for the degradation of phenacetin (PNT), *Chem. Eng. J.*, 2020, **395**, 125094.

179 Y. Yang, J. Zhu, Q. Zeng, X. Zeng, G. Zhang and Y. Niu, Enhanced activation of peroxydisulfate by regulating pyrolysis temperature of biochar supported nZVI for the degradation of oxytetracycline, *J. Taiwan Inst. Chem. Eng.*, 2023, **145**, 104775.

180 Y. Yang, X. Xu, S. Zhang, G. Wang, Z. Yang and Z. Cheng, *et al.*, Two novel and efficient plant composites for the degradation of oxytetracycline: nanoscale ferrous sulphide supported on rape straw waste, *Environ. Sci. Pollut. Res.*, 2022, **29**(42), 63545–63559.

181 Z. R. Jiang, Y. Li, Y. X. Zhou, X. Liu, C. Wang and Y. Lan, *et al.*, Co$_3$O$_4$–MnO$_2$ nanoparticles moored on biochar as a catalyst for activation of peroxymonosulfate to efficiently degrade sulfonamide antibiotics, *Sep. Purif. Technol.*, 2022, **281**, 119935.

182 F. Sang, Z. Yin, W. Wang, E. Almatrafi, Y. Wang and B. Zhao, *et al.*, Degradation of ciprofloxacin using heterogeneous Fenton catalysts derived from natural pyrite and rice straw biochar, *J. Cleaner Prod.*, 2022, **378**, 134459.

183 Y. Yao, H. Hu, H. Zheng, H. Hu, Y. Tang and X. Liu, *et al.*, Nonprecious bimetallic Fe, Mo-embedded N-enriched porous biochar for efficient oxidation of aqueous organic contaminants, *J. Hazard. Mater.*, 2022, **422**, 126776.

184 M. Xiong, J. Yan, G. Fan, Y. Liu, B. Chai and C. Wang, *et al.*, Built-in electric field mediated peroxymonosulfate activation over biochar supported-Co$_3$O$_4$ catalyst for tetracycline hydrochloride degradation, *Chem. Eng. J.*, 2022, **444**, 136589.

185 K. Xiao, F. Liang, J. Liang, W. Xu, Z. Liu and B. Chen, *et al.*, Magnetic bimetallic Fe, Ce-embedded N-enriched porous biochar for peroxymonosulfate activation in metronidazole degradation: Applications, mechanism insight and toxicity evaluation, *Chem. Eng. J.*, 2022, **433**, 134387.

186 T. Liu, Q. Wang, C. Li, M. Cui, Y. Chen and R. Liu, *et al.*, Synthesizing and characterizing Fe$_3$O$_4$ embedded in N-doped carbon nanotubes-bridged biochar as a persulfate activator for sulfamethoxazole degradation, *J. Cleaner Prod.*, 2022, **353**, 131669.

187 J. Liu, J. Jiang, M. Wang, J. Kang, J. Zhang and S. Liu, *et al.*, Peroxymonosulfate activation by cobalt particles embedded into biochar for levofloxacin degradation: Efficiency, stability, and mechanism, *Sep. Purif. Technol.*, 2022, **294**, 121082.

188 J. Chen, X. Bai, Y. Yuan, Y. Zhang and J. Sun, Printing and dyeing sludge derived biochar for activation of peroxymonosulfate to remove aqueous organic pollutants: Activation mechanisms and environmental safety assessment, *Chem. Eng. J.*, 2022, **446**, 136942.

189 S. Fu, Y. Zhang, X. Xu, X. Dai and L. Zhu, Peroxymonosulfate activation by iron self-doped sludge-derived biochar for degradation of perfluorooctanoic acid: A singlet oxygen-dominated nonradical pathway, *Chem. Eng. J.*, 2022, **450**, 137953.

190 H. Huang, T. Guo, K. Wang, Y. Li and G. Zhang, Efficient activation of persulfate by a magnetic recyclable rape straw biochar catalyst for the degradation of tetracycline hydrochloride in water, *Sci. Total Environ.*, 2021, **758**, 143957.

191 Z. Jiang, J. Li, D. Jiang, Y. Gao, Y. Chen and W. Wang, *et al.*, Removal of atrazine by biochar-supported zero-valent iron catalyzed persulfate oxidation: Reactivity, radical production and transformation pathway, *Environ. Res.*, 2020, **184**, 109260.

192 B. Liu, W. Guo, H. Wang, Q. Si, Q. Zhao and H. Luo, *et al.*, Activation of peroxymonosulfate by cobalt-impregnated biochar for atrazine degradation: The pivotal roles of persistent free radicals and ecotoxicity assessment, *J. Hazard. Mater.*, 2020, **398**, 122768.

193 Z. Li, Y. Sun, Y. Yang, Y. Han, T. Wang and J. Chen, *et al.*, Biochar-supported nanoscale zero-valent iron as an efficient catalyst for organic degradation in groundwater, *J. Hazard. Mater.*, 2020, **383**, 121240.

194 F. Qin, Y. Peng, G. Song, Q. Fang, R. Wang and C. Zhang, *et al.*, Degradation of sulfamethazine by biochar-supported bimetallic oxide/persulfate system in natural water: Performance and reaction mechanism, *J. Hazard. Mater.*, 2020, **398**, 122816.

195 X. Zhang, P. Sun, K. Wei, X. Huang and X. Zhang, Enhanced H$_2$O$_2$ activation and sulfamethoxazole degradation by Fe-impregnated biochar, *Chem. Eng. J.*, 2020, **385**, 123921.

196 S. F. Jiang, L. L. Ling, W. J. Chen, W. J. Liu, D. C. Li and H. Jiang, High efficient removal of bisphenol A in a peroxymonosulfate/iron functionalized biochar system: Mechanistic elucidation and quantification of the contributors, *Chem. Eng. J.*, 2019, **359**, 572–583.

197 V. T. Nguyen, T. B. Nguyen, C. W. Chen, C. M. Hung, C. P. Huang and C. D. Dong, Cobalt-impregnated biochar (Co-SCG) for heterogeneous activation of peroxymonosulfate for removal of tetracycline in water, *Bioresour. Technol.*, 2019, **292**, 121954.

198 T. A. Nguyen and S. Oh, Biochar-mediated oxidation of phenol by persulfate activated with zero-valent iron, *J. Chem. Technol. Biotechnol.*, 2019, **94**(12), 3932–3940.

199 J. Chen, X. Yu, C. Li, X. Tang and Y. Sun, Removal of tetracycline *via* the synergistic effect of biochar adsorption and enhanced activation of persulfate, *Chem. Eng. J.*, 2020, **382**, 122916.

200 C. Lai, F. Huang, G. Zeng, D. Huang, L. Qin and M. Cheng, *et al.*, Fabrication of novel magnetic MnFe$_2$O$_4$/bio-char composite and heterogeneous photo-Fenton degradation of tetracycline in near neutral pH, *Chemosphere*, 2019, **224**, 910–921.

201 Q. Mao, Y. Zhou, Y. Yang, J. Zhang, L. Liang and H. Wang, *et al.*, Experimental and theoretical aspects of biochar-supported nanoscale zero-valent iron activating H$_2$O$_2$ for ciprofloxacin removal from aqueous solution, *J. Hazard. Mater.*, 2019, **380**, 120848.

202 H. Fu, S. Ma, P. Zhao, S. Xu and S. Zhan, Activation of peroxymonosulfate by graphitized hierarchical porous bio-char and MnFe$_2$O$_4$ magnetic nanoarchitecture for organic pollutants degradation: Structure dependence and mechanism, *Chem. Eng. J.*, 2019, **360**, 157–170.

203 L. Chen, S. Yang, X. Zuo, Y. Huang, T. Cai and D. Ding, Biochar modification significantly promotes the activity of Co$_3$O$_4$ towards heterogeneous activation of peroxymonosulfate, *Chem. Eng. J.*, 2018, **354**, 856–865.

204 J. Deng, H. Dong, C. Zhang, Z. Jiang, Y. Cheng and K. Hou, *et al.*, Nanoscale zero-valent iron/biochar composite as an activator for Fenton-like removal of sulfamethazine, *Sep. Purif. Technol.*, 2018, **202**, 130–137.

205 D. Ma, Y. Yang, B. Liu, G. Xie, C. Chen and N. Ren, *et al.*, Zero-valent iron and biochar composite with high specific surface area *via* K$_2$FeO$_4$ fabrication enhances sulfadiazine removal by persulfate activation, *Chem. Eng. J.*, 2021, **408**, 127992.

206 M. Chen, T. Yang, L. Zhao, X. Shi, R. Li and L. Ma, *et al.*, Manganese oxide on activated carbon with peroxymonosulfate activation for enhanced ciprofloxacin degradation: Activation mechanism and degradation pathway, *Appl. Surf. Sci.*, 2024, **645**, 158835.

207 X. Li, S. Zhang, M. Zhang, M. Yu, H. Chen and H. Yang, *et al.*, One-step synthesis of mixed valence FeO$_x$ nanoparticles supported on biomass activated carbon for degradation of bisphenol A by activating peroxydisulfate, *J. Hazard. Mater.*, 2021, **409**, 124990.

208 Z. Yang, Y. Li, X. Zhang, X. Cui, S. He and H. Liang, *et al.*, Sludge activated carbon-based CoFe$_2$O$_4$-SAC nanocomposites used as heterogeneous catalysts for degrading antibiotic norfloxacin through activating peroxymonosulfate, *Chem. Eng. J.*, 2020, **384**, 123319.

209 W. W. Loo, Y. L. Pang, S. Lim, K. H. Wong, C. W. Lai and A. Z. Abdullah, Enhancement of photocatalytic degradation of Malachite Green using iron doped titanium dioxide loaded on oil palm empty fruit bunch-derived activated carbon, *Chemosphere*, 2021, **272**, 129588.

210 J. Zhao, Y. Sun, Y. Zhang, B. T. Zhang, M. Yin and L. Chen, Heterogeneous activation of persulfate by activated carbon supported iron for efficient amoxicillin degradation, *Environ. Technol. Innovation*, 2021, **21**, 101259.

211 J. M. Dangwang Dikdim, Y. Gong, G. B. Noumi, J. M. Sieliechi, X. Zhao and N. Ma, *et al.*, Peroxymonosulfate improved photocatalytic degradation of atrazine by activated carbon/graphitic carbon nitride composite under visible light irradiation, *Chemosphere*, 2019, **217**, 833–842.

212 H. Erdem and M. Erdem, Ciprofloxacin Degradation with Persulfate Activated with the Synergistic Effect of the Activated Carbon and Cobalt Dual Catalyst, *Arabian J. Sci. Eng.*, 2023, **48**(7), 8401–8415.

213 D. V. Nguyen, H. M. Nguyen, Q. L. N. Bui, T. V. T. Do, H. H. Lam and T. M. Tran-Thuy, *et al.*, Magnetic Activated Carbon from ZnCl$_2$ and FeCl$_3$ Coactivation of Lotus Seed-pod: One-Pot Preparation, Characterization, and Catalytic Activity towards Robust Degradation of Acid Orange 10, *Bioinorg. Chem. Appl.*, 2023, **2023**, 384845.

214 C. Wang, H. Liu, P. Sun, J. Cai, M. Sun and H. Xie, *et al.*, A novel peroxymonosulfate activation process by single-atom iron catalyst from waste biomass for efficient singlet oxygen-mediated degradation of organic pollutants, *J. Hazard. Mater.*, 2023, **453**, 131333.

215 Y. Chen, X. Bai, Y. Ji and T. Shen, Reduced graphene oxide-supported hollow Co$_3$O$_4$@N-doped porous carbon as peroxymonosulfate activator for sulfamethoxazole degradation, *Chem. Eng. J.*, 2022, **430**, 132951.

216 X. Zhou, Y. Wang, H. Liu, Y. Zhang, Y. Fan and S. Mo, *et al.*, Novel amino-modified bamboo-derived biochar-supported nano-zero-valent iron (AMBBC-nZVI) composite for efficient Cr(vi) removal from aqueous solution, *Environ. Sci. Pollut. Res.*, 2023, **30**(57), 119935, DOI: **10.1007/s11356-023-30351-9**. Available from: .

217 P. Kaur, S. Kumar, J. Rani, J. N. Babu and S. Mittal, Comparison of surface adsorption efficacies of eco-sustainable agro/animal biomass-derived activated carbon for the removal of rhodamine B and hexavalent chromium, *Environ. Sci. Pollut. Res.*, 2024, **31**(39), 52371–52390, DOI: **10.1007/s11356-024-34686-9**. Available from: .

218 S. Kumar, P. Kaur, J. Rani, J. Singh, S. Kaushal and J. N. Babu, *et al.*, Synergistic impact of rice husk biomass derived carbon supports on the performance of biogenic Fe^0-catalyzed advanced oxidation processes for oxytetracycline remediation, *Environ. Sci.: Water Res. Technol.*, 2025, **11**(2), 242–261, DOI: **10.1039/D4EW00912F**. Available from: .

219 P. Thamarai, V. C. Deivayanai, S. Karishma, A. Saravanan, P. R. Yaashikaa and A. S. Vickram, Adsorption Strategies in Surface Modification Techniques for Seaweeds in Wastewater Treatment: Exploring Environmental Applications, *Rev. Environ. Contam. Toxicol.*, 2024, **262**(1), 18 Available from: **https://link.springer.com/10.1007/s44169-024-00071-3**.

220 J. Chen, S. Deng, W. Jia, X. Li and J. Chang, Removal of multiple heavy metals from mining-impacted water by biochar-filled constructed wetlands: Adsorption and biotic removal routes, *Bioresour. Technol.*, 2021, **331**, 125061

Available from: https://linkinghub.elsevier.com/retrieve/pii/S0960852421004004.

221 V. Katheresan, J. Kansedo and S. Y. Lau, Efficiency of various recent wastewater dye removal methods: A review, *J. Environ. Chem. Eng.*, 2018, **6**(4), 4676–4697. Available from: https://linkinghub.elsevier.com/retrieve/pii/S2213343718303695.

222 L. Wang, Y. Chang and Q. Liu, Fate and distribution of nutrients and heavy metals during hydrothermal carbonization of sewage sludge with implication to land application, *J. Cleaner Prod.*, 2019, **225**, 972–983. Available from: https://linkinghub.elsevier.com/retrieve/pii/S0959652619310637.

223 J. O. Eniola and B. Sizirici, Investigation of biochar-modified biosand filter performance for groundwater treatment for drinking water purposes: A laboratory and pilot scale study, *J. Water Process. Eng.*, 2023, **53**, 103914. Available from: https://linkinghub.elsevier.com/retrieve/pii/S2214714423004336.